Master's thesis

NTNU
Norwegian University of Science and Technology
Faculty of Engineering
Department of Geoscience and Petroleum

Vahid Marashi

Northern Lights Project: Aurora Model Investigation with Sensitivity Studies and Using Different Simulation Methods

Master's thesis in Petroleum Engineering
Supervisor: Ashkan Jahanbani Ghahfarokhi
Co-supervisor: Per Eirik Bergmo, Cathrine Ringstad
December 2021

NTNU
Kunnskap for en bedre verden

Vahid Marashi

Northern Lights Project: Aurora Model Investigation with Sensitivity Studies and Using Different Simulation Methods

Master's thesis in Petroleum Engineering
Supervisor: Ashkan Jahanbani Ghahfarokhi
Co-supervisor: Per Eirik Bergmo, Cathrine Ringstad
December 2021

Norwegian University of Science and Technology
Faculty of Engineering
Department of Geoscience and Petroleum

NTNU
Norwegian University of
Science and Technology

Abstract

The Norwegian *"Longship"* full-scale carbon capture and storage (CCS) project was defined over the Norwegian Continental Shelf (NCS) following the successful Sleipner CO_2 storage operation. The Northern Lights project is part of the Longship project, responsible for transporting CO_2 captured from industrial sources via ship and pipeline and storing the captured CO_2 in the subsurface. The Aurora complex, southwest of Troll Field, has been identified as a storage site for this purpose. This storage site comprises two sandstone formations that have been treated as one saline aquifer with promising storage capacity for long-term CO_2 storage.

Numerical reservoir simulations can be very useful for CO_2 sequestration projects since they provide a great deal of information about the best storage sites for optimal injection strategies by simulating the physics of the rock/fluid inside the formation and forecasting the possible CO_2 distribution along with the formation before an expensive injection operation. It is feasible to utilize Schlumberger's ECLIPSE software to adapt the black-oil model for CO_2 storage (ECLIPSE 100) and the CO2STORE module in compositional modeling (ECLIPSE 300). Additionally, sensitivity studies must be carried out to assess the impact of uncertain parameters on pressure changes, the amount of CO_2 dissolved in the brine phase, and the likely distribution pathway of injected CO_2 in the reservoir over a long period.

The given Aurora model was initially refined and updated in this project to create a new base case model. The Aurora model (black-oil) was then converted to a compositional model using the CO2STORE option, employing the equation of state and solubility models to assess the quantity of dissolved CO_2 in the brine phase over time. CO2STORE module uses dedicated storage output parameters for mobile, immobile, and dissolved CO_2, whereas the black-oil model does not. According to the results, the differences in computations between these two simulation methods were minor. The black-oil simulation is a wiser choice for sensitivity studies with several simulations needed due to their low computation time, while the compositional simulation is more suitable for achieving more accurate results. In addition, a sensitivity analysis was carried out to account for the uncertainty of six reservoir parameters. According to the findings, pore volume and rock compressibility have the most impact on pressure build-up and stabilization, while permeability ratio, fault transmissibility, and relative permeability curve have the greatest influence on CO_2 plume distribution over the reservoir.

Acknowledgment

The master's thesis (30 Credits) is submitted to the Department of Geosciences and Petroleum, Norwegian University of Science and Technology (NTNU), in the candidacy of Master of Science in Petroleum Engineering (120 Credits), following the Reservoir Engineering and Petrophysics specialization. The thesis is a part of CEORS Gemini-Center activities (CO_2 Enhanced Oil Recovery and Storage), a strategic collaboration between NTNU and SINTEF (https://www.ntnu.edu/ceors). This project is also a part of the SINTEF Industry's project, known as COSMOS (Controlled Source Electromagnetic Monitoring of CO_2 Storage Sites), and started in September 2021, after receiving permission from Gassnova to use the Aurora reservoir model.

I would like to express my gratitude to my supervisor, Ashkan Jahanbani Ghahfarokhi (NTNU), who always provided me with his helpful advice, knowledge, and full support as a professor and supervisor whenever possible. I would like to thank Cathrine Ringstad as my co-supervisor from the SINTEF group, who had confidence in me and gave me an excellent opportunity to be a part of this exciting project. In addition, my appreciation also goes to Per Eirik Bergmo as my other co-supervisor from the SINTEF group, who was always there for me whenever I needed his guidance and shared his ideas and knowledge through the project. It was indeed an honor working with people that have a lot to offer both to academia and the industry. Lastly, I would like to thank my incredible family for being a constant source of support. I appreciate everything you've done for me.

Despite the fact that I only had a limited amount of time to work on this project, I did my best to develop the work as much as possible in order to prepare it for future studies, as there is a lot more that could be tested and done with this project. I tried to make the thesis a valuable reference for future students who are interested in CO_2 storage and simulation topics. I hope you enjoy reading the thesis and learning more about this fascinating subject.

Trondheim, December 2021

Vahid Marashi

Table of Contents

List of Figures

List of Tables

List of Abbreviations

AI	Acoustic impedance
AIM	Adaptive implicit
BHP	Bottom hole pressure
$CaCl_2$	Calcium chloride
CCS	Carbon capture and storage
CO_2	Carbon dioxide
E100	ECLIPSE 100 black-oil simulator
E300	ECLIPSE 300 compositional simulator
EOR	Enhanced oil recovery
EoS	Equation of state
FDM	Finite difference method
FEM	Finite element method
Gt	Giga tonnes
H_2O	Water
IMPES	Implicit pressure, explicit saturation
IPM	Invasion percolation method
km	Kilometer
m	Meter
Mt	Million tonnes
NaCl	Sodium chloride
NCS	Norwegian continental shelf
PHIE	Effective porosity
PHIT	Total porosity
PVT	Pressure, volume, temperature
VCL	Volume of clay
VE	Vertical equilibrium

1 Introduction

This study is a continuation of reservoir simulations performed on the Aurora model by research groups at the University of Oslo, SINTEF group, Gassnova, and Equinor (Gassnova, 2012; Lothe et al., 2019; Sundal et al., 2015). It includes different sensitivity studies on model uncertainties, utilizing two different numerical reservoir simulators, comparing, and contrasting their similarities and differences, and finally observing the strengths and limitations of each one in the case of an actual CO_2 plume distribution in the reservoir. This section introduces the motivation, the study area, and the main research objectives of the project.

1.1 Motivation

Global warming is undeniably a significant concern that has the potential to threaten modern human life. The majority of proposed strategies to fight climate change, such as renewable energy sources, are effective approaches with major improvements during the recent years, yet they are currently unable to meet 100% of global energy demand. We believe that fossil fuel combustion is the primary source of CO_2 emission to the atmosphere, which causes the earth's temperature to rise. However, since energy consumption is escalating due to industrialization and an increasing worldwide population, fossil fuels will continue to be the primary energy source for people and industry in the coming years. Fortunately, CCS technology was introduced as a quick and functional solution to comply with the Paris Agreement's goal of keeping the global mean temperature rise below two degrees by 2100 and achieving net zero emissions from the energy sector by 2050 (Beck & Mahony, 2018).

Sleipner, as the world's first commercial CCS project that has injected an annual rate of approximately 1 million tonnes of CO_2 since 1996, can be a solid practical benchmark for the following CCS projects around the world, especially in the North Sea due to its geographical location (Solomon, 2007). After this successful large-scale project, the Norwegian government started issuing the feasibility of putting all parts of the CCS value chain, i.e., capture, transport, and storage, on a single project. After the positive outcomes, the government defined a concrete plan to construct and develop a new full value chain CCS project, named *Longship* (Langskip in Norwegian), with the ambition to give an effectual contribution to the development of long-term CCS with cost-effective approaches, not only for Norway but for other European countries (Equinor, 2020). This demonstration project encompasses capturing CO_2 at Norcem's cement

factory in Brevik first, and possibly Fortum Oslo Varme's waste-to-energy facility in Oslo, then transporting captured CO_2 by ships to a new receiving terminal (Naturgassparken) in Øygarden municipality (Figure 1.1). From the terminal, the CO_2 will be transported via pipelines and injected into a deep saline aquifer within two colossal potentials of the Johansen and Cook formations, located in the southwest part of the giant Troll Field and approximately 2.6 km below the seabed (Bakke, 2020; Sundal et al., 2016). As part of the Longship CCS project, the *Northern Lights* is responsible for transporting and storing CO_2 in the subsurface and is a joint venture with Equinor ASA as the project operator, A/S Norske Shell, and Total E&P Norge AS as other partners. In January 2019, Northern Lights received the award of exploitation license 001 (EL001) south of giant Troll West Field (Figure 1.2). In early 2020, the 'Eos' confirmation well was drilled to test the Dunlin Group, consisting of potential saline aquifers for CO_2 storage. Phase one of the project aims to store up to 1.5 Mt of CO_2 per year over ten years, possibly developing the facility to store 5 Mt of CO_2 per year for the subsequent second phase. The *Oseberg A* platform will be utilized for controlling and monitoring the injection well via an umbilical line (Figure 1.2) (Furre et al., 2020). The storage site for the early stages of the project is called *Aurora* and lies in the *Horda* Platform together with the Smeaheia area and the Troll Field. Aurora storage site will be developed as a subsea development (Furre et al., 2020).

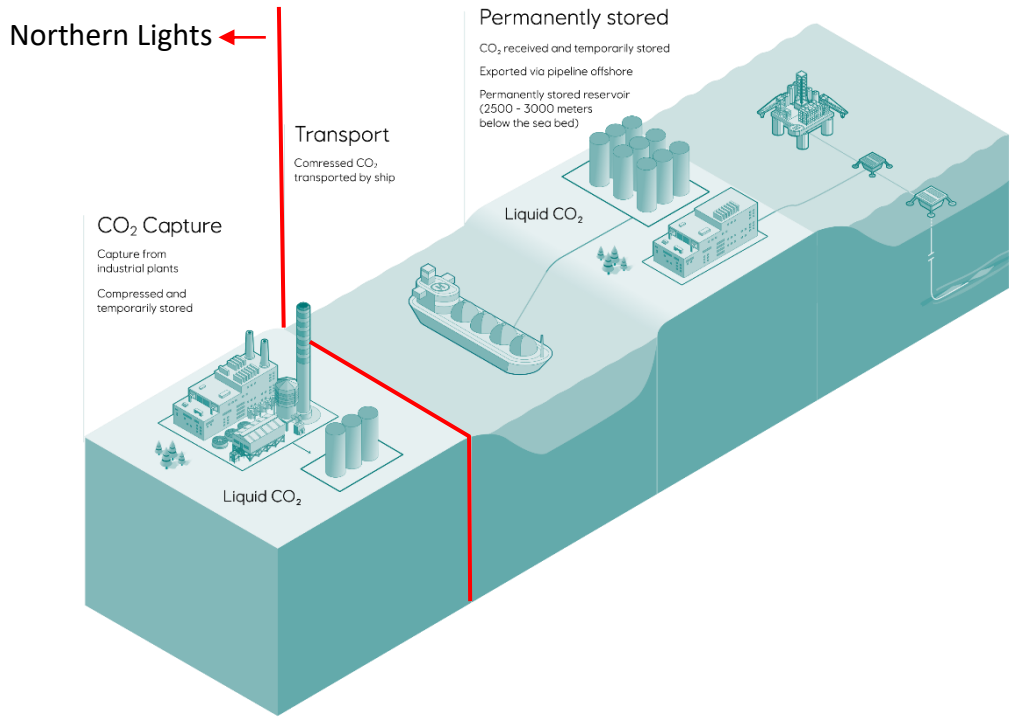

Figure 1.1 Sketch of full-scale CCS project. CO_2 is captured at industrial plants and compressed at high pressures to form a liquid. The first transportation is done by ship to an onshore terminal and from the terminal CO_2 is transported to a geological storage site via a pipeline (Modified from Equinor-Northern Lights CCS).

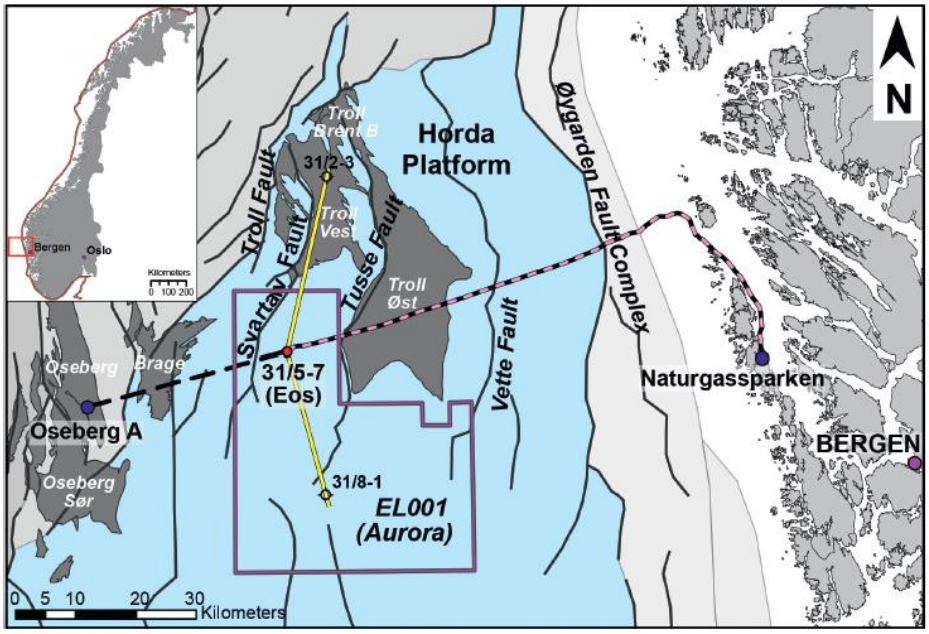

Figure 1.2 Map indicating the Exploitation License EL001 in the Aurora site, south of the Troll Field, as well as the Eos confirmation well shown in red point. The Horda Platform covering the Troll Field and the exploitation license EL001 is shown in light blue. Control umbilical and cable route shown by black stippled line. Yellow line is the trace of the cross section shown in Figure 1.3 and the Pink stippled line is the pipeline route. Blue point indicates the onshore terminal, Naturgassparken, located in Øyegarden, west of Bergen municipality (Furre et al., 2020).

1.2 The Aurora Exploitation License (EL1001)

The Aurora Exploitation License was granted to the Northern Lights project by the Norwegian government in January 2019. The license is located in the Horda Platform, an established hydrocarbon producing region approximately 60 km west of Naturgassparken, in Øygarden municipality. The gas production from the Troll Field affects the pore pressure in the whole Horda Platform area. The effect east of the Vette Fault, i.e., Smeaheia area, is still uncertain because of having very few drilled wells in that area (Lothe et al., 2018). Due to the uncertainty on the density of CO_2 at Smeaheia area and the risk of possible spill-over of expanding CO_2 into the Øygarden Fault complex, Norwegian authorities decided to shift the focus of Northern Lights project to grant the Aurora exploitation license (EL001), which covers the southern part of Troll West and Troll East fault blocks with the early Jurassic Johansen Formation with a CO_2 storage capacity of at least 150 Mt (Gassnova, 2012; Lothe et al., 2019; Sundal et al., 2015; Sundal et al., 2016).

As a confirmation of suitable storage sites, including promising sealing units within Aurora, the 31/5-7 confirmation well, named Eos, was drilled by the Northern Lights project from December 2019 to March 2020. This well is located around 10 km south of the border between

the Aurora site and the Troll License (Figure 1.3). The temporarily abandoned Eos well will be later re-entered, side-tracked, and used as a CO_2 injection well (Furre et al., 2020).

Aurora complex consists of the Lower Jurassic, the Dunlin Group, within license EL001. The Johansen and Cook formations are the primary sandstone reservoirs, overlaid by the Drake Formation as the primary sealing unit to ensure containment of the injected CO_2 in the saline aquifer. In addition to the Drake Formation, a shallower sealing system (overburden) exists which encompasses the Draupne Formation, a proven hydrocarbon barrier for many fields in NCS such as the Troll West and Troll East, followed by the Cromer Knoll, Shetland, and Rogaland groups, and is believed to be an effective barrier, retaining the injected CO_2 in the subsurface. The injected CO_2 in the Johansen Formation is deemed to migrate upwards into the overlying Cook Formation with an N-S structural of approximately 2 degrees (Furre et al., 2020). The part of injected CO_2 that is not trapped during migration will migrate up-dip, and after several decades, it is expected to cross the license boundary. Eventually, the remaining free CO_2 will be possibly trapped in the Cook Formation, approximately 400 m below the hydrocarbon contact Troll West Field, more than 20 km north of Eos well. The target area for CO_2 injection and storage is situated in the middle of the Johansen Formation, south of the Troll Field. The reason is that the Troll Field is producing hydrocarbons from Late Jurassic sandstones of the Viking Group, assuming the injected CO_2 in the Johansen Formation will not be in contact with the overlying hydrocarbon reservoirs.

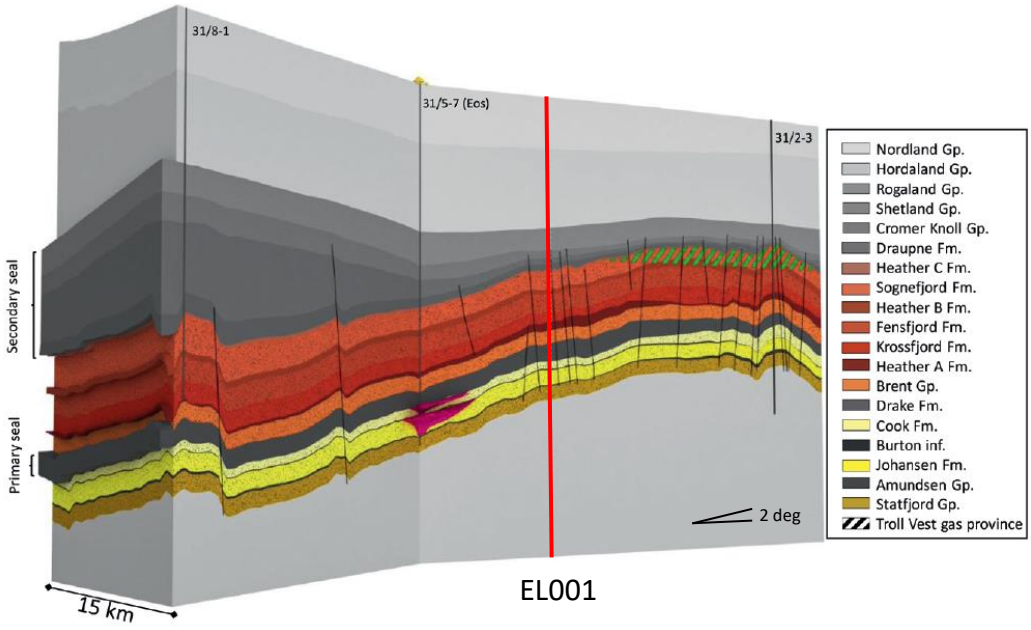

Figure 1.3 Schematic of the subsurface going from south to north through the 31/5-7 (Eos) confirmation well. The CO_2 plume extent after 37.5 Mt injection is illustrated in magenta. The red line indicates the extent of the exploitation license EL001 (Modified from Furre et al. 2020).

1.3 Research objectives

As a part of studying the Aurora storage site, a model was established by Anja Sundal and her team at the University of Oslo to propose the possible scenarios that can occur in the Johansen Formation as the primary reservoir unit of the Aurora site (Sundal et al., 2015). In addition, the model will be refined and updated with new findings and during the injection periods. As a continuation of previous investigations on the Aurora model, the main objectives of the research are the following:

I. Update the model and place the injection well (Eos) in the real geographical coordinate.
II. Convert the black-oil model to the compositional model by changing the DATA file.
III. Compare the performance of the black-oil and compositional simulators.
IV. Sensitivity studies on some uncertain parameters using the black-oil simulator.

1.4 Thesis outline

The thesis consists of six chapters and four appendices. Chapter one introduces the motivation, the Aurora site as the study area, and the research objectives. Chapter two summarizes the most important aspects of CO_2 sequestration in saline aquifers. Chapter three explains the methodology and process of the reservoir simulation and the software and tools utilized for the project. Chapter four describes the features of the default Aurora model and the new Aurora base case model and gives an overview of the model. Chapter five reveals the results obtained from ECLIPSE 100, the black-oil simulator, and ECLIPSE 300, the compositional simulator, their performance, and compares both simulation methods. In addition, the results from sensitivity analysis of six reservoir parameters are described using the black-oil simulator. Finally, chapter six presents the conclusion and recommendations for future works on this project.

Appendix A covers the important conversions, and Appendix B covers the DATA file of the black-oil and compositional simulators. Appendix C shows the integrated biostratigraphy of the area of interest and the formation tops resulting from the Eos well. Lastly, the link to all the simulations done in this project has been attached in Appendix D.

2 Geological CO_2 storage concept

In the early 1970s, the first engineered CO_2 injection started as a part of EOR (enhanced oil recovery) in Texas, the USA, followed by many other EOR projects worldwide utilizing CO_2 as a fluid to increase hydrocarbon recovery (Metz et al., 2005). What is expected in all EOR projects using CO_2 is the accumulation of some proportion of the injected CO_2 in the reservoir. In addition, it is highly accepted that the natural accumulation of gases such as methane and CO_2 in deep underground reservoirs trapped by overlying impermeable caprocks has been a widespread natural phenomenon for millions of years. After the concerns about climate change due to the increasing concentration of greenhouse gases resulting from fossil fuel combustion to produce energy and other industrial emitter sources such as steel and cement plants, the idea of CO_2 capturing and sequestration in geological formations to mitigate emissions to the atmosphere was revealed in the late 70s (Marchetti, 1977). In 1996, Equinor (former Statoil) and its partners initiated the first large-scale CCS project at the Sleipner Gas Field in the North Sea, successfully storing nearly 1 Mt of CO_2 per annum until today. Several long-term storage sites with porous reservoirs containing water or hydrocarbon have been proposed that are able to retain the CO_2 in the subsurface in a secure manner (Figure 2.1). Deep saline aquifers, depleted hydrocarbon fields, and unminable coal seams have been introduced as the most suitable potential storage sites in terms of their capacity (Table 2.1). However, other storage possibilities exist, including shale units, volcanic rocks, and underground caverns (Metz et al., 2005).

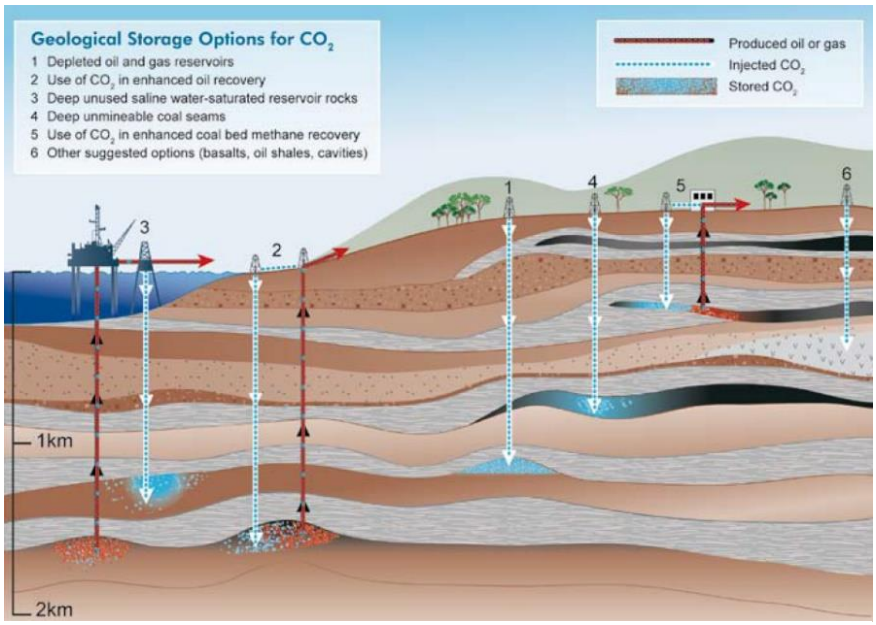

Figure 2.1 Different options for geological storage of CO_2 underground. (Metz et al., 2005).

Table 2.1 Storage capacity of different geological storage options, including non-economical storage options (Metz et al., 2005)

Reservoir type	Lower estimate of storage capacity (Gt CO_2)	Upper estimate of storage capacity (Gt CO_2)
Deep saline aquifers	1000	10,000
Hydrocarbon fields	657	900
Unminable coal seams	3-15	200

CO_2 is in the gaseous phase at standard conditions, meaning that it is highly compressible and has low viscosity and density. Depending on the geothermal gradient, the density of CO_2 increases with depth. When the CO_2 reaches the critical depth (nearly 800 m) or greater, the injected CO_2 will be in a new phase known as the *super-critical* phase (Bachu, 2002) (Figure 2.2). Being CO_2 in the super-critical (dense) phase is always preferred in that it occupies much less volume in comparison to the gaseous phase, leading to a more effective storage operation. Depth is also crucial for increasing the security of the storage site since at depths around 800 m or more, the chances of existing sealing units such as shales, faults, and salt units above the injection formation increases. Natural gas and CO_2 have been trapped beneath the impermeable seals for millions of years in deep formations, and as a result, the potential for long-term CO_2 storage is clearly high (Ringrose, 2020).

CO_2 flow dynamics in the subsurface is a complex process and hence needs a deep understanding of the physical process and driving forces occurring during the injection and post-injection period. Reservoirs behave differently when introduced to the injected fluid depending on their geology, pressure-temperature, heterogeneity, thickness, and other essential parameters. After finding the accurate interval of the zone of interest, the well is perforated where it faces the formation, and CO_2 is injected in saline aquifers by pumping the fluid down into the well with a higher pressure than the reservoir pressure. CO_2 injected into a deep saline aquifer can be present in three forms: a free CO_2 phase, a dissolved state in pore water, and an immobilized state through geochemical reactions with formation minerals. A low-permeable, thick caprock should overlie the storage injection zone with a depth usually

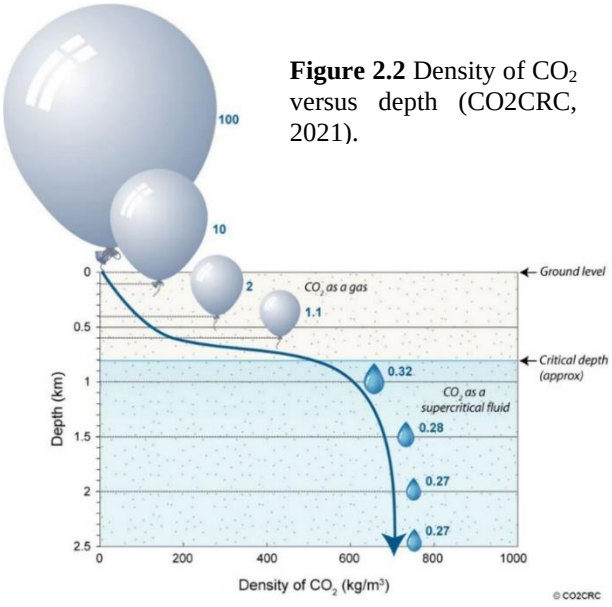

Figure 2.2 Density of CO_2 versus depth (CO2CRC, 2021).

greater than 800 - 1000 m as CO_2 becomes super-critical and will have a liquid-like phase density, providing the potential for efficient utilization and increasing the safety of storage (Metz et al., 2005).

The pressure needed at the bottomhole must be higher than the formation's average pressure, letting CO_2 fluid entering the pore spaces to displace the *in situ* formation water (brine). Pressure build-up in the formation depends on the permeability and thickness of the formation, injection rate, faults that can act as sealing or conduit units, depending on the nature of the faults and the stress conditions, and the reservoir's heterogeneity (Metz et al., 2005). It needs to be considered very carefully to have a secure injection operation without creating additional fractures in the overlying low-permeable formation, leading to CO_2 leakage in a short or long-time period. For saline aquifer cases, CO_2 in the form of a liquid or liquid-like super-critical (dense) phase is immiscible with the water inside the formation. Before modeling or predicting the CO_2 plume growth in the reservoir, it is vital to understand the physical processes during injection and post-injection operation, such as the interplay between fluid driving forces, i.e., viscous, gravitational, and capillary force, before starting an actual CO_2 injection project.

2.1 Injection process

When the injected CO_2 enters the formation in the near-well region, the dominating driving force flow is the viscous force due to the pressure gradient induced by the high injection pressure, pushing away the *in situ* brine and occupying some fraction of the pores near the injection well in the *drainage* process. While two distinct phases share the pores on a small scale, there will be a limited exchange of mass between two phases, where a small amount of CO_2 starts dissolving into the brine, and a smaller amount of brine evaporates into the CO_2. However, dissolution will not have a strong impact in this stage. CO_2, when at the super-critical (dense) phase, has much less viscosity than that of the brine phase (by order of magnitude or more). The very low viscosity of super-critical CO_2 will lead to flow instability in the CO_2-brine interface resulting in fingering in some reservoir regions. This means that instead of having a uniform piston-like CO_2 front distribution, some front parts will flow considerably faster and form fingers inside the brine phase. Fingering and channeling can also occur due to the heterogeneity of the rock formation, leading to channelizing the injected CO_2 to permeable paths due to the spatial variation of permeability of the formation. Gravitational force will also have an important role in the flow direction, where due to the high-density difference between phase fluids, the injected CO_2 tends to move vertically and fill the top of the formation until the sealing unit blocks the vertical movement. After reaching the top of the formation, CO_2 needs

to exceed the capillary entry pressure of the sealing unit for further vertical movements. The geometry of the plume depends on many factors such as reservoir heterogeneity, flow rate, and the density difference between the CO_2 and brine. A high fluid flow rate will cause more viscous force near the wellbore region, while a significant density difference will cause more vertical migration and lateral distribution on top of the formation, away from the well. Driving out 100% of the *in situ* brine by injecting CO_2 is impossible since a residual amount of water will always remain trapped in the pores or adsorbed by the grain surfaces. In the laboratories, it is possible to estimate the fraction of *irreducible water saturation* as the amount of water that remains in the pores in the drainage process and cannot be extracted by the injected CO_2. The amount of trapped brine will decrease gradually due to brine evaporation into the dry CO_2 injected in the saline aquifer, leading to salt precipitation as a solid matter within the pores which can cause injectivity reduction (Miri & Hellevang, 2016).

Two main mechanisms play a vital role in providing extra space needed to store the CO_2 in the formation with less concern about the limit exceeding pressure elevation that can lead to fracturing the sealing unit. The first mechanism is the gradual migration of brine, either through the caprock, into the neighboring formations, or across lateral boundaries. Even though the injected CO_2 faces difficulties entering the caprock through the mechanism of capillary exclusion, the brine can pass through the low-permeable caprock at a very slow pace. The second mechanism is through the compressibility. As the pressure increases in the reservoir due to the constant CO_2 injection, the density of CO_2 and brine starts to increase slightly, and as a result, more amount of fluid is allowed to occupy the reservoir. In addition, the pressure-buildup will cause slight rock expansion due to the rock compressibility and thus increase the overall volume of the available pore space. It should be noted that pressure elevation can also cause changes in the rock matrix's global stress field, which can lead to rock fracturing and fault reactivation if the pressure elevation is not controlled and kept within safe limitations. Lastly, since most of the saline aquifers, such as the Aurora site, are formed at high depths, thermal effects can affect the injection process since the injected CO_2 is injected at much lower temperatures (25 ˚C) compared to the formation temperature (up to 100 ˚C) which could lead to thermal fracturing, fault reactivation or completion design issues (Thompson et al., 2021).

2.2 Migration process

When the injection stops and the well is shut off, the pressure build-up resulting from the CO_2 injected starts to dissipate gradually in the formation. The domination of viscous forces a bit away from the well will be replaced by advection, and the fluid phases start to find the equilibrium in the porous media, driven by gravitational and capillary forces, where the upper part of the CO_2 continues expanding outwards as a thin plume below the caprock. As the CO_2 migrates upward due to gravitational force, the trail of the CO_2 plume will be displaced by the *in situ* brine in the *imbibition* process, as the reverse of the drainage process. As with irreducible water saturation, the imbibition process cannot displace 100% of the CO_2, and a fraction of CO_2 will remain in the pores and be trapped by capillary forces, known as *residual trapping*. Once CO_2 reaches the top of the formation, the sealing unit (caprock) prevents further vertical movement. However, The CO_2 is still mobile and will slowly distribute in the upslope direction below the caprock, known as *hydrodynamic trapping*. During the upslope migration of CO_2, some portion of CO_2 can become permanently trapped as it can collect in local pockets, sealed fault blocks, salt domes along the way, referred to as *structural trapping*. The same case type of trapping can be due to unconformities, pinch-outs, or rock type change within the storage called *stratigraphic* trapping. As the plume extends laterally, the CO_2-brine interface will be more extended, and the brine starts to dissolve CO_2 in the *dissolution trapping* process until it becomes a CO_2-rich brine, which is denser than the undersaturated brine and sinks toward the bottom of the formation in a process called *convection enhanced dissolution*. After years, depending on the chemical composition of the brine and rock, pressure, and temperature, CO_2-rich brine can precipitate as carbonate minerals in a pretty slow process known as *mineral trapping*. The migration process and the trapping mechanisms that contribute to the CO_2 storage process are shown in Figure 2.3.

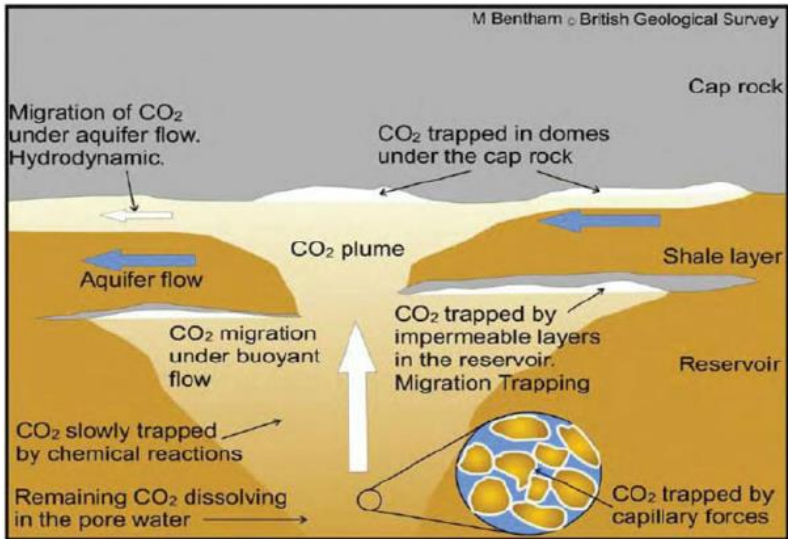

Figure 2.3 CO_2 migration process and various trapping mechanisms in the reservoir (Gough et al., 2006).

2.3 Trapping mechanisms

Following injecting CO_2 in the subsurface, a couple of mechanisms could control the movement of the injected fluid and prevent CO_2 from leakage, some by immobilizing the CO_2 over time and some by trapping the CO_2 under confining layers which can avoid possible leakages to the sea and eventually the atmosphere. These storage mechanisms can occur simultaneously, yet with different contributions over a specific time. From a theoretical perspective, the containment of CO_2 in the geological storage site is classified into *physical* and *chemical* trapping shown in Table 2.2.

Table 2.2 Different types of trapping mechanisms

Trapping type	Trapping mechanism
Physical	Stratigraphic and Structural
	Hydrodynamic
	Residual
Geochemical	Dissolution
	Mineralization

Physical trapping: stratigraphic and structural

The initial trapping mechanism controlled by the rock architecture of the storage complex appears below caprocks with low permeability and high capillary entry pressure. This mechanism is similar to hydrocarbon or saline water accumulation in the reservoir and is the most dominating mechanism for secure storage in the early time frame. Sedimentary basins occupied by hydrocarbons and saline water have closed structures that preserve CO_2 in the subsurface. Stratigraphic traps are formed by changes in rock type made by variation in the rocks' setting, while structural traps cover those formed by folded or fractured rocks. Faults can sometimes serve as preferential pathways for the fluid flow and sometimes as permeability barriers. To avoid caprock fracturing or reactivation of faults, significant attention must be taken into consideration to keep the allowable overpressure at a safe limit. As mentioned before, since caprocks are usually composed of small grains and pore throats, CO_2 will not be able to penetrate the caprock to a great extent, and a finite pressure increase must overcome the capillary pressure limit for CO_2 to enter the caprock (Figure 2.4). For pressure differentials lower than entry capillary pressure, CO_2 will not enter the caprock at all. Interfacial tension is an essential factor since it controls the size of natural or artificial accumulations of CO_2. Berg (Berg, 1975) proposed a formula wherein the thickness of a gas that can be retained against the gravity by the capillary entry pressure of the sealing rock is defined as:

$$z_g = \frac{2\gamma cos\theta \left({}^{1}/_{r_{cap}} - {}^{1}/_{r_{res}}\right)}{g(\rho_w - \rho_g)} \qquad 2.1$$

Where γ is the interfacial tension, θ is the fluid contact angle, r_{cap} and r_{res} are the pore throat radii in the caprock and reservoir, respectively, ρ_w and ρ_g are the densities of water and gas and g is the gravitational constant. Therefore, having all the parameters makes it possible to estimate the maximum CO_2 column height that can be held below a given caprock. It should be noted that with the presence of a fracture in the caprock, the effective pore radius in the fracture can be much more significant, and thus, the capillary entry pressure of the caprock will be less, leading to more quantity of CO_2 entering the sealing unit (Niemi et al., 2017).

Physical trapping: hydrodynamic

Hydrodynamic trapping occurs in saline formations without a closed trap, where fluids migrate at a plodding velocity over large ranges. When CO_2 is injected into a reservoir, it tends to displace saline water, mostly on top of the formation, due to the gravitational force caused by the density difference between CO_2 and brine. CO_2 continues to migrate as a separate phase on top of the formation until it is trapped in local stratigraphical or structural traps within the sealing formation or by reaching residual CO_2 saturation in regions that brine has displaced the injected CO_2 in the imbibition process. A huge amount of CO_2 will dissolve in the formation water (brine) phase on a long time scale. Suppose the distance from the injection site to the end of the overlying impermeable formation is hundreds of kilometers. In that case, millions of years are needed for fluid to reach the surface from the deep basin (Metz et al., 2005).

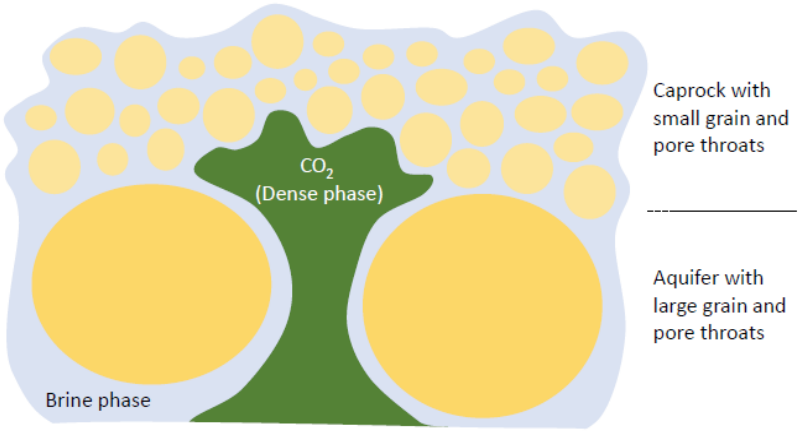

Figure 2.4 Sketch of capillary trapping of a CO_2 phase in super-critical (dense) phase in a completely water-wet porous medium. Due to smaller pore throats of caprock with small grains compared to larger pore throats in the aquifer, the gas column will rise quite slightly (Ringrose, 2020).

Physical trapping: residual trapping

As CO_2 plume is formed and migrates upwards due to gravitational forces, a trail of residual gas/liquid is left behind the plume due to pore-scale trapping of CO_2. The significance of residual trapping contribution is dependent on pore throat size, interfacial tension, and wettability. Two important processes control the retainment of CO_2 as residual phase; the pore-scale behavior that is typically measured after drainage and imbibition flooding cycles, giving relative permeability curves where residual CO_2 saturation and irreducible water saturation can be estimated; the rock heterogeneity and plume dynamics that are observable better when using dynamic flow simulations (Figure 2.5). Despite the general premise of CO_2 behaving as the non-wetting phase in sandstone reservoirs, some circumstances exist, particularly in carbonate and clay mineral surfaces, wherein CO_2 somewhat becomes a wetting phase. Fluid distributions of CO_2 and water within the pore space differ for drainage, where CO_2 as a non-wetting phase displaces brine as a wetting phase, and imbibition, where brine as the wetting phase displaces CO_2 as the non-wetting phase. The residual saturation of the non-wetting phase is usually large during the imbibition cycle (20-30%), which means a large quantity of CO_2 will be trapped and immobile in the pores, leading to a more secure storage operation. CO_2-brine relative permeability curves that indicate the drainage and imbibition flooding cycles are used for estimating the residual CO_2 saturation, but since it is highly dependent on the rock heterogeneity and fluid dynamics on a large scale, a more valid quantity of residual CO_2 trapping is computed using dynamic flow simulations, and sometimes analytical approaches can also be utilized. However, precise measurement of residual CO_2 trapping is still in development and an active field of research (Ringrose, 2020).

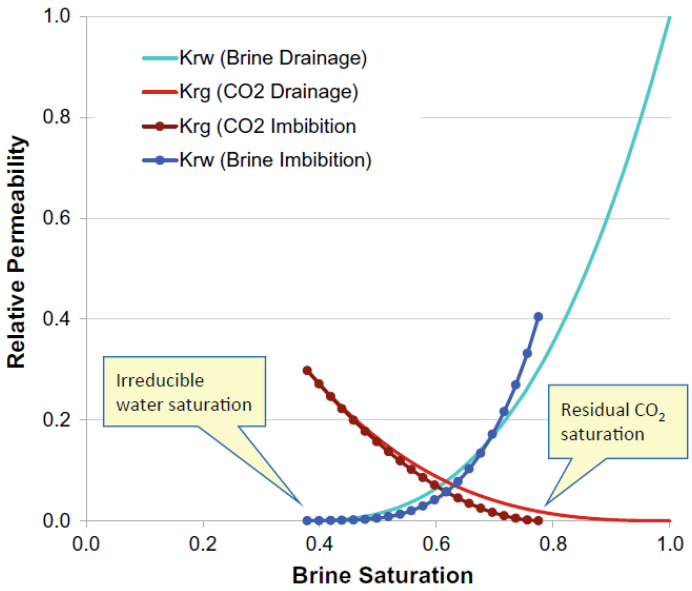

Figure 2.5 CO_2-brine relative permeability curves with interfacial tension as 56.2 mN/m. The drainage of brine by CO_2 shows irreducible water saturation as 40% and imbibition of brine into CO_2 phase shows residual CO_2 saturation as 22% (Bennion & Bachu, 2006).

Geochemical trapping: dissolution

A free phase CO_2 plume with a lower density than the *in situ* formation water spreads horizontally along the formation, beneath the caprock. Due to the continuous CO_2-brine interface over the formation, a significant portion of CO_2 can dissolve into the brine over a long period. The process known as *dissolution trapping* is the most crucial geochemical reaction for safe CO_2 storage and can play a vital role in stabilizing a long-term CO_2 storage project. Dissolution of CO_2 in formation water is represented by the chemical reaction:

$$CO_2\,(g) + H_2O \leftrightarrow H_2CO_3 \leftrightarrow HCO_3^- + H^+ \leftrightarrow CO_3^{-2} + 2H^+$$

When dissolution starts, the free CO_2 phase decreases in volume and pressure because the CO_2-rich brine phase is formed with a much higher viscosity than a free phase CO_2 and 1-2% denser than the *in situ* brine, which is willing to sink towards the bottom of the formation instead of migrating upwards and filling the top of the formation. CO_2 dissolution is initially controlled by molecular diffusion from the CO_2-brine interface, a slow process with mass flux evolving proportional to $t^{-1/2}$, t being time (Niemi et al., 2017). Over time, more CO_2 is dissolved into the brine; thus, a diffusive boundary layer is formed on top of the formation, and when a specific thickness of diffusive boundary layer and gravitational instability is achieved, a process called *convection* happens, wherein the CO_2 saturated brine that is slightly heavier (denser) than its surrounding brine sinks downwards and will be displaced by less dense brine (Figure 2.6). This stirring effect will cause CO_2 to be in contact with more undersaturated brine, and therefore, it is a faster dissolution process compared to molecular diffusion. The critical time (t_c) for convection to happen can take from 10 days to 2000 years, and the characteristic wavelength (λ_c) would be in the range of 0.3 m to 200 m based on the *in situ* fluid conditions and geological conditions it can be estimated how fast this process proceeds (Riaz et al., 2006). The solubility of CO_2 in brine increases with decreasing pressure, increasing temperature and salinity, where 20-60 kgCO_2 can dissolve in 1 m^3 of formation fluid. (Holt et al., 1995).

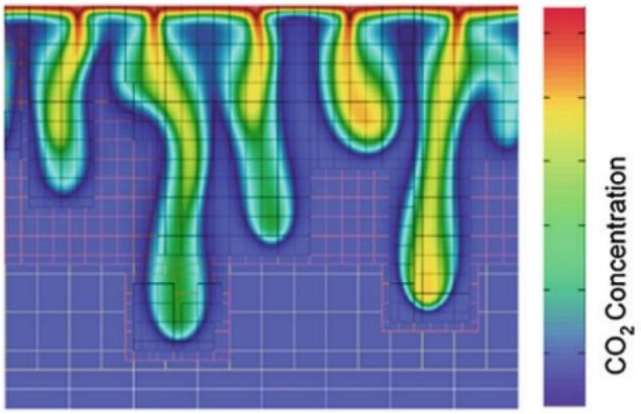

Figure 2.6 Sketch of the CO_2 sequestration process in a simple geometry. A free CO_2 phase accumulates along the impermeable top boundary. It slowly dissolves into the underlying brine, forming a heavier boundary layer. The resulting gravitational instability leads to convection (Ringrose, 2020).

Geochemical trapping: mineralization

Dissolution of CO_2 in the aqueous phase produces a weak acid that can react with chemical elements such as the sodium, calcium, magnesium, iron carbonate, potassium basic silicate, and silicate minerals in the reservoir to form bicarbonate ions by the following chemical reaction:

$$3\,K-feldspar + 2H_2O + 2CO_2 \leftrightarrow Muscovite + 6\,Quartz + 2K^+ + 2HCO_3^-$$

Carbonate minerals form after continuous reaction of bicarbonate ions with silicate minerals such as clays, chlorites, micas, feldspars, and also other chemical elements such as calcium, magnesium, and iron present in the formation; however, the rates of reaction are pretty slow and could take hundreds to thousands of years for the injected CO_2 precipitate as a result of reaction with carbonate minerals. Generally, mineralization is the most effective trapping mechanism in terms of safety, however, it could take thousands of years for possible chemical reactions and eventually form carbonate minerals.

Storage safety

When the injection operation begins, different types of trapping mechanisms start to contribute to retaining the CO_2 in the subsurface. Over time the safety of the storage increases if any leakage does not occur during injection and post-injection. Despite all the debates and discussions about the actual contribution of each trapping mechanism at different time scales, a general principle is accepted by everyone involved in this field. Figure 2.7 indicates how the contribution of different trapping mechanisms will be over 10,000 years. Structural and stratigraphical trapping will be the dominant contributor in the first ten years due to a high-quality sealing unit on top of the injection formation. Residual trapping is expected to progressively contribute after 10-100 years, while dissolution trapping is relatively less effective during the first 100 years, with more contribution afterward. Eventually, mineralization will appear after 100 years with little contribution, but more contribution after 1,000 years. The contribution of all physical and chemical trapping mechanisms is vital to assure having safe storage.

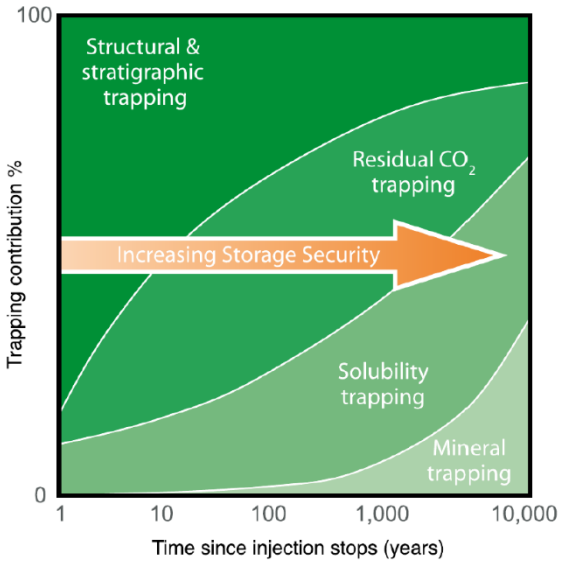

Figure 2.7 Projected contribution of different trapping mechanisms over 10,000 years (Metz et al., 2005).

As explained before, all of the trapping mechanisms will have a contribution to immobilize the injected CO_2 under physical or chemical processes and thus increase the safety of the CO_2 sequestration. Figure 2.8 is a perfect indicator of the contribution of all trapping mechanisms during and after the injection operation.

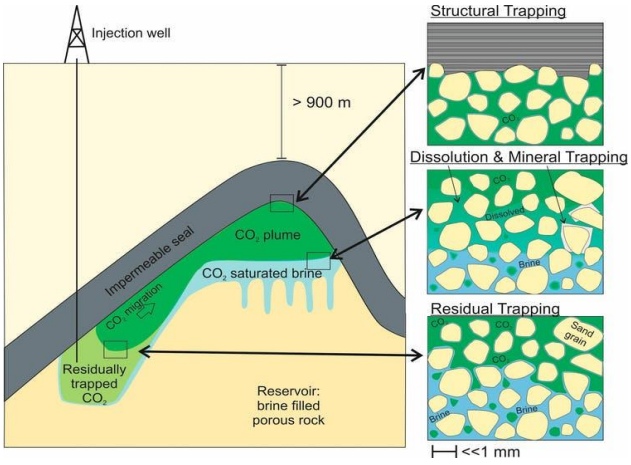

Figure 2.8 Sketch showing different trapping mechanisms retaining CO_2 underground, physically and geochemically (Flude & Alcade, 2021).

2.4 CO_2 properties

CO_2 is a thermodynamically stable gas, heavier than air, with the density of 1.87 kg/m^3 at atmospheric condition, and it is pretty compressible. However, as shown in Figure 2.9, at deep saline aquifer reservoirs, where the pressure and temperature are high, CO_2 forms a liquid phase, and after a certain pressure and temperature (critical point at T = 30.98 ˚C, P = 73.8 bara), it forms a super-critical phase with a density that can range from 150 to more than 800 kg/m^3 (Bachu, 2002). As mentioned previously, CO_2 being in a dense phase, either liquid or super-critical, is more effective than the gaseous phase of CO_2 as it consumes much less volume, which allows the operators to inject more CO_2 into the formation. Thus, the CO_2 is first compressed to form a liquid after the capture process, transported to the wellhead facilities, and is typically injected in the reservoir in liquid form. Eventually, due to the high pressure-temperature at reservoir conditions, CO_2 becomes super-critical and possibly stays in the same

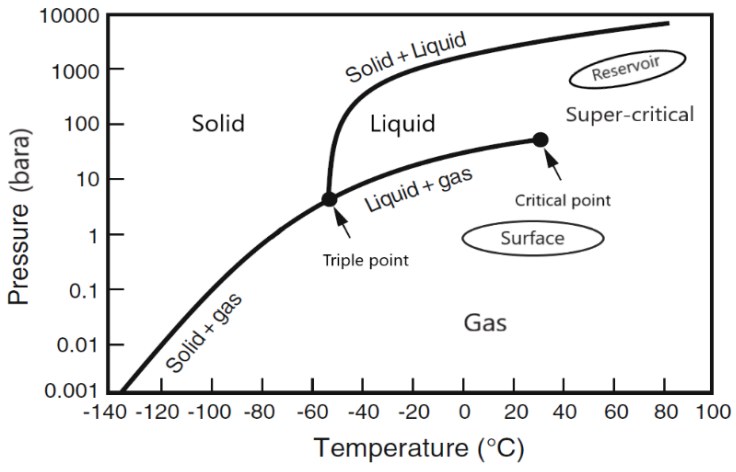

Figure 2.9 CO_2 pressure- temperature phase diagram (Modified from Niemi et al. 2017).

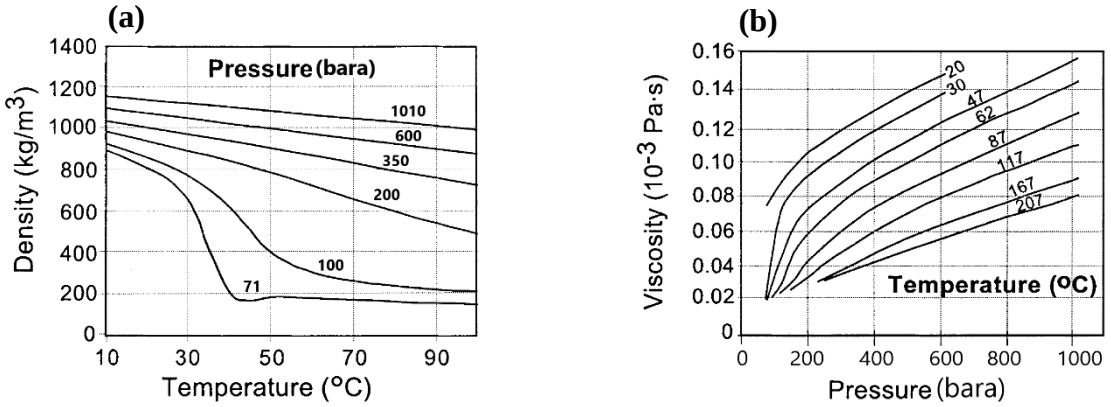

Figure 2.10 (a) liquid and super-critical CO_2 density-pressure and temperature relationship **(b)** liquid and super-critical CO_2 viscosity-pressure and temperature relationship (Modified from Bachu 2002).

phase in the reservoir. The porous medium is initially saturated 100% with brine and usually has a salinity range between 10 – 100 g /L (Niemi et al., 2017).

The fluid phase at each point (x) and each instant of time (t) have the density of $\rho=\rho(x,t)$ as a state variable that mainly depends on two other state variables pressure (p) and temperature (T). To describe the relationship among the state variables and properties of each of the CO_2-brine phases under a given set of physical conditions, such as pressure, volume, and temperature (PVT), *Equation of State* (EoS) is utilized as a thermodynamical equation. According to Gibbs phase rule, the number of degrees of freedom for a two-phase fluid system such as CO_2 injection in saline aquifers is two, where two phases exist in the system, one as the *in situ* brine phase and the other as the CO_2 phase, and the number of components is two. Gibbs phase rule for this type of system is shown by:

$$F = C - P + 2 = 2 - 2 + 2 = 2 \qquad 2.2$$

Where F is the number of degrees of freedom, C is the number of components, and P is the number of phases. Two degrees of freedom means that with having two state variables such as pressure, temperature, composition, the third state variable such as density can be yielded, meaning a multiphase system can be defined. The state of aggregation of CO_2 as a function of two variables of state, pressure, and temperature, is shown in Figure 2.9. Depending on the pressure and temperature, the CO_2 phase can exist in solid, liquid, or gas form or co-exist as a two-phase system. In addition, two specific conditions can happen; one is the triple point that three phases co-exist at a specific pressure and temperature, the second is the critical point wherein there's a smooth transition between the gaseous and liquid phase. Above the critical point, CO_2 can exist in the super-critical phase, which is the expected phase at deep saline aquifer conditions since the pressure and temperature usually exceed the critical point. The

diagram (a) in Figure 2.10 indicates that at a specific pressure, increasing the temperature decreases the density, and increasing the pressure also increases the density. Since density is known as the mass per unit volume of a substance, increasing pressure will decrease the volume of CO_2, thus increasing its density. Increasing temperature will expand CO_2 and occupy more volume, and therefore density decreases. Thus, density is directly related to the pressure and inversely related to the temperature. The diagram (b) in Figure 2.10 reveals that increasing pressure will increase the viscosity at a specific temperature, and the viscosity decreases as the temperature increases at a specific pressure. In gases, the viscosity increases with increasing temperature; however, when CO_2 is in the liquid or super-critical phase, the thermal energy of CO_2 increases, and molecules overcome the attractive forces binding them together easier. Plus, increasing pressure will bring the molecules significantly closer together, and as a result, viscosity increases. The state variables in an equation of state do not necessarily need to be density, pressure, and temperature, and other state variables can come into play to describe the state of matter. Specific volume as one of the state variables that can be used in the equation of state is defined as the volume per mass unit and is conversely proportional to density, i.e., $\upsilon = 1/\rho$. Figure 2.11 indicates $T=T(p,\upsilon)$, meaning the temperature at which a specific volume is found for a given pressure. Thus, it describes the state variable T as a function of two other state variables, υ, and p, in addition to the state of the fluid. The diagram shown below indicates not only the state of aggregation and the value of a third state variable, but it also indicates that at lower temperatures, the fluid consumes less storage volume per unit of storage mass. This is one of the primary reasons that CO_2 is preferred to be injected at lower temperatures; however, a high temperature difference between the formation and the injected fluid could cause damages in the formation and caprock, which is unwanted.

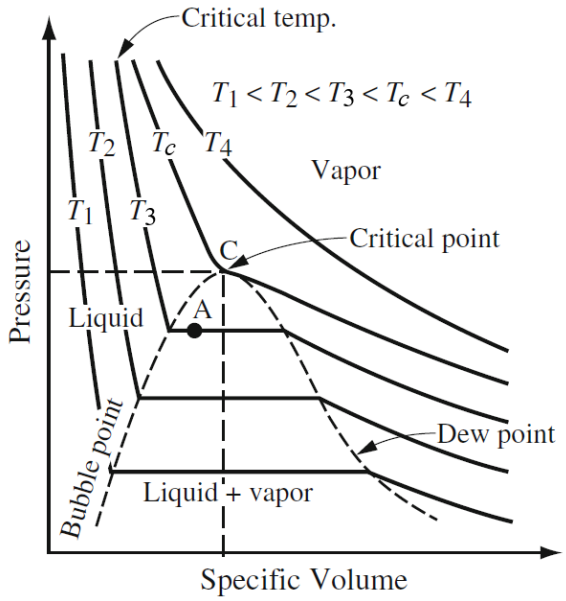

Figure 2.11 Temperature diagram as a function of specific volume and pressure (Niemi et al., 2017).

3 Reservoir simulations and modeling

Reservoir simulation is an approach of imitating the reservoir performance in the subsurface through using software to solve fluid flow equations numerically, including conservation of mass, momentum, and energy, along with equations of state to describe fluid phase behavior as a function of pressure and temperature (PVT). Since temperature changes are considered a weak parameter in terms of affecting rock and fluid properties, PVT data are collected under isothermal conditions. It is wise to note that thermal effects near the well-region area might be considerable in injection projects like CO_2 storage, causing fractures in the formation and caprock (Thompson et al., 2021). Reservoir simulations can handle fluid compositions differently; the black-oil model contains three (pseudo-) components: water, gas, and oil, which can exist in three phases: gaseous, oleic, and aqueous; the compositional model allows more multiple components to be added to a simulation, and composition variations of fluid phases are handled via the equation of state (EoS), making the simulation more computationally expensive than the black-oil model.

3.1 Modeling strategies employed for CO_2 storage

CO_2 storage projects require a considerable investment and a high-level evaluation of the risks associated with different sequestration scenarios. Researchers have developed several analytical and numerical CO_2 modeling methods to predict the CO_2 distribution and its behavior in the reservoir. Nordbotten et al. (2005) proposed an analytical solution to predict the plume migration growth in a CO_2 storage site. Zhou et al. (2008) developed an analytical solution to approximately measure the storage capacity in saline aquifers and the expected pressure build-up during storage operation. Mathias et al. (2009) proposed a solution to estimate the expected pressure elevation in aquifers with vertical equilibrium assumption and accounting for the Forchheimer flow of CO_2 and brine. Although these analytical solutions can help provide quick insights into the feasibility of a project, the assumptions in analytical models are too simplistic and thus not reliable for risk evaluation and/or final decision makings (Ajayi et al., 2019). Three different numerical modeling approaches have been applied for CO_2 storage; vertical equilibrium (VE) modeling, grid-based numerical modeling, and streamline simulation. In VE models, all layers are treated as one homogeneous/heterogeneous layer, and the discretization of the simulation will be performed only in the horizontal direction, leaving one layer in the

vertical direction. The model focuses on the large density difference between super-critical CO_2 and the *in situ* brine, leading to a strong vertical migration of CO_2 and neglecting the effect of viscous forces. The primary assumption is that the flow system is in vertical equilibrium, meaning the analytical expression can determine the vertical distribution of fluid phases. Since the VE modeling technique utilizes the 2D simulation, it is a relatively fast computation approach and can obtain beneficial insight into the CO_2 distribution laterally and the segregation between super-critical CO_2 and brine in the porous medium; nevertheless, it cannot model heterogeneity in the vertical direction. Streamline simulation splits the simulation domain into small grid blocks and models the pressure in each grid block using a finite difference technique. Since the flow equations are reduced to 1D equations along the streamlines, streamline simulation is a practical approach in terms of computation time as well as being suitable for processes where pressure changes are limited; however, it is limited by the assumption of incompressible flow, which is not the case in reality (Ajayi et al., 2019).

3.2 Numerical simulation over other modeling methods

The selection of which modeling method to apply for reservoir performance prediction relies on the kind of problem, available data, and the nature of research. The analytical and numerical modeling techniques introduced earlier can be used for CO_2 plume migration prediction; however, they are restricted to specified cases and cannot be generalized for all potential CO_2 storage sites. To overcome the shortcomings from other modeling techniques suggested, numerical reservoir simulations can be utilized with the possibility of CO_2 storage modeling to recommend optimal injection strategies, leading to both reducing the costs and possible risks linked with the CO_2 injection, wherewith the help of numerical mathematics, the simulation can mimic the physics of the rock/fluid inside the reservoir to observe the CO_2 distribution along the reservoir before injection operation, as well as optimizing the placement of the well(s) needed to be utilized for that purpose. One of the merits of applying numerical simulation with discretization techniques is their ability to incorporate all relevant physics such as heterogeneities and pressure elevation in both the vertical and horizontal directions and coupling important physical phenomena such as geochemistry, thermal changes, and geomechanics. Numerical simulation allows one to use finite difference, finite element, and finite volume approaches to solve the transport (conservation of mass) and flow (Darcy's law) equations with precise estimations. Companies, universities, and research institutes have developed different reservoir simulation software, allowing engineers to propose different scenarios and observe the results for short and long-term periods. Numerical reservoir

simulation can be computationally expensive and not accurate at the early stages of a project due to the uncertainty of collected data and factors such as heterogeneity, petrophysical properties, faults, and fluid behavior, which can significantly affect the pressure changes and fluid flow in the porous medium. However, multiple approaches exist to reduce the uncertainties over time, such as seismic surveys, core analysis, well logging, and well testing. As time goes by, models can be updated when further measurements and new data are collected. Later history matching can be a great aid to make the model give results as realistic as possible. The rock numerical models should be used to estimate reservoir performance and monitor fluid distribution with relatively accurate findings. As a result, reservoir simulation is one of the most critical aspects of governmental and operational decision-making. Moreover, numerical simulation is the only effective method of determining storage capacity before injection. (Ajayi et al., 2019).

3.3 Numerical two-phase CO_2 storage modeling

Analytical solutions for reservoir problems are only helpful when the reservoir is assumed to be simple in terms of geometry, petrophysical and fluid properties, and boundary conditions; however, they suffer to solve real reservoir problems where the rock and fluid properties vary at different parts of the reservoir. Therefore, for real reservoir cases, the equations need to be solved with numerical solutions that involve major steps to arrive from the general formulation at the solution. This process involves the following steps:

1. Discretization
2. Formulation
3. Linearization

Discretization

Numerical formulations do not search for a continuous solution, instead, they look for approximated values of the solution on a finite set of grid points at discrete time intervals. The simplest case of discretization is when the space and time of the system are broken into constant grid block sizes Δx and constant time-step sizes Δt. After dividing the continuous system into discrete distances and time levels, the numerical approximation of pressure and saturation of each phase can be obtained at each grid and time step. The grid blocks are assigned indices *i, j, k* in the Cartesian indexing grid and in natural ordering, where *i* index changes faster than *j*, *k* indices and *k* index changes slower than *i*, *j* indices. There exist two types of grids systems known as *block-centered* and *point-distributed* that are being used by the industry. In a *block-*

centered grid, the grid boundaries are associated with properties such as the flux into and out of the cells. The other properties such as pressure, saturation, porosity, and permeability are calculated in the grid cell centers (Figure 3.1). The block-centered grid systems are more adapted to the distribution of the reservoir properties such as porosity and permeability. Moreover, it is easier to calculate the pressure and saturation in the middle of a grid, making it more favorable than the point-distributed grid system. However, point-distributed grid systems have shown more consistency when using finite difference methods for models with varying grid sizes (Berg & Slotte, 2020).

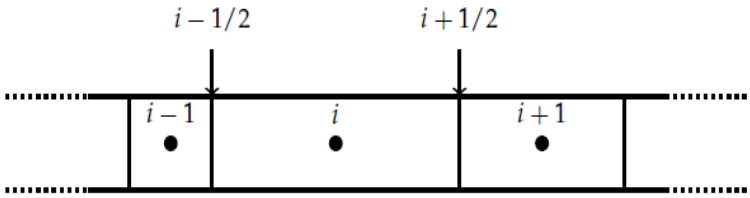

Figure 3.1 Block-center grid with grid boundaries and centers with different sizes (Berg & Slotte, 2020).

The most common grid type supported by most reservoir simulators and the most widely used gridding format is the *cornerpoint* gridding (Figure 3.2). Grid blocks follow Cartesian coordinates and are labeled using *i*, *j*, *k* scheme, with corners between four and eight. A grid cell with eight corners represents a complete square or rectangular grid cell, and a grid cell with four corners represents a vertically collapsed grid cell that does not contain a volume, meaning it consists of only a surface. Pillars are not usually vertical but rather normal to the layering due to better K-orthogonality (Berg & Slotte, 2020). With different grid blocks being in different depths along the pillar for the same logical corner, it could be understood that faults and non-reservoir gaps are represented in the reservoir model.

Figure 3.2 Cornerpoint gridding (From Sintef website). Each grid is constructed using the corners that are defined on pillars.

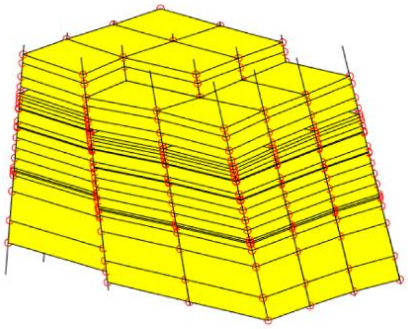

Formulation

The numerical formulation simulates the real physics of interactions between fluids inside the porous medium and the interaction between fluids and the reservoir rock. The process of solving the equations is simplified using numerical formulation where a set of partial differential equations, constraints, and initial and boundary conditions are presented. Numerical simulation of geological carbon storage, which is used to predict the fluid movement in the subsurface, is

based on the conservation of mass, as a mathematical representation of the fact that mass neither arises nor disappears, thus the difference between mass flowing into and out of an elementary volume (grid block in modeling) should be equal to the mass accumulation inside that elementary volume. After shrinking the elementary volume and time interval to their infinitesimal limits, the conservation of mass principle can be expressed in the form of a continuity equation, where two-phase immiscible flow is assumed without dissolution or evaporation of one phase into the other:

$$\frac{\partial(S_p \rho_p \phi)}{\partial t} + \nabla \cdot (\rho_p u_p) = \psi_p \qquad 3.1$$

The first term on the left-hand side of the equation indicates the *accumulation term* where S_p, ρ_p represent the saturation and density of each phase, respectively, with ϕ as the porosity of the reservoir rock. The second term represents the *flux term,* including the phase density and Darcy velocity, while ψ_p on the right-hand side represents the *source term*. Fluid flow in the porous media is related to the phase pressures using the extended Darcy's law for two-phase fluid system (known as momentum equation), which relates the fluid velocity of the non-wetting (CO_2) and wetting phase (brine) u_{nw} and u_w to the pressure gradient as well as two terms, permeability, and viscosity, representing the rock and the fluid, respectively:

$$u_{nw} = \frac{\bar{k} k_{rnw}}{\mu_{nw}} \nabla (P_{nw} + \rho_{nw} g z) \qquad 3.2$$

$$u_w = \frac{\bar{k} k_{rw}}{\mu_w} \nabla (P_w + \rho_w g z) \qquad 3.3$$

Where $\bar{k}$ is the absolute permeability tensor, k_{rnw} and k_{rw} are the relative permeabilities of each phase, μ_{nw} and μ_w are the phase viscosities. $\nabla(P)$ is the phase pressure gradient in the space *(x, y, z)*, and $\nabla(\rho g z)$ is the pressure gradient due to gravity, ρ_{nw} and ρ_w are the phase densities, *g* is the acceleration due to gravity, and *z* is the height above a datum. The relative permeability of a phase is defined as the ratio of the effective permeability over the absolute permeability $\bar{k}$ of the porous rock. In reality, relative permeability depends on different factors, including pressure, saturation, temperature, and composition of the phase, however in practice, they are assumed to be only functions of saturation, and the relationship between them denotes the hydraulic property of a porous medium (Liu et al., 2014). Relative permeability being only a function of saturation is a fair assumption as long as the saturation changes monotonically and

the rates are in a limited range (Berg & Slotte, 2020). In the presence of a two-phase fluid system in the reservoir, rock capillary forces will drive the flow towards an equilibrium where each phase has a different pressure, known as the phase pressure. Phase pressures are linked via capillary pressure, which is defined as the difference between the non-wetting pressure P_{nw} and wetting pressure P_w. Capillary pressure mainly depends on fluid properties, the structure of the reservoir rock, and wettability. Having a porous medium containing pores of different sizes, which is often the case, it is a fair approximation to express capillary pressure as an empirical function of saturation, where the relationship between capillary pressure and fluid saturation represents the static characteristic of the reservoir rock and can be experimentally measured against saturation (Liu et al., 2014).

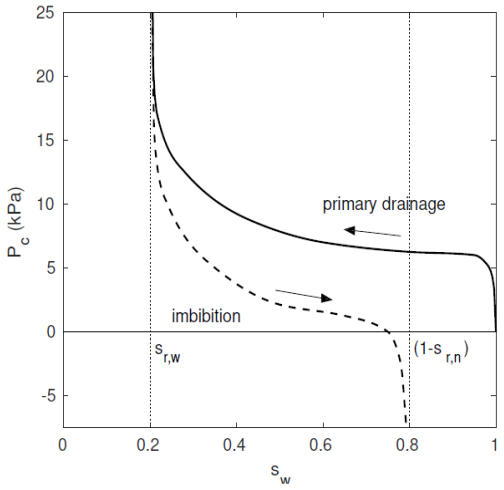

Figure 3.3 Capillary pressure during drainage and imbibition against saturation (Sketch by Odd Andersen).

$$P_c(S_p) = P_{nw} - P_w = P_{CO_2} - P_b \qquad 3.4$$

Figure 3.3 indicates that during the primary drainage, the super-critical CO_2 attempts to enter the system that is fully saturated with water ($S_w=1$); however, a specific amount of capillary pressure, here nearly 5 kPa, is needed for CO_2 to enter the porous medium and displace the *in situ* formation water. An essential point for the primary drainage curve is that when the irreducible water saturation ($S_{r,w}=0.2$) is reached, the capillary pressure goes to infinity while 20% of the water remains in the pores or cannot be displaced. Suppose the capillary pressure is assumed to be zero. In that case, the pressure of the non-wetting and wetting phase will be equal at each time step, meaning calculating one fluid pressure will lead to obtaining the other fluid pressure. Since k_{rn} , k_{rw} and P_c are all functions of phase saturation, these equations for two-phase immiscible flow are non-linear. After defining the initial and boundary conditions and inserting k_{rn} , k_{rw} and P_c as inputs to the simulation, four unknowns consisting of fluid pressures at each phase and fluid saturations at each phase are calculated iteratively. One constraint in the formulation is the summation of CO_2, and brine saturation that must be equal to 100% as the porous medium in the subsurface is always filled with fluids.

$$S_{CO_2} + S_b = 1 \tag{3.5}$$

As mentioned, the flow equation for each phase needs to be solved using partial differential equations in three dimensions. Using central differences for the spatial approximation and forward difference in time, the finite difference approximation of flow equation is:

$$\frac{u^t_{i+1,j,k} - 2u^t_{i,j,k} + u^t_{i-1,j,k}}{(\Delta x)^2} + \frac{u^t_{i1,j+1,k} - 2u^t_{i,j,k} + u^t_{i1,j-1,k}}{(\Delta y)^2} + \frac{u^t_{i1,j,k+1} - 2u^t_{i,j,k} + u^t_{i1,j,k-1}}{(\Delta z)^2} = \frac{u^{t+1}_{i,j,k} - u^t_{i,j,k}}{\Delta t} \tag{3.6}$$

Where superscripts *t+1* and *t* denote the next and current timesteps in simulation, respectively and subscripts *i*, *j*, *k* denote the coordinates of a 3D grid cell in the model. In addition, *Δx*, *Δy,* and *Δz* represent the length of the grid cell in three directions. Usually, two main approaches to deal with partial differential equations are known as *explicit* and *implicit*. If the left-hand side of Equation 3.6 is evaluated at the current time step *t*, the equation then can be solved *explicitly* for the solution $u^{t+1}_{i.j.k}$ as the only unknown in the equation, finding the solution and the next step *t+1* for all grid cells (*i*, *j*, *k)*. In contrast, if the left-hand side is evaluated at the next time step *t+1*, all the terms are unknown except $u^t_{i.j.k}$, meaning in the system needs to be solved simultaneously to find unknowns, meaning the system needs to be solved *implicitly*.

The implicit method has been proven to provide more stability for large time steps than the explicit method. The primary reason for the implicit method being stable is that when errors occur at a specific time step, it has the ability to approach the correct solution for the next time steps, while the explicit method suffers from having errors due to the reason that the error of a specific time starts to grow with time, meaning the solution will be more inaccurate as the simulation continues running. Three options are available (in ECLIPSE reservoir simulator) to solve the flow equations; fully-implicit, IMPES (IMplicit Pressure and Explicit Saturation), and AIM (Adaptive Implicit Method).

The fully-implicit method solves both the pressures and saturation unknowns implicitly. It evaluates the unknowns at the next time step, where it utilizes Newton's method to find the solutions after a few or several iterations. Although the fully-implicit method is associated with longer computation time and numerical dispersion when solving the equations, it is totally stable for large time steps. IMPES method firstly solves the pressures implicitly at the next time

step, and then the saturation is updated explicitly for the next time step. IMPES is potentially unstable; however, it does not suffer from numerical dispersion, and sometimes the simulation is faster using the IMPES method. The AIM method is a combination of fully-implicit and IMPES methods. It has the flexibility to utilize both methods depending on the difficulty of the region the simulator is trying to solve the equations.

In general, three main types of model method can be utilized for solving two-phase flow problems after discretization of the model, which is the following:

1. Two-phase finite-difference method (FDM)
2. Two-phase finite-element method (FEM)
3. Invasion Percolation method (IPM)

The finite difference method (FDM) is the most common class of numerical techniques to replace the non-linear, analytical partial differential equations by finite difference quotients and solving the resulting algebraic system where the pressure and saturation are functions of space and time, the spatial domain and time interval are broken into grid blocks and time-steps, respectively, then the flow equations can be solved numerically for each time step. However, there are some limitations to FDMs, especially such as lack of grid geometry flexibility, while FEMs are more computationally expensive, yet allow high flexibility in terms of grid geometry since grid meshes are defined by nodes at each corner of the grid cell, which will make the grid cells able to deform with time. IPM is another approach of modeling when capillary/gravity force is assumed to dominate the physical process of CO_2 flow dynamics, and the Darcy equation, which is representative of viscous forces is neglected. FEM is not an option for general flow simulation and is being used when the reservoir model needs to be tested in geochemical or geomechanical problems. IPM method is only suitable for modeling long-term CO_2 plume growth far from the near-wellbore region, where gravitational and capillary forces dominate the fluid flow (Ringrose, 2020). FDMs are generally the most efficient method in terms of computation with robustness in terms of accuracy and ease of obtaining a solution (Schlumberger, 2020).

Linearization

Each non-linear equation needs to be solved by a linear system of equations, which consumes the most significant computation time in the simulations. One of the powerful and accurate methods to solve non-linear iterations is the Newton method, where the simulation linearizes the equations, solve them and check if the linear solution gives a satisfying non-linear solution;

if yes, it moves to the next time step; otherwise, it goes back to linearize the equation again to find the best solution. The Newton method attempts to determine the root of a continuous function of all variables in a reservoir model as precisely as possible. For the sake of simplicity, only one variable is used to illustrate the method, to evaluate the value of for which $f(x) \simeq 0$. The algorithm starts with an initial guess x_0, leading to the tangent line of $f(x)$ at that point, which crosses the x-axis to find a new point x_1:

$$x_1 = x_0 + \frac{f(x_0)}{f'(x_0)} \tag{3.7}$$

If the magnitude of $f(x_1)$ is less than $f(x_0)$ the solution is improved and closer to the root function. This procedure is repeated until a point that is sufficiently close to zero is reached, where *convergence* occurs. The size of f(x) is called *residual*, and when it is sufficiently small, the solution is said to converge; however, it is crucial to understand when the solution is 'good' enough. ECLIPSE 100 (E100) and ECLIPSE 300 (E300) have different convergence approaches, where the former utilizes the residual method, and the latter utilizes the solution change method (Figure 3.4). The main reason for having different approaches is the inclusion of flash calculations in E300 when calculating the residuals, which is computationally expensive. In E100, the residual for each phase for each grid cell is calculated, and then, the largest of these values is compared with its default value. In E300, each component's pressure and molar density are the solution variables. After finding the maximum change for each of these variables over cells, it is directly compared to its target, and the component molar density changes are converted to effective saturation changes.

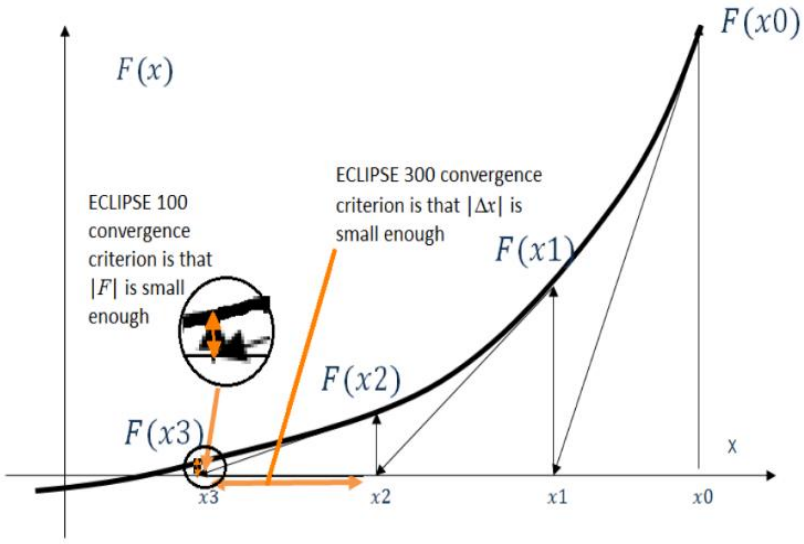

Figure 3.4 Solving a non-linear problem using two approaches for ECLIPSE 100 and ECLIPSE 300 (Schlumberger, 2020).

3.4 ECLIPSE Schlumberger reservoir simulator

ECLIPSE Schlumberger is a hydrocarbon reservoir simulator software that offers a comprehensive and up-to-date set of methods for accurate numerical solutions of reservoir flow equations to predict the dynamic characteristics of all types of reservoirs, along with development planning and operations. This software can be used for various purposes, including chemical enhanced oil recovery, waterflooding, and heavy oil recovery. It covers all types of simulations, including the black-oil, compositional, thermal, vertical equilibrium, and streamline simulations. This project utilized the black-oil and compositional simulators for CO_2 storage simulation.

ECLIPSE simulator compromises two main stages: an initial stage, where the reservoir and fluid data of the reservoir is read and processed at an initial date, and an actual simulation stage, where time is advanced from the initial date in a set of timesteps, and the reservoir condition in terms of pressure and saturation is calculated at each timestep based on the calculations from the previous time step. An ECLIPSE data file comprises eight sections, consisting of five required and three optional sections (Table 3.1). SCHEDULE is the simulation controlling section, where timesteps and well specifications are defined, while other sections (RUNSPEC, GRID, EDIT, PROPS, REGIONS, SOLUTION, SUMMARY) provide the data for initialization, such as rock and fluid properties and in general request for the simulation output. These sections need to come in the prescribed order; however, the keywords in each section should not necessarily be sequential. The simulator will automatically organize the simulation and run the DATA file.

Table 3.1 The Data section needed to be defined in ECLIPSE DATA file to run the simulation.

Section	Function
RUNSPEC	The overall setting of the simulation; title, unit system, phases present, start date, simulation grid dimension
GRID	Grid dimensions and shape, porosity, permeability, fault
EDIT (Optional)	Change grid structure defined in GRID section
PROPS	Fluid and rock properties; PVT data, relative permeability
REGIONS (Optional)	Define sub-regions of the reservoir
SOLUTION	Equilibration data and initialization of the model
SUMMARY (Optional)	Define what needs to be saved from the simulation
SCHEDULE	Well definitions, description of operating schedule, time step reports

Black-oil simulator: ECLIPSE 100

ECLIPSE 100, also known as E100, is a black-oil simulator that can contain one, two, or three-phase systems, where a two-phase system of gas-oil including gas dissolving in oil (DISGAS keyword) was used in the CO_2 storage simulation, gas representing the CO_2 and oil representing the brine as well as the option of CO_2 dissolution in brine phase. The oil phase represents the brine because gas is assumed to be soluble in oil but not usually in water. In E100, the method to simultaneously solve equations for pressure and saturation is fully implicit since it provides high stability over time is able to reduce the residuals to values close to zero, leading to low material balance errors.

The fully-implicit method in the black-oil simulator uses Newton-Raphson's (mostly known as Newton's) method to solve non-linear equations. The Jacobian matrix is fully expanded in all variables to ensure fast convergence. The linear equations arising at each Newton iteration are solved simultaneously by Nested Factorization accelerated by Orthomim as a fast iterative technique devised for the solution of large sets of sparse linear equations and can keep the material balance at each iteration accurately (Schlumberger, 2020). The E100 black-oil simulator utilizes PVT relations to assign the variation of physical properties such as density, viscosity, and compressibility depending on temperature and pressure.

PVT tables contain data that can relate the surface and reservoir conditions, with properties such as formation volume factors and the solution gas/oil ratio (the ratio of dissolved gas in water in our case). It is worth noting that PVT relations are obtained either from laboratory experiments, a matched equation of state, or correlations with the assumption of no compositional changes with temperature and pressure. The density of different phases as one of the important physical properties in the reservoir is supplied to the ECLIPSE simulator at standard condition values (pressure of 1 bar, temperature of 15˚C). The surface condition then is converted to reservoir conditions using formation volume factors, as the ratio of a unit volume of fluid at reservoir conditions to the volume of the same amount of fluid occupies at standard conditions:

$$B_p = \frac{V_{p,RC}}{V_{p,SC}} \tag{3.8}$$

Where B_p denotes the formation volume factor of the phase, $V_{p.RC}$ and $V_{p.\ SC}$ represent the phase volumes at reservoir conditions (Rm^3) and standard conditions (Sm^3), respectively. The solution gas-oil ratio R_s (dissolution of CO_2 in water) is defined as the gas volume measured at standard

conditions that can be dissolved in one standard conditions unit volume of oil (water in our case) if both fluids are taken to the reservoir conditions. Having density values at surface conditions, formation volume factors, and solution gas-oil ratio values at different pressures, it is possible to determine the fluid density of different phases at reservoir conditions:

$$\rho_{g,RC} = \frac{\rho_{g,SC}}{B_g} \tag{3.9}$$

$$\rho_{o,RC} = \frac{\rho_{o,SC} + \rho_{g,SC} R_s}{B_o} \tag{3.10}$$

Compositional simulator: ECLIPSE 300

The compositional simulation in ECLIPSE, known as ECLIPSE 300, was initially developed for miscible gas injection plans in EOR projects, gas condensates, and volatile crude oil reservoirs. E300 is a multi-component simulator where more than three components can be defined. The PVT properties of oil and gas phases are fitted to a cubic equation of state or pressure-dependent K-values and black-oil modeling. The standard cubic equations of state used in the compositional simulation are Redlich-Kwong, Soave-Redlich-Kwong, Peng-Robinson, and Zudkevitch-Joffe (Schlumberger, 2020). E300 utilizes the procedure of Adaptive IMplicit (AIM) as a compromise between IMPES and fully implicit methods, which allows grid cells in complex regions to remain fully implicit while employing the advantage of an IMPES description in easy regions. Since compositional simulation is usually computationally expensive, especially for large models, using only a fully implicit method can be quite prohibitive in CPU time and memory, especially for local computers.

Several options have been provided in E300 in recent years, specifically for CO_2 storage studies under different conditions; study CO_2 storage in hydrocarbon reservoirs (CO2SOL), coal bed methane reservoirs (COAL), and saline aquifer reservoirs (CO2STORE). Since saline aquifers have been proven to provide the largest storage sites for CO_2 storage, the CO2STORE module was made available in E300 for CO_2-brine systems (H_2O containing salt). In this module, three phases are considered, a CO_2-rich phase, a H_2O-rich phase, and a solid phase to represent the salinity of water. To calculate the phase equilibrium and the mutual solubilities of CO_2 and H_2O, a procedure was given by Spycher and Pruess to match the experimental data for CO_2-H_2O systems from 12 to 100 ˚C and up to 600 bar, which are relevant to geological CO_2 storage

conditions (Spycher & Pruess, 2005, 2010). Two main reactions express the equilibrium between CO_2 and H_2O:

$$H_2O_{(l)} \Leftrightarrow H_2O_{(g)} \qquad K_{H_2O} = f_{H_2O(g)}/a_{H_2O(l)} \qquad 3.11$$

$$CO_{2_{(aq)}} \Leftrightarrow CO_{2_{(g)}} \qquad K_{CO_{2_{(g)}}} = f_{CO_2(g)}/a_{CO_2(aq)} \qquad 3.12$$

K is the equilibrium constant defined as fugacity *f* ratio for gaseous H_2O and CO_2 to activities (*a*) for liquid water and aqueous CO_2. The subscript *g* refers to the CO_2-rich phase, either gas, liquid, or super-critical phase. Activity is defined as the following:

$$\text{On a molality scale} \quad a_i = \gamma_i m_i \qquad 3.13$$

$$\text{On a mole-fraction scale} \quad a_i = \gamma_i x_i \qquad 3.14$$

i represents the component in the mixture, in this case, CO_2 or H_2O, *m* designates the molality, and *x* and *y* indicate the mole fractions in the aqueous and compressed gas, respectively. For the departure from ideality, including concentration effects, γ as the activity coefficient for aqueous components and liquid water were included in the activity. The fugacity in the gaseous phase is defined as:

$$f_i = \Phi_i p_i = \Phi_i y_i P \qquad 3.15$$

Where Φ is the fugacity coefficient for gaseous components, *p* is the partial pressure of the gaseous phase, and *P* is the total pressure. Equilibrium constants are expressed using fugacity values defined with respect to a reference state fugacity of 1 bar, with activity values defined on a mole fraction scale (water) and a molality scale for aqueous CO_2. Margules expressions measure the activity coefficient of CO_2 and H_2O. In cases with temperatures less than 100 ˚C, A_M , which represents a Margules parameter is zero, meaning both γ_{H_2O} and γ_{CO_2} will be equal to one.

$$ln(\gamma_{H_2O}) = (A_M - 2A_M\, x_{H_2O}){x_{CO_2}}^2 \qquad 3.16$$

$$ln(\gamma_{CO_2}) = 2A_M\, x_{CO_2}{x_{H_2O}}^2 \qquad 3.17$$

The water mole fraction in the CO_2 rich phase (y_{H_2O}) and the CO_2 mole fractions in the aqueous phase (x_{CO_2}) are expressed as:

$$y_{H_2O} = \frac{K^0_{H_2O}\gamma_{H_2O}}{\Phi_{H_2O}P_t} exp\left(\frac{(P - P^0)\overline{V}_{H_2O}}{RT}\right) \quad 3.18$$

$$x_{CO_2} = \frac{\Phi_{CO_2}P_t\left(1 - y_{H_2O}\right)}{55{,}508\,\gamma'_x K_{CO_2}} exp\left(-\frac{(P - P^0)\overline{V}_{CO_2}}{RT}\right) \quad 3.19$$

$\overline{V}$ is the average molar volume, γ'_x is the ratio of the mole fraction of CO_2 dissolved in water divided by the mole fraction dissolved in brine. The subscript *t* and superscript *0* refer to the total and reference value, respectively. A tuned cubic equation measures the gas density to give the most accurate compressed gas-phase density. A modified version of Redlich-Kwong cubic equation of state is utilized, with attraction parameters being temperature-dependent:

$$P = \left(\frac{RT_K}{V - b_{mix}}\right) - \left(\frac{a_{mix}}{T_K^{0,5}V(V + b_{mix})}\right) \quad 3.20$$

Where P is the pressure, R is the universal gas constant, T_K is the temperature in Kelvin, V is the molar volume and a_{mix} and b_{mix} are the measures of intermolecular attraction and repulsion, respectively. More information about the procedure can be obtained by referring to Spycher Pruess (2005, 2010). The brine density calculated in the CO2STORE module is based on an analytical form of the water density proposed by *The International Association for the Properties of Water and Steam* (Schlumberger, 2020).

3.5 Petrel E&P software by Schlumberger

Petrel is a software platform that has been utilized for the exploration and production of the oil and gas industry with several options available for geological and geophysical interpretation, fault analysis, well design, creating the reservoir models, designing development strategies for reservoir optimization, and visualizing the dynamic reservoir simulation results. Due to its collaborative workflow, it helps geophysics, geology, and reservoir engineer groups to integrate operations to maximize reservoir performance. Making the users able to import several simulation cases, specifically for comparisons and saving time, are only some of the advantages of this platform. In addition, Petrel has several visualization options such as a high-quality 2D and 3D view of the model, intersection view, single or multiple curves plotting for observing the changes of different properties, and histogram Figures to observe the distribution of properties in the reservoir.

Petrel is utilized as the post-processing tool for the reservoir simulations in this project, and different visualization tools were included. To observe the CO_2 plume migration when reaching the top of the reservoir after some years, a 2D view was used for different simulation cases for comparison purposes. Observing more details that would have been lost by looking at them in a 2D view was achieved using 3D visualization, wherein each segment of the reservoir can be examined with details for more accurate comparisons.

Since injected CO_2 tends to migrate up when entering the formation, particularly away from the injection area, the ideal tool for observing the dominance of gravity force and the extension of the CO_2 plume is the intersectional view, which is available in Petrel as a valuable tool for that purpose. The Petrel charting window was used to monitor pressure variations in the reservoir and the amount of free or dissolved CO_2 over a long period. Although other software packages may offer various visualization options, Petrel is the most comprehensive software platform, providing all visualization types that can be used and customized.

3.6 Simulations of Johansen Formation

In simulation studies of a specific model, it is always better to investigate and learn from previous works since models are evaluated from different reservoir engineering aspects, especially for formations where the injection/production operation has not started yet. Over the years of evaluating a project, new seismic surveys and wells help modify the models with more accurate data, leading to more realistic results. Uncertainty or lack of data on porosity and permeability measurements, PVT and saturation tables, state of faults regarding acting as sealing units or conduits, pore volume estimation, and many other important factors can lead to misleading, unrealistic simulation results which can lead to failure of a project economically and environmentally. In this section, some of the most important studies on the Johansen Formation as the main reservoir unit of the Aurora storage site that has been done by geology and reservoir engineering groups have been sorted and explained briefly with the focus of each study and conclusion points.

To evaluate the feasibility of using the Johansen Formation as a possible CO_2 storage site, several simulations, including different scenarios and sensitivities, have been reported by geology and reservoir engineering groups during the last fifteen years. The model used for CO_2 storage simulations of the Johansen Formation is based on mapping the existing high-quality 3D seismic data in the Troll Field area and a 2D seismic grid with good quality from the 1990s south of the field in the current Aurora License. In addition, log data from 12 exploration wells

in the Troll Field and some additional wells located in neighboring fields that have penetrated the Johansen Formation and core samples were also utilized to increase the quality of the model (Eigestad et al., 2009).

Bergmo et al. (2009) were one of the first groups working on the western part of the Johansen Formation model to evaluate the reservoir as a potential storage site for future utilizations. They used the ECLIPSE 100 black-oil simulator, using one vertical CO_2 injection well set to 3 Mt per year for 110 years. Two different simulation grids were built since two main simulation scenarios were proposed. The first scenario only represents the Johansen Formation having an aerial grid block size of 200 × 200 m with 18 layers varying from 2 to 50 m, where CO_2 plume distributes only within the formation due to being entirely sealed by overlying formations. Since the Johansen Formation model is confined and smaller than the mapped Johansen Formation, a numerical aquifer as the southern boundary with increasing the pore volume in the grid blocks was modeled. It was concluded that assuming the pore volume is more than 170 Gm^3, the increased formation pressure due to CO_2 injection is relatively lower than the fracture pressure, promising no cap rock failure. The second scenario represented all the formations from the Statfjord Formation below the Johansen Formation to the topmost Sognefjord Formation with an average areal size of 500 × 500 m with 16 layers, where CO_2 migration extends out of the Johansen Formation through faults, assuming non-zero fault transmissibility and vertical permeabilities in overlying formations. As a result of using four different fault transmissibility values, one case with no CO_2 dissolution and the last one with the Dunlin Group as the sealing unit, it was concluded that in the worst-case scenario without dissolution of CO_2 into the formation, CO_2 will reach the top layer, wherein the Troll Gas Field is producing from, after 150 years, while it can take more than 245 years in the other scenarios. They also concluded that dissolution of CO_2 will be more critical on a 1000 year scale, and the amount of CO_2 dissolved in the formation water depends on the magnitude of contact between these two fluids.

Eigestad et al. (2009) performed different simulations on the simplified model of the southern part of the Johansen Formation. They used ECLIPSE 100 for dynamic simulation, limiting the flow fluid simulation to two-phase immiscible flow, neglecting the effect of solubility of CO_2 in the native brine system. One vertical CO_2 injection well with the annual rate of 3.5 Mt for 110 years with 500 years of post-injection period to observe CO_2 saturation profile over a long time. A sector model with 100 × 100 × 11 grid cells, including five layers of the Johansen Formation, sealed by five layers of the Dunlin shale on top and overlaying one layer corresponding to the Amundsen shale. The geometry of the formation, together with

petrophysical, fluid data, has been published online to provide the opportunity for further research and studies on this model (Sintef, 2009). Different types of three different boundary conditions to compare the bottom hole pressure (BHP) for the proposed injection well. Additionally, they wanted to observe the CO_2 migration using various grid resolutions due to the highest possible impacts of coarsening grids on the CO_2 saturation distribution when accounting for relative permeability, capillary pressure, and PVT data. Lastly, they tested the impact of different relative permeability curves since the amount of residual trapped CO_2 in the simulation is strongly dependent on the residual CO_2 saturation. Their analysis concluded that the choice of lateral boundary condition, the extent of vertical grid refinement, and different relative permeability models would significantly change the spreading of CO_2 and simulation results.

In another study by Sundal et al. (2015), which was initiated by Eigestad et al., with adding new 3D seismic data that Gassnova acquired in 2010 to merge with older surveys covering the Troll Field, to add more scientific knowledge base for further steps in consideration of the Johansen Formation as a potential CO_2 storage site (Gassnova, 2012). In this study, the simulation was performed using the CO2STORE option in the compositional simulator ECLIPSE 300, including mutual solubilities of CO_2-brine and estimating the contribution of different trapping mechanisms with different model scenarios. Boundary grid cells were assigned a communicating pore volume multiplier of 10^4, ensuring pressure dissipation in the reservoir. One vertical CO_2 injection well through the lower part of the Johansen Formation, with the annual CO_2 injection rate of 3.2 Mt for 50 years were used. Two main scenarios were proposed in this study. In the regional model scenarios with grid numbers 78×130 ×170, two alternative down-slope and up-slope well placements were used and tested to compare with the base case model with grid size 250 × 250 m. The results indicated that the down-slope injection alternative led to the most immobilization of CO_2 in a 1000 year post-injection period. In the local model with grid numbers 112×121×170, thirteen different scenarios were proposed for 150 years, including low and high case porosity, directional permeability anisotropy on migration paths, various geological heterogeneities such as discrete layers of low-permeability mudstone, tight calcite cemented layers, grid orientation, using horizontal well and lastly omitting the Cook formation as the secondary reservoir unit. Four sets of relative permeability curves were used according to the facies to enhance preferential migration and bypass zones. Among all the scenarios, applying a base case using a horizontal well increased the immobilization fraction to 83%.

The last study was done by Lothe et al. (2019) to evaluate the four potential storage sites in the Horda CO_2 storage hub, including the Aurora site, and propose a possible roadmap for the future. The reservoir model used in this study was defined by Gassnova (2012) and Sundal et al. (2015), which covers an area of 475 km^2 from the southern part of the Troll Field. They used the ECLIPSE 100 black-oil simulator for their study with a model resolution of 250 × 250 m, with 120 vertical layers, including the Johansen and Cook formations. In this model, the full connected volume of the Johansen and Cook formations is modeled by using high pore volume multipliers on the northern boundary of the model, where the boundaries to the east, west, and south are closed. Based on a supply scenario where new sources will be added to the Longship Project, the simulation of CO_2 was done with gradually increasing rates and drilling a new vertical well each time the total annual rate exceeds the capacity of a single, which was assumed to be 3 Mt annually. Two different sensitivities were done in this study; one sensitivity was simulating and observing the CO_2 footprint using one, two, and six wells for an injection period of 27 years; the other sensitivity was run with the pore volume multipliers along the northern boundary of the model give a total pore volume of 280 and 50 Gm^3, assuming a large and small pore volume in connection with the Johansen and Cook formations, respectively. The simulation result of pore volume sensitivity showed that the smaller model volume impacts the injection rate of the wells and reduces the distribution of the CO_2 insignificantly.

4 Model setup

A benchmark study on CO_2 storage in the Johansen Formation was first done by Eigestad et al. (2009), using 2D seismic data and long distance well data interpolation to build the grid model available online for further studies (Eigestad et al., 2009). To confirm the previous studies on the Johansen Formation as a potential for CO_2 storage, new 3D seismic data were collected by Gassnova in 2010, followed by attribute analysis and property modeling of the seismic dataset (Gassnova, 2012). Based on these studies and data collection and additional mineralogical sampling and re-interpolation of wells, a revised model for the Johansen Formation was proposed by Sundal et al. (2015), which is the benchmark model of this study. The wells involved in creating the model, the stratigraphy of the reservoir and sealing units, petrophysical properties, fluid properties, and modifications on the default model to create a new base case model will be explained.

4.1 Database

The aim is to store CO_2 in the Johansen Formation, a sandy saline aquifer as the main reservoir unit, overlaid by an additional volume, the Cook Formation. 16 exploration wells have penetrated parts of the Johansen Formation in the Horda Platform, including the Smeaheia area, the Troll Field, and the Aurora site (study area). In addition, the Eos confirmation well was added in 2019 to confirm the feasibility of the Johansen Formation, which includes core and well log data but is not used for the model that was made before 2015. The information about the wells, such as well log measurements and cores taken, are available through Gassnova's interim report for Johansen Formation (https://ccsnorway.com/). The well data collected for the Eos confirmation well is also available through Equinor Open Data (https://data.equinor.com/).

Figure 4.1 indicates the Horda Platform area, including the giant Troll Field, the Smeaheia area, and the Aurora site with the Cook-Johansen formations as the saline aquifer reservoir. In addition, the outline of the velocity model used for depth conversion and 2D, 3D seismic data interpretation is shown by the yellow color. To achieve a consistent seismic database for seismic interpretation, inversion, and analysis, the 3D seismic surveys GN1001, NPD-TW-08-4D-TROLLCO2, and NH0701 were merged by processing from field data into a new seismic volume GN10M1. GN1001 is the last 3D seismic survey, which was collected in 2010 by

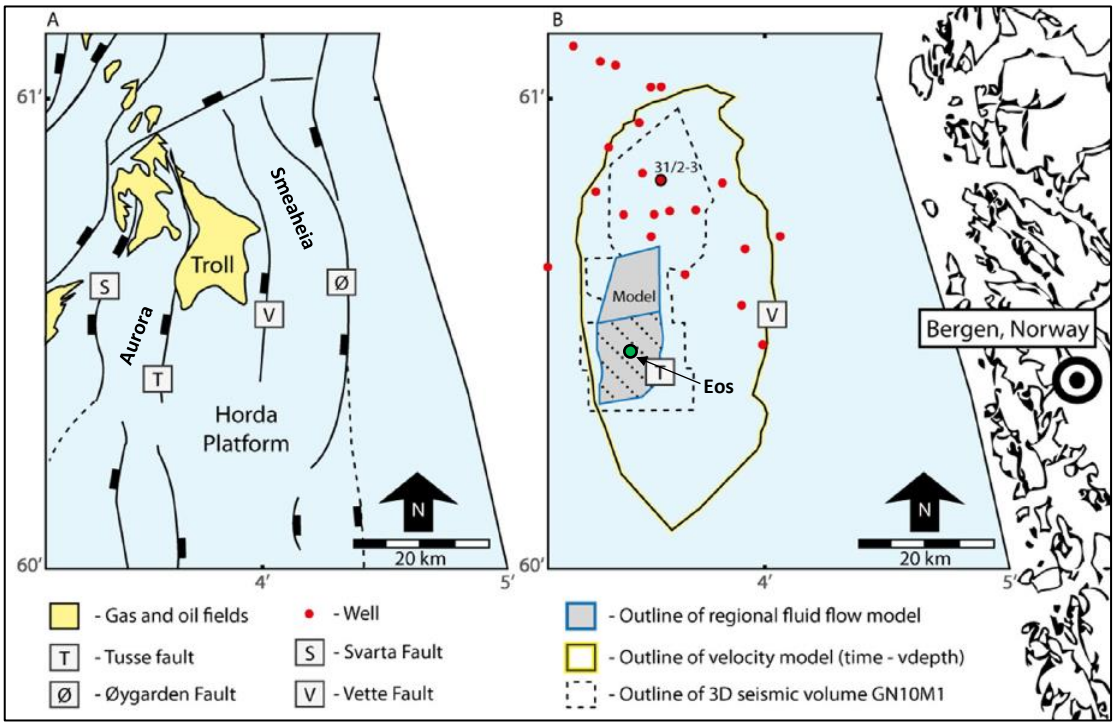

Figure 4.1 The study area, approximately 100 km West of Bergen (**A)** Structural setting of Horda Platform compromising Svarta, Tusse, Vette and Øygarden faults (**B)** Data coverage (Modified from Sundal et al. 2015).

Gassnova, mainly aiming at mapping the reservoir potential for CO_2 storage, covering from the top of the Draupne formation (second sealing unit) down to the Statfjord formation (below the reservoir unit) with excellent quality, where the rest are older surveys are covering the Troll Field. The reflection from seismic data can create an image of the subsurface, containing the reservoir, sealing units, faults, and other parameters by measuring the time (ms) that a seismic wave propagates down to an interface and reflects up to the receiver. Time depth conversion and formation thickness maps were generated using a velocity model, hiQbeR, utilizing sonic log data and providing low uncertainties in well-correlated areas (Sundal et al., 2015).

4.2 Stratigraphy

The Early Jurassic Johansen and Cook formations as parts of the geological layering Dunlin Group are deposited on the Horda Platform area. The Dunlin Group outlines a primary marine transgressive sequence overlying the Statfjord Group. including the Johansen, Amundsen, Cook, Burton, and Drake formations of the late Sinemurian – Toarcian age (Marjanac & Steel, 1997). The Johansen Formation consists of the fine-grained sandstones and siltstones, creating a large westward- and northward- prograding and wedging sandstone body represented as an extensive delta (Marjanac, 1995). The Lower Jurassic Johansen Formation sandstones depict shallow-marine deposits at the Horda Platform (Vollset & Doré, 1984).

Multiple interlayers of siltstone and mudstone with low porosity values are detected within the Johansen Formation associated with flooding events (Sundal et al., 2016). The observed siltstone/mudstone interlayers are witnessed laterally over a kilometer scale. Frequent calcite cemented sandstones (carbonate layers) have been recognized mainly less than one meter thick within the Johansen Formation (Sundal et al., 2015). The Johansen Formation has more than 2000 m depth with 116 m thickness confirmed by the Eos confirmation well. The Early Jurassic Cook Formation is dominated by sandstone tongues interfingering with the Drake mudstones at several distinct stratigraphic levels (NPD, 2014). The Cook Formation consists of clean sandstones with subordinate thin heterolithic intervals that also overlies stratigraphically above the Johansen Formation, which in some parts of the Horda Platform entirely lies on the Johansen Formation, and in some other parts, it is separated by the shaly Amundsen Formation (Lothe et al., 2019; Marjanac & Steel, 1997). The Eos well confirmed 57 m thickness for the Cook Formation. According to studies by Sundal et al. (2015, 2016), the Johansen Formation can be granted as a proper reservoir for CO_2 storage for various reasons. Based on the cores taken from the reservoir unit, The Johansen Formation is capable of high residual trapping, and the CO_2 plume is expected to develop effectively along the migration path due to the geological heterogeneities. Lastly, high porosity and permeability and ideal pressure and temperature conditions have caused the Johansen Formation to be a reservoir with tremendous potential for safe and efficient CO_2 storage.

The Amundsen Formation comprises laterally extended marine silts and mudstones deposited on a shallow marine shelf, separating the Johansen and Cook formations in parts of the northern Horda Platform (Lothe et al., 2019). The Burton Formation is essentially composed of marine mudstones, founded over most of the Dunlin Group. The Drake Formation with 128 m thickness confirmed by the Eos well acts as a primary sealing unit toward the underlying sandstone formations. This sealing unit is divided into the Lower Drake unit as the primary seal composed of mainly clays and the Upper Drake unit, with poorer sealing quality, mainly composed of siltstones. An overburden, serving as the secondary seal system, is composed of the Draupne Formation, Cromer Knoll, Shetland, and Rogaland groups and can act as a sealing barrier to the plume with a high degree of confidence. The Draupne Formation has served as a confining layer to many fields in the NCS, and its presence has been proven by the 31/5-7 (Eos) well. The integrated biochronostratigraphy and palaeoenvironmental summary from the Hordaland Group on top (900 m depth) to the Statfjord Group (2800 m depth) of the 31/5-7 (Eos) well as well as the formation tops of the Dunlin Group are included in Appendix C.

4.3 Petrophysical properties

To model the petrophysical features of the reservoir, i.e., porosity and permeability, the inversion of the GN10M1 3D seismic dataset was used. The seismic inversion is mainly aimed at the Dunlin Group and Cook-Johansen formations. One of the main objectives of the seismic inversion was to quantify the Acoustic Impedance (AI) as the product of the bulk rock density (ρ) and the compressional wave velocity (v), which is inversely related to porosity and can be used as a proxy for lithology prediction since velocity and rock density vary as a function of depth and petrophysical properties. (Rasmussen & Maver, 1996). Although correlating AI with total porosity (*PHIT*) is a standard procedure, effective porosity (*PHIE*) as a more relevant feature to flow properties were calculated using density-neutron model corrected for volume of clay (VCL). As shown in the cross-sectional view in Figure 4.3, The porosity is distributed within the Johansen Formation, lying in the range PHIE = 7.3-31.4% with corresponding acoustic impedance values of AI=6.1E-6 - 9.0E-6. Horizontal permeability was modeled as $K=1000(\ PHIE^{4.5}/S_w\ )$, with adjusting the water saturation as a calibration parameter to fit core measurements (Gassnova, 2012) (see Figure 4.4).

In addition, the permeability values of the Cook-Johansen formations measured from the wells 31/2-3, 30/3-2, and 30/3-4 were plotted against porosity to generate model functions. AI and PHIE were correlated using well logs, and AI-derived *PHIE* volumes with associated permeability assigned as a fitted function were used to populate the models. The vertical to horizontal permeability ratio was set to $K_V/K_H=0.1$ which is usually a fair assumption for sedimentary basins (Lothe et al., 2019). Porosity and permeability values are based on the wells far from the injection area; thus, they are not quite uncertain; however, they remained unchanged in this project until further evaluations on the Aurora model.

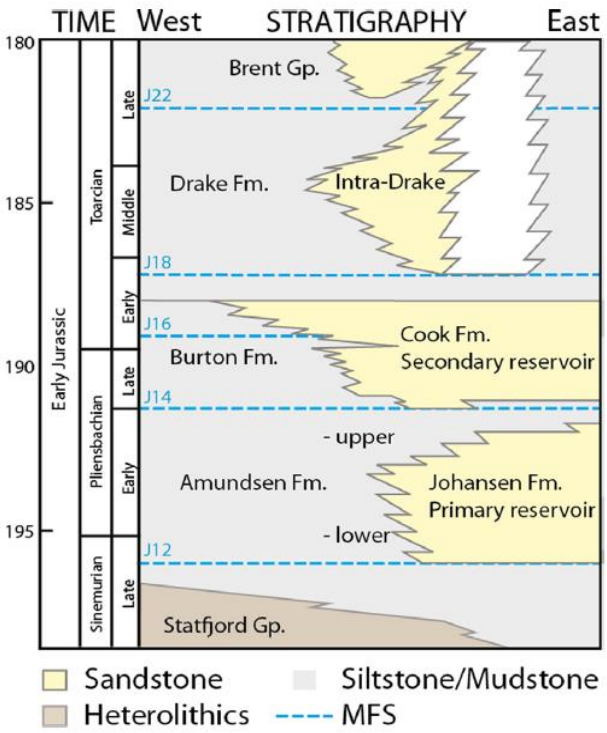

Figure 4.2 Stratigraphy of the Early Jurassic Dunlin Group; comprising the Amundsen, Johansen, Cook and Drake formations. Johansen and Cook Formations as the reservoir units sealed by the Drake Formation mudstones (Sundal et al., 2015).

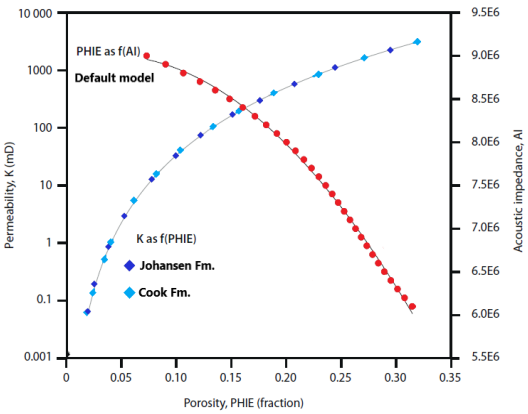

Figure 4.3 The effective porosity (PHIE) measured as a function of acoustic impedance (AI) by Gassnova. Calculating permeabilities as a function of effective porosity using a fitted function $K=467866.3973\times(PHIE^{4.5581})$ (Modified from Sundal et al. 2015).

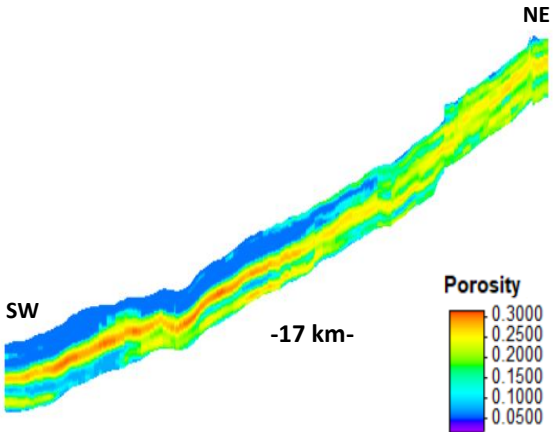

Figure 4.4 Intersectional view of the Aurora model showing the porosity distribution over the reservoir.

4.4 Fluid data and initialization

Two-phase immiscible flow with CO_2 as the nonwetting phase and the formation water (brine) as the wetting phase were utilized by a data set for relative permeability of the brine and the CO_2 phase, without accounting for hysteresis effect, which generally depends on the sweeping history. PVT relations were supplied based on properties of brine and CO_2 at a constant reservoir temperature of T= 98˚C, where densities, viscosities, and formation volume factors vary with pressure. Isothermal condition assumption is far from the reality since temperature varies at different depths; injecting cold CO_2 into a hot saline aquifer will affect the temperature. However, we need to live with that since a new PVT table must be defined for each reservoir temperature value. The fluid densities at surface conditions were reported as ρ_{water}= 1110 kg/m^3 and ρ_{CO_2}=1.87 kg/m^3 with 15% of salinity. Fluid densities measured at surface condition are converted to density values at reservoir condition, using formation volume factors in PVT data. The CO_2 injected in the porous medium was assumed to be pure in a super-critical condition based on the pressure-temperature condition of the reservoir. The effect of capillary pressure has been neglected in this study, possibly due to the cores that could not be representative of capillary pressure measurements. However, measuring accurate capillary pressure values could dramatically affect the CO_2 plume distribution in the reservoir in numerical simulations for CO_2 storage cases, and thus, it should be taken into consideration for further studies (Liu et al., 2014).

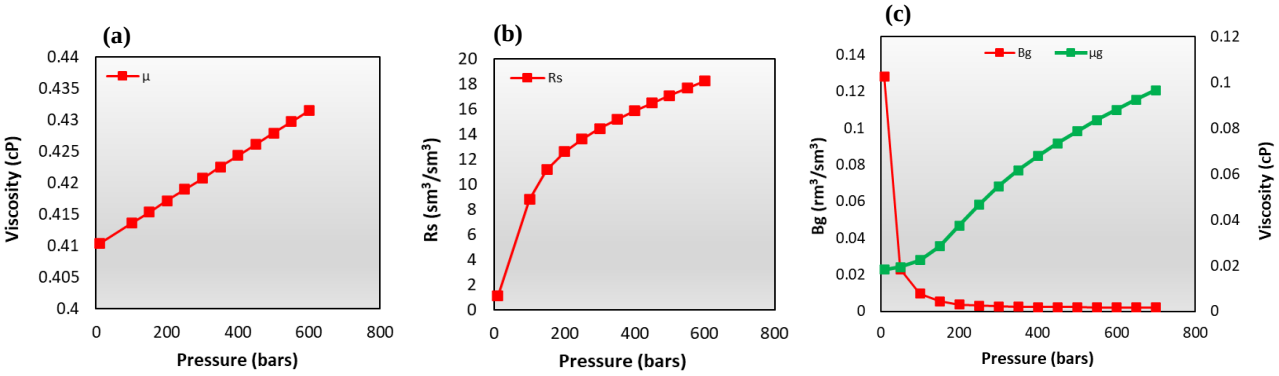

Figure 4.5 PVT relations for brine and CO_2 at constant reservoir temperature of 98 ˚C **(a)** Brine PVT; viscosity-pressure relationship for saturated table **(b)** Brine PVT; R_s-pressure relationship for saturated table **(c)** CO_2 PVT; viscosity & formation volume factor – pressure relationships for saturated table.

In the black-oil modeling adapted for CO_2 storage in saline aquifers, oil represents brine, hydrocarbon gas represents super-critical CO_2, including dissolved gas in live oil keyword to mimic the amount of dissolved CO_2 in brine over time. Thus, three keywords, OIL, GAS, and DISGAS, were used in the data file to include the active phases present during the simulation. Figure 4.5 illustrates some of the important PVT relationships for both CO_2 and brine phases, where for brine PVT, the viscosity, and the solution CO_2/brine (gas/oil in ECLIPSE) experience increases with pressure increase. For CO_2 PVT, the viscosity increases with pressure increase, while the formation volume factor is close to 0 except for low pressures. It is assumed that the Johansen-Cook formations are initially in hydrostatic equilibrium, and at the datum depth of 2600 m, the pressure is set to 260 bars (Figure 4.6). The initial pressure ranges between 220 and 350 bar depending on the depth of the formation (Figure 4.6). The pressure build-up during the injection period and stabilization after the decease of CO_2 injection is an essential part of the study for CO_2 injection simulation with different cases.

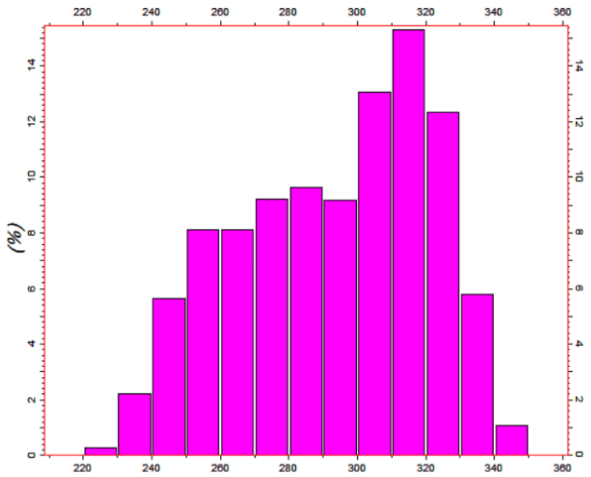

Figure 4.6 Histogram of Initial Pressure distribution lying between 220-350 bar.

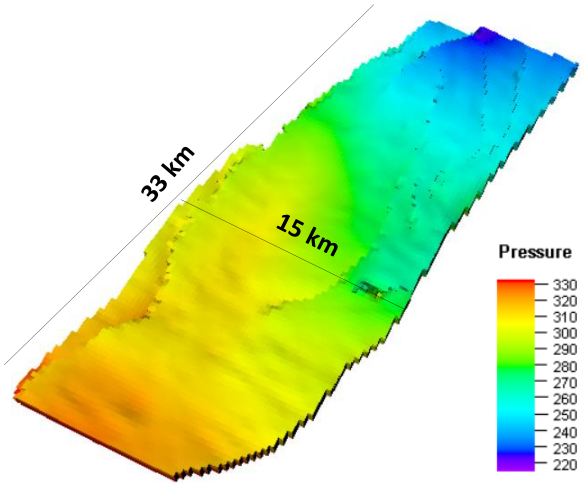

Figure 4.7 3D view of the Aurora model's initial pressure distribution.

4.5 Faults

3D view of Aurora model's pressure property with initial pressure distribution

Aurora storage site is located in Troll West's fault, an eastward tilted fault block bounded by Tusse fault zone to the east and Svarta fault zone to the west with significant fault throws along their fault strike. In addition to these thick-skinned fault zones, several intra-block faults with throws less than the primary sealing unit (the Drake Formation) intersect the storage complex present in the Aurora model (Furre et al., 2020). There has not been a published study by the industry specifically on the impact of intra-block faults on the migration of CO_2. However, according to the last across-fault assessment on Aurora storage site, the eastern, north-eastern dipping intra-block faults are likely to baffle fluid flow compared to western and south-western dipping faults (Holden, 2021).

13 small-scale faults within the Aurora model have been characterized by Sundal et al. (2015), shown in Figure 4.8. All fault transmissibility values are set to MULTFLT = 1 except for F1, F6 with MULTFLT = 0.1 and F7 with MULTFLT = 0.5. F6 can be considered the most important fault in this study since it covers a huge area in the model, and it is the closest fault to the Eos well. Since the injection operation has not started yet and uncertainties about how faults act when facing the fluid flow are still high, a sensitivity study was done on F6 to observe its effect acting as a sealing fault or conduit, which will be explained in the sensitivity analysis section.

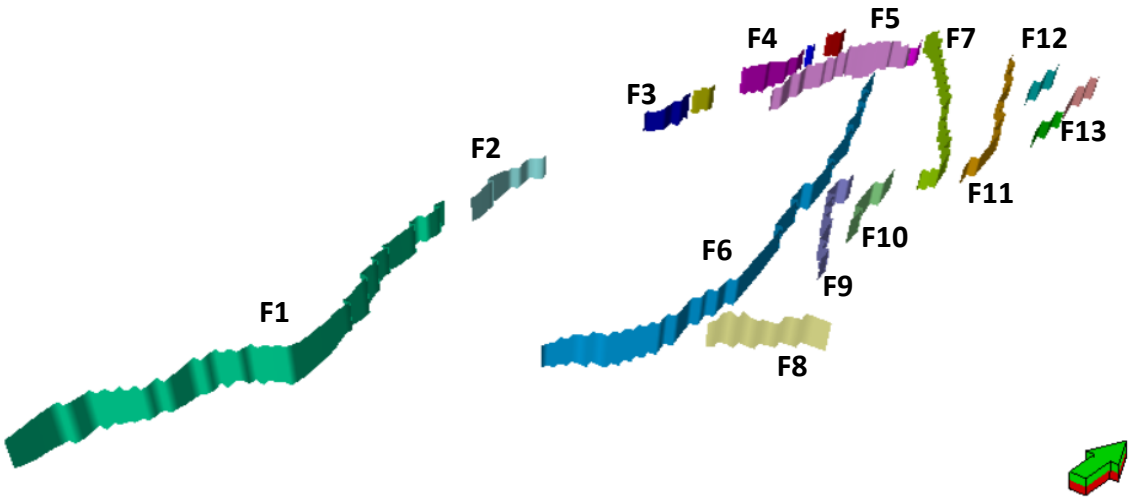

Figure 4.8 Small-scale (intra-block) faults within the Aurora model.

4.6 Model modifications

Before running the simulations using the black-oil and compositional model and comparing their performance and sensitivity studies on uncertain parameters, a new base case model was vital to be constructed by modifying the Aurora model made in 2015. Thus, the simulations to compare E100 and E300 and all the sensitivity studies are based on the base case described in this section. To avoid any confusion, the model given to start this project is called the *default model*, and the modified model is called the *base case model*.

Well placement

Two injection wells, 'WGI-1' and 'WGI-2,' were defined in the default model in the southern part of the formation at around 3100 m depth with a distance of 2 km; however, their placement in the formation and injection plans are not the same as the Northern Lights project. The confirmation well 31/5-7 (known as the Eos well) was drilled approximately 19 km south of the nearest exploration well in the Troll Field, at geographical coordinate E: 524299.5 N 6715849, grid block 43, 49 (*i,j*) and will later be used as an injector within the Aurora storage complex. At roughly 2700 m depth, the Eos well is partially perforated (100 m). Phase one of the project involves injecting up to 1.5 Mt CO_2 into the reservoir. The amount of CO_2 stored per year varies depending on the amount of CO_2 captured in capture plants; however, for 30 years of injection, 1.5 Mt equivalent to 2,200,000 Sm^3/day CO_2 is assumed (conversions in Appendix A). Figure 4.9 illustrates that the Eos well is relatively close to the northern part of the model, which can be challenging after 30 years of continuous CO_2 injection and a long period needed for observing the CO_2 plume growth. The simulation period should be at least 200 years since CO_2 storage projects aim for hundreds of years and rely on long-term trapping mechanism effects to improve project safety and retain the injected CO_2 inside the formation with almost no leakage risk. Moreover, it is possible to obtain a useful estimation of the CO_2 plume migration in the reservoir, the pressure build-up, and stabilization during injection and post-injection. The simulation starts with injection operation from 2024 to 2054, and the results will be obtained until the year 2500.

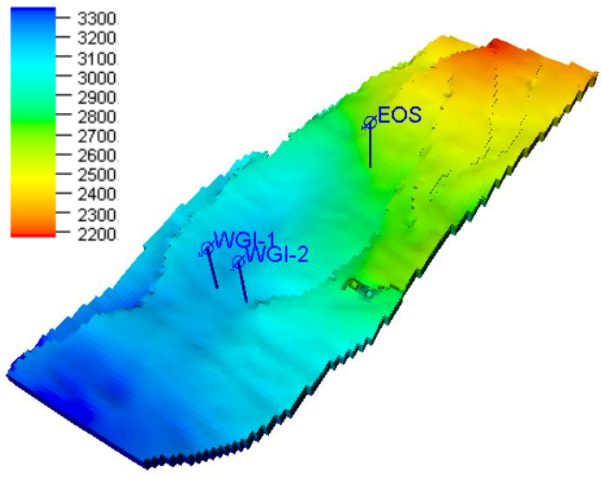

Figure 4.9 Depth property of Aurora default model, showing well placement of confirmation well (Eos) at a shallower depth compared two proposed injection wells in the southern part of Aurora.

Grid and boundary condition

The total number of grid cells is 1,216,800 cells (78 ×130×120), while the total number of active cells in the default model is 742,637 cells, with the grid formats being cornerpoint constructed in Petrel SE software platform. Since computation time is one of the constraints of the black-oil and compositional model, especially when dealing with multiphase systems and millions of grid cells, it is vital to improve the simulation performance as many different cases need to be run. As mentioned before, the previous works on the Aurora model mainly focused on the southern part of the model for the well placement to be at a sufficient distance from the Troll Field and inject in the maximum possible depth. In this project, the cells from the lower central part of the model towards the southern part were deactivated, and a new southern boundary was defined, mainly based on two reasons:

1. The base case model is based on the confirmation well 31/5-7 (Eos) located at the almost central part of the model, which will later be side-tracked and completed for injection operations (Furre et al., 2020).
2. Due to the N-S structural dip of the reservoir and the fact that CO_2 has a low density, gravitational force will dominantly make the injected CO_2 migrate upwards, meaning the grid cells beyond the injection well will not contribute to the injection plan anymore.

After defining the new southern boundary, almost half of the remaining active cells will be deactivated in the J-direction, and 374,814 cells will remain for pressure and saturation calculations (Figure 4.10). The pore volume of the new southern boundary with 19,672 cells has approximately the same pore volume as the removed part of the model. With doing that, the pore volume will remain constant while the overall simulation time will decrease significantly (Figure 4.11).

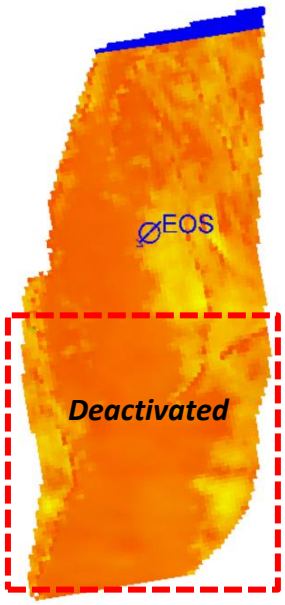

Figure 4.10 The Aurora default model. Red dashed line is indicating the deactivated area to improve computation performance.

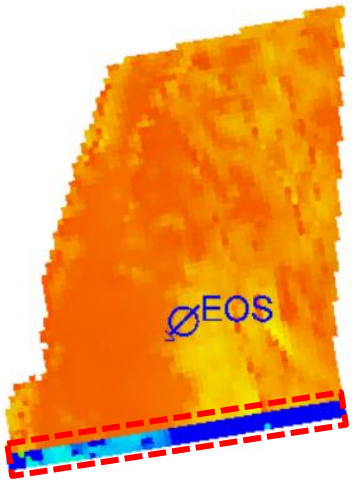

Figure 4.11 The Aurora base case model with reduced grid cells. Red dashed line is indicating the new southern boundary that represents the pore volume of the deactivated grid cells beyond the injection well.

Pore volume

The Norwegian CO_2 storage Atlas has estimated the pore volume of the combined Johansen and Cook formations to be approximately 90 Gm^3. In the default model, made by Sundal et al. (2015), the total pore volume is approximately 280 Gm^3, assuming a quite large pore volume in connection with the Johansen and Cook formations. This was achieved by assigning the communicating pore volume multiplier of 10^4 using MULTPV=1000 in the northern boundary to ensure that the reservoir has an open/semi-closed boundary and consequently, the pressure dissipates out of the reservoir. In the base case model, the total pore volume was based on the work done by Lothe et al. (2019). The Johansen and Cook formations of only the western part of the Tusse fault were considered with estimating the total pore volume of 50 Gm^3. One of the sensitivity studies on this project used different total pore volume values to observe their impact on pressure build-up and CO_2 plume migration. The uncertainty about the true connected pore volume of the Aurora site is high since the proper estimation is achievable only after several years of injection by monitoring and modeling the injection pressure (Lothe et al., 2019).

In order to reach the total connected pore volume of 50 $Gm^{3,}$ both the northern and southern boundary was modified, and as, in the southern boundary, three rows of grid cells (J-direction) were assigned MULTPV=18.5 to account for the removed grid cells in the southern part of the model, while in the northern boundary, five rows of grid cells (J-direction) from layer 60 to 120 were assigned MULTPV=215. The first 60 layers in the northern boundary have MULTPV=1, unlike the default model where grid cells in the northern boundary were assigned MULTPV=999 (Figure 4.12). The main reason is that in the base case model, the placement of the injection well has changed from the southern part to the central part of the model, where the Eos well is located in the real geographical coordinate. Thus, when the CO_2 injection starts, the plume reaches the northern boundary after 200 years since the well is closer to the northern region. With the pore volume of the grid cell being too high, CO_2 starts to dissolve in the water phase immediately, which will overestimate the total dissolved CO_2 in the simulation. To avoid this issue, the first 60 layers of the northern boundary cells have regular pore volume multipliers MULTPV=1 while the last 60 layers have MULTPV=215, which will act as a pressure buffer to the model since the base case model is assumed to have the total pore volume of 50 Gm^3. Although adding pore volume multiplier is an effective method to mimic the effect of the boundary far from the injection point, other approaches of modeling the boundary could be

applying pressure-driven production wells in the boundaries or adding external aquifers that are in communication with the reservoir at the boundaries.

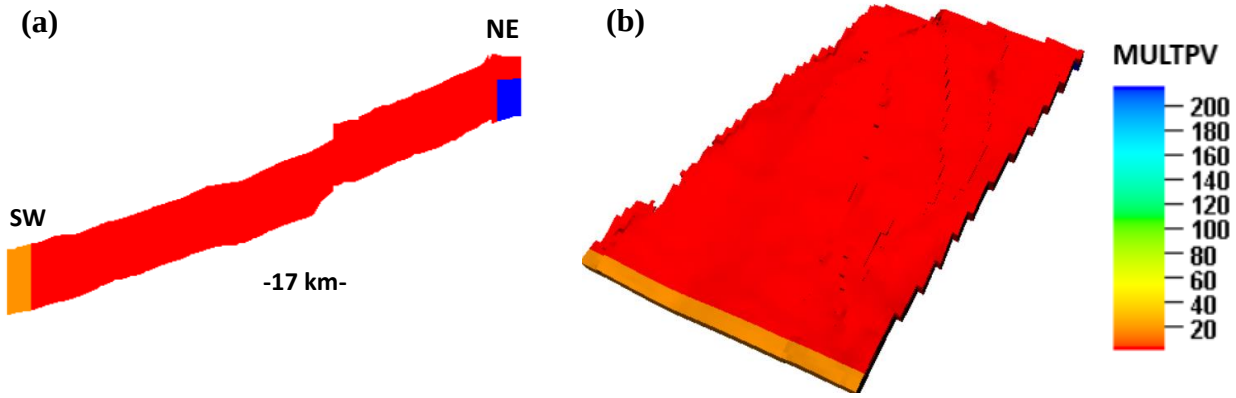

Figure 4.12 Pore volume multiplier property of Aurora base case model, with the new southern and northern boundaries, **(a)** Intersectional view **(b)** 3D view. The majority of the grid cells were assigned MULTPV=1 shown by red color. In the southern boundary, MULTPV=18.5 was assigned to the grids shown by orange color. In the northern boundary, MULTPV=215 was assigned to the grids shown by blue color.

Relative permeability curve

Another important modification was changing the saturation end-point values for the base case model. The main reason is that the saturation dependent data used in the default model is based on the saturation end-point values of the Utsira formation with residual gas saturation of $S_{gr}=0.2$ and $S_{wirr}=0.07$; however, they might not be representative values for the Cook Johansen formations. The CO_2 stored in the Utsira formation is at a depth of 800 – 1000 m below the sea surface with a high porous (>30%) and extremely permeable (>1 *Darcy*) sandstone, while the first injection plan is located at a depth of nearly 2700 m below sea level in the Johansen Formation which has a porosity range of 7.3 to 31.4 % with permeability range of 0.1 to 500 millidarcy (*mD*) (Sundal et al., 2015; Williams & Chadwick, 2021). In Gassnova's report (2012), the combination of Johansen cores from well 31/2-3 located in the Troll Field was used to measure the saturation end-point values where $S_{gr}=0.298$ and $S_{wirr}=0.337$ reported as the residual gas saturation and irreducible water saturation, respectively (see Table 4.1).

Table 4.1 Saturation end-point values reported for the Utsira, Johansen, and Tubåen formations

Formation	End-point values	
	S_{gr}	S_{wirr}
Utsira	0.200	0.070
Johansen	0.298	0.337
Tubåen	0.330	0.100

A set of saturation-dependent data obtained from the Tubåen's formation, the primary reservoir unit in the early years of the Snøhvit CO_2 injection project (around 2500 m), was included in the DATA file but was not used in the default model. However, since the relative permeability curves were not included in Gassnova's report, the water and gas relative permeability values of the Tubåen's formation were used, and the saturation end-point values were changed to the Johansen's formation values. Figure 4.13 indicates the CO_2 relative permeability curve obtained from Tubåen's data; however, residual gas saturation was changed for this project. Since the shape of the gas relative permeability values closest to a straight line typically produces more realistic simulation results, the CO_2 relative permeability curvature was converted to a straight line (upscaled). The brine relative permeability curve shown in Figure 4.13 is obtained from Tubåen's saturation dependent data from the default model, where the irreducible water saturation was changed from $S_{wirr}=0.07$ to $S_{wirr}=0.337$. Even though the saturation end-point values in this project are the most representative so far, there's no guarantee that they are accurate since the well 31/2-3 is in the northern part of Aurora model, where the Johansen Formation was drilled at a depth of approximately 2000 m below sea level, 700 m above the one drilled by the Eos well in the southern part of the Johansen Formation which has different pressure and temperature condition as well as different deposition possibility. Due to the uncertainty of these values and the fact that CO_2 movement and the amount of CO_2 trapped in

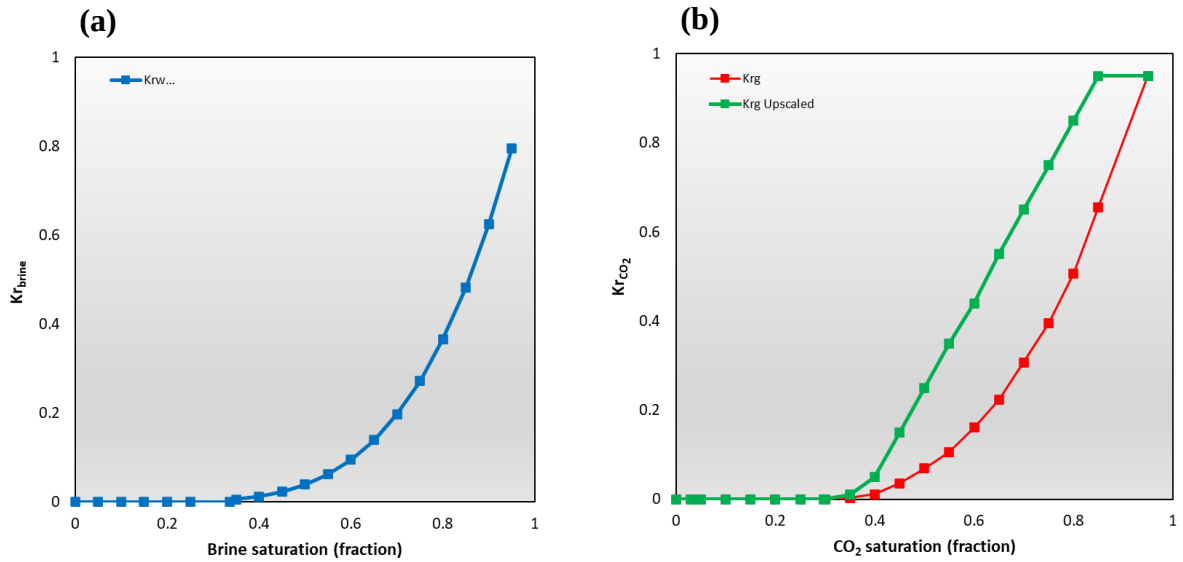

Figure 4.13 (a) Brine relative permeability curve for a drainage process **(b)** CO_2 relative permeability curves for a drainage process; red curve is indicating CO_2 relative permeability curve obtained from the Tubåen Formation., green curve is indicating the upscaled form of red curve to use for the base case model.

the pores are highly dependent on saturation end-point values (especially S_{gr}), two types of sensitivity analysis were done in this project, which will be explained in the sensitivity analysis section. Since the model is relatively small, especially after the well placement change, it is essential to have an idea about the amount of CO_2 that reaches the northern boundary, as it represents a larger pore volume connected to the model than the northern grid cells themselves. By defining two '*Fluid in Place'* regions (FIPNUM in ECLIPSE), one for the northern boundary and the other for the rest of the model, to observe how much CO_2 injected will migrate to the boundary region and how much remain in the rest of the model.

4.7 Simulator

The simulations in this project were performed using E100 and E300, the black-oil and compositional simulators provided in ECLIPSE software. E100 is used for black-oil modeling where a two-phase system with gas representing the super-critical CO_2 and oil representing the brine and the option of CO_2 dissolution in brine based on the PVT relations obtained at isothermal conditions. E300 is used for multi-component modeling of CO_2 storage projects using CO2STORE module where two phases are considered: a CO_2 rich phase and a H_2O rich phase where the mutual solubilities and phase partitioning of CO_2 and H_2O are calculated to match the experimental data for typical CO_2 storage conditions (12-250 ˚C and up to 600 bars), with the procedure given by Spycher and Pruess (2005, 2010). Three components as CO_2, H_2O, and NaCl, were introduced to E300, where NaCl's total mole fraction was set to 0.15 to account for the salinity of the formation water. $CaCl_2$ was not considered in this model to decrease the computation time. A local computer was used to perform the simulations in this project with 16 GB RAM and 4 physical CPU cores, and 8 logical processors. The most important parameters of the Aurora model used in this project are shown in Table 4.2.

The following assumptions were made for the simulation:

- The capillary pressure difference between the non-wetting and wetting phases is zero.
- The process during the injection and post-injection is in isothermal conditions
- Pure CO_2 is injected into the porous media in super-critical condition
- The model contains 100% formation water initially
- The mineral trapping is ignored
- Solid precipitation is neglected

Table 4.2 Aurora base case overview

Parameter	**Value**
Reservoir	Johansen, Cook Fms
Reservoir thickness	173 m
Slope	2 ˚ N-S
Porosity	7.3 - 31.4 %
Horizontal Permeability	0.1 to 500 mD
Vertical to horizontal Permeability ratio	0.1
Well name	Eos
Well location	(43, 49) I, J
Well depth	2700 m
Perforation	Partially perforated
Injection Rate	1.5 Mt/year
Injection period	30 years
Pore volume	50 Gm^3
Grid type	Cornerpoint
Grid dimension	78 × 130 × 120
No. of active grids	374,814
No. of faults	13
Fluid In place region	2
Initial condition	260 bar at 2600 m
Temperature	98 ˚C
Water density at SC	1110 kg/m^3
CO_2 density at SC	1.87 kg/m^3
Salinity	15%
Residual gas saturation	0.298
Irreducible water saturation	0.337
Simulation start	Jan 2024
Simulation end	Dec 2499
Simulator	E100 E300
Visualization	Petrel SE
Computer specifications	16 GB RAM, 4 physical CPU cores 8 logical processors

5 Results and Discussion

The black-oil model was transformed to the compositional model after preparing the base case model based on the default Aurora model to assess the performance and compatibility of these two simulation approaches. Furthermore, various cases were created for sensitivity studies of some of the unknown parameters, namely to examine pressure changes, the quantity of CO_2 that will remain free or dissolved in the brine phase after 45 Mt of injection, and lastly, the CO_2 footprint over time. Following the presentation of the data, the possible causes of any changes will be addressed in depth.

5.1 Black-oil & compositional simulation

The E100 black-oil simulator was adapted for CO_2 storage in this project, where oil represents the brine phase and gas represents the CO_2 phase. The main parameters used for the investigation of the black-oil simulator were the pressure at the well injection area (BPR), free gas in place (FGIPG), and solution gas in place (FGIPL). The CO2STORE module was used in the E300 compositional simulator, specifically developed for CO_2 storage in saline aquifers. The main parameters used for investigation of the compositional simulator were the pressure at the well injection area (BPR), CO_2 mobile in the gas phase (FGCDM), CO_2 trapped in the gas phase (FGCDI), and CO_2 dissolved in the water phase was used to compare the findings of these simulations (FWCD). In addition, 3D pictures and intersectional views were employed to compare CO_2 distributions. The compositional model used similar parameters so that the focus in both models was on the CO_2 distribution differences and the PVT properties of the fluids.

The initial pressure for the compositional case with E300 is 283 bar, 5 bar higher than the initial pressure for the black-oil case with E100. The pressure rises rapidly after CO_2 is introduced in the formation from 2024 to 2054 and reaches 296 bar for the compositional case and 293 bar for the black-oil case. As expected, the pressure starts falling in both cases following injection; however, the pressure in the black-oil case decreases more than the pressure in the compositional model, presumably due to more CO_2 dissolved in the brine phase. After around 100 years, pressure stabilizes. The compositional base case stabilizes at around 286.3 bar, marginally higher than the black-oil case stabilizing at around 285.6 bar (see Figure 5.1).

CO_2 injection projects deal with mass values such as millions of tonnes rather than volume terms because CO_2 volume is highly dependent on pressure and temperature. In standard

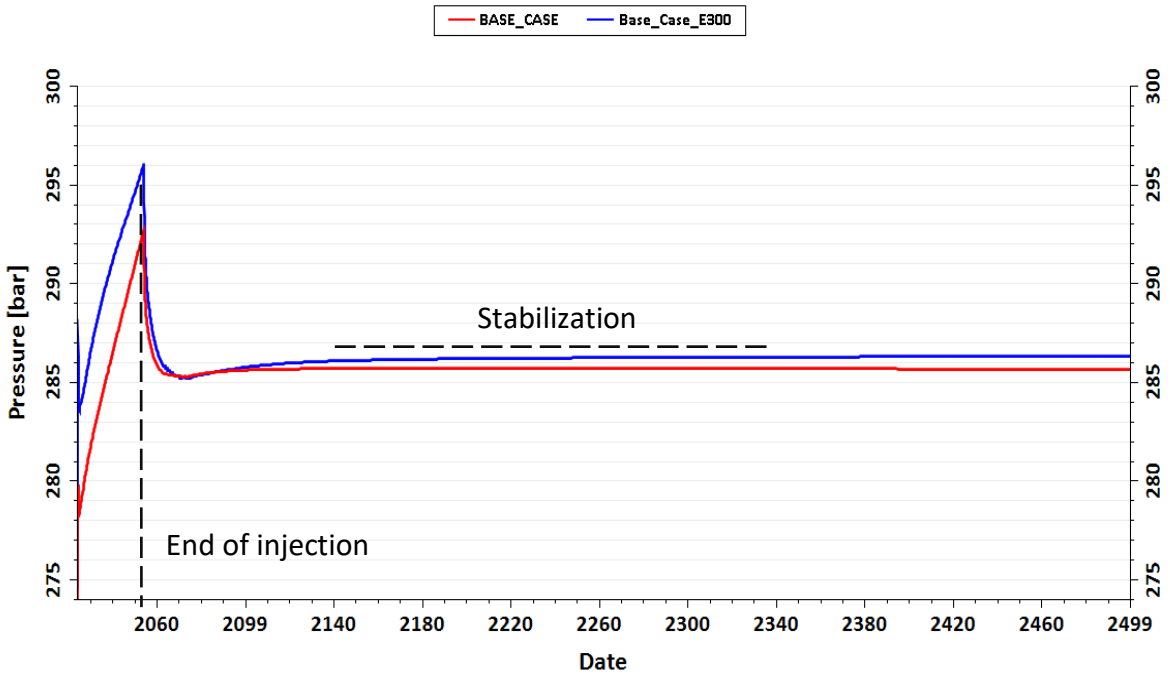

Figure 5.1 Reservoir pressure in the injection area (Grid 43,49,44) using Eclipse 100 and Eclipse 300.

conditions, one tonne of CO_2 has a volume of 534 m^3, which was used for conversion purposes in the project. The CO2STORE module, as previously stated, can indicate the amount of trapped, mobile, and dissolved CO_2 in *kg-mole*. The kilo-mole word can be translated to mass since 1 kg-mole of CO_2 equals 44.01 $kgCO_2$. Since it was originally created for hydrocarbon production, black-oil simulation only reports the volume of dissolved or free CO_2 (refer to Appendix A for conversions).

The result of CO_2 storage utilizing the CO2STORE module in the E300 compositional simulation is shown in Figure 5.2. The amount of trapped, mobile, and dissolved CO_2 increased during the injection period from 2024 to 2054; however, the majority of the injected CO_2 was trapped. Around 50% of the injected CO_2 has been trapped, 40% stays mobile in the gas phase, and 5% dissolves into the water phase after the injection of around 45 Mt of CO_2 has stopped. After 50 years, the amount of trapped and dissolved CO_2 increases, with the trapped CO_2 having greater relevance while the mobile CO_2 decreases significantly. As a result, by 2100, 82% of CO_2 will have been trapped, 11% will still be mobile, and 7% will have been dissolved in the brine phase. Around 1% of the CO_2 injected in 2300 reached the northern boundary, where it was trapped for the most part. At the same time, the amount of trapped CO_2 has climbed to 86%, with 8% dissolved, while the amount of mobile CO_2 has decreased to 6% in the model region. CO_2 trapped and dissolved will stabilize and rise quite gradually in the middle of the simulation, but mobile CO_2 will continue to decrease by the end of the simulation. In the year 2500, 97% of the CO_2 injected remained in the model region, with only 3% reaching the northern barrier, which mimics the rest of the formation in reality. After 45 Mt of CO_2 injection

in the Johansen Formation, 88% will be confined in the reservoir, 8% will dissolve to the brine phase, and just 4% will be mobile after 500 years.

Table 5.1 The amount of trapped, mobile CO_2 in the gas phase and the amount of dissolved CO_2 in the water phase in the boundary and the model region of the compositional case over three time intervals 2100, 2300, and 2500.

45 Mt injection	**E300**					
	Trapped CO_2 in gas phase (Mt)		**Mobile CO_2 in gas phase (Mt)**		**Dissolved CO_2 in water phase (Mt)**	
Year	**Model**	**Boundary**	**Model**	**Boundary**	**Model**	**Boundary**
2100	36.40	0.00	4.83	0.00	3.37	0.00
2300	38.60	0.35	2.00	0.03	3.61	0.01
2500	38.67	0.53	1.12	0.64	3.63	0.01

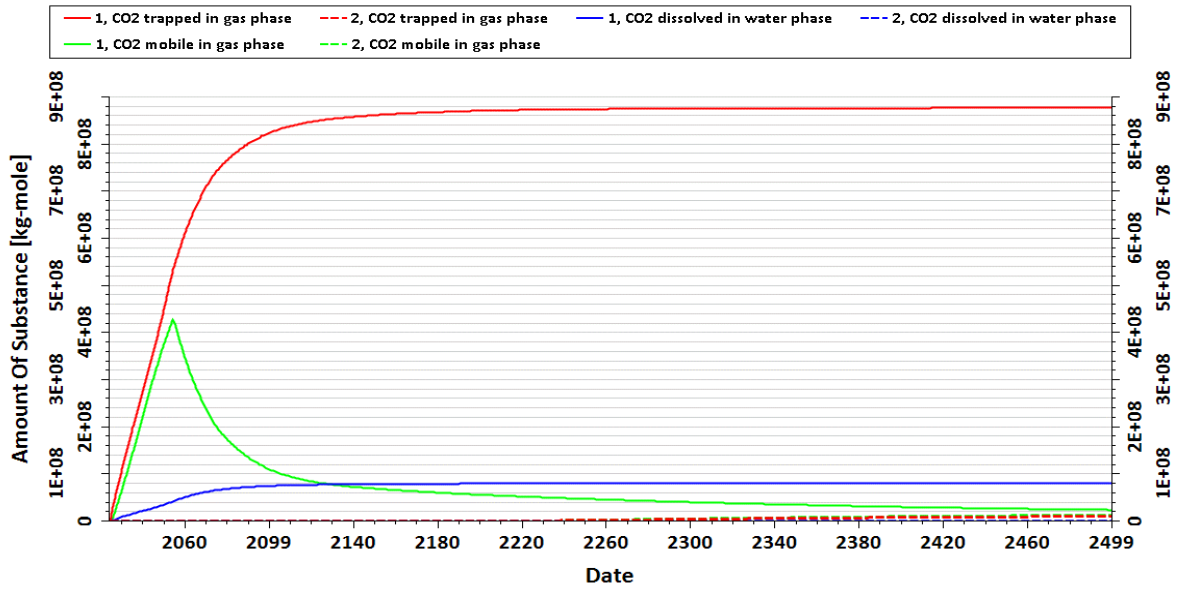

Figure 5.2 Plot of the cumulative trapped, mobile CO_2 in gas phase and the amount of dissolved CO_2 in terms of mass-mole using E300 for fluid in places 1 and 2, representing the model and boundary regions, respectively. The simulations begins in 2024 with 30 years of injection and ends in the year 2500.

The results of CO_2 storage utilizing the black-oil simulator option, which adapts CO_2 characteristics to gas and brine properties to oil in the data file, are shown in Figure 5.3. The graph shows that during the injection period from 2024 to 2054, free CO_2 increases significantly and peaks at roughly 42.3 Mt of injected gas, or 94%, whereas only 6% of the CO_2 is dissolved in the brine phase. Following a period of injection, the amount of free CO_2 begins to decrease gradually, while the amount of dissolved CO_2 grows. Less than 1% of the CO_2 plume, mostly free CO_2 with low dissolved CO_2, reached the northern boundary in 2300. The amount of free

CO_2 has fallen to 88% over the same period, resulting in 11% of CO_2 being dissolved in the brine phase. By 2500, 1% of the CO_2 plume, mostly free CO_2, has reached the northern border. After 45 Mt of CO_2 injection in the Johansen Formation, 88% of the CO_2 will remain in the reservoir as free CO_2, and 11% will dissolve into the brine phase after nearly 500 years.

After obtaining the results for CO_2 storage using the black-oil and the compositional simulators, it can be stated that free CO_2 in E100 or '*free gas in place'* is equivalent to the summation of *'*CO_2 *trapped and mobile in gas'* in E300, and the dissolved CO_2 or *'solution gas in place*' in E100 is equivalent to *'*CO_2 *dissolved in water phase'* in E300 simulator. After the end of the simulation and observing the results, it can be seen that the dissolved CO_2 in the water phase for the black-oil case is 11%, with the free CO_2 being 4% less than the summation of trapped and mobile CO_2 in the gas phase for the compositional model which is 92% of the total CO_2 injected. Using E100 with the pre-deterministic PVT properties gives close results to simulation using the CO2STORE module from E300.

There's no keyword in E300 compositional simulator to request the model's field density and/or viscosity values. Consequently, it is impossible to compare the field density-viscosity values of the black-oil model and the compositional model. The only way to compare these values is through requesting density-viscosity values at a specific grid block(s). Therefore, the grid block (44, 40, 44) was chosen to obtain the density-viscosity values of each phase separately for both the black-oil and the compositional model. The results shown in Table 5.3 indicate that even though the viscosity and density calculations of the black-oil and compositional simulators are identical for the gas phase, there are considerable differences when calculating the same properties for the brine phase. The calculated brine density for the specified grid cell is ρ_{brine}=1253 kg/m^3 when using the compositional simulator, while the black-oil simulator has the brine density of ρ_{brine}=1076 kg/m^3, confirming a high density difference between the two simulation methods. The calculated viscosity for the specified grid cell is μ_{brine}=0.71 cP for the compositional simulator, considerably higher than the brine viscosity given in the black-oil simulator, which is μ_{brine}=0.42 cP.

When employing the black-oil and compositional simulators, different pressure values were obtained during the injection and post-injection periods, as shown in Figure 5.1. This could be due to differing brine density values acquired from both simulations. Both simulation cases are initialized at the same reference depth and pressure. However, when the calculated brine density increases, the initial pressure at the grid blocks below the reference depth also increases since they are directly proportional. Thus, the primary reason that the pressure is in total higher for

the compositional case is due to the fact that the brine density obtained from the compositional case is greater than the brine density calculated in the black-oil case.

Table 5.2 The amount of free/dissolved CO_2 in the boundary and the model region of the black-oil case over three time intervals 2100, 2300, and 2500.

45 Mt injection	**E100**			
	Free CO_2 in gas phase (Mt)		**Dissolved CO_2 in gas phase (Mt)**	
Year	**Model**	**Boundary**	**Model**	**Boundary**
2100	40.60	0.00	4.40	0.00
2300	39.94	0.06	5.06	0.00
2500	39.26	0.43	5.30	0.01

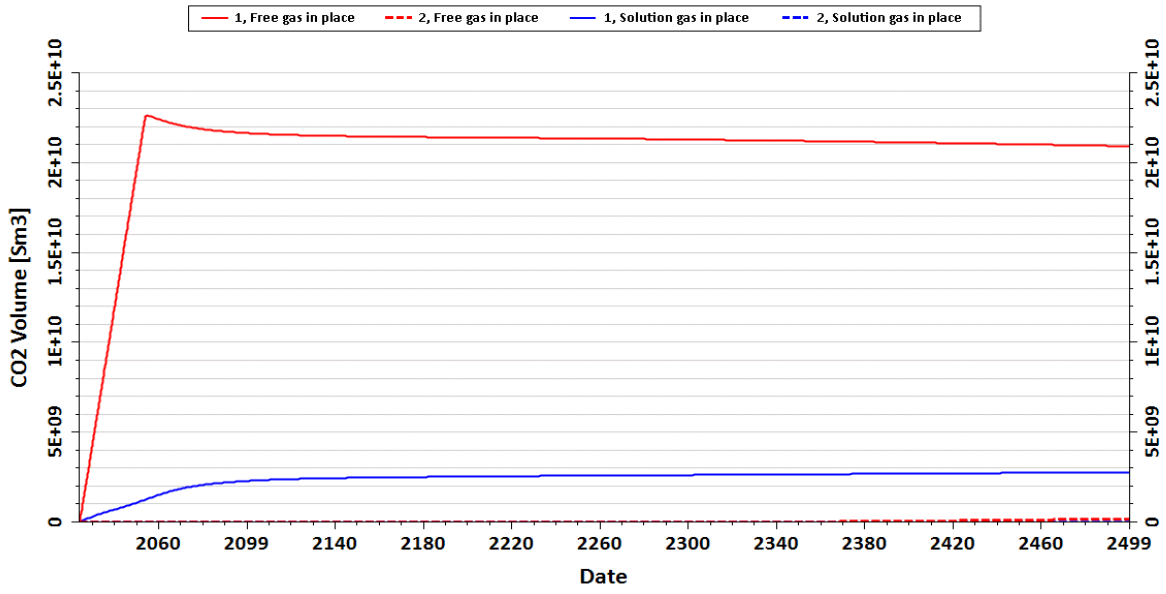

Figure 5.3 Plot of the cumulative free and dissolved CO_2 in terms of volume using E100 for fluid in place 1, 2 representing the model and boundary regions, respectively. The simulations begin in 2024 with 30 years of injection and ends in the year 2500.

Table 5.3 The density and viscosity obtained at the grid block 44, 40, 44 for each phase, using E100 and E300

Grid block 44,40,44	**Brine**		**CO_2**	
	E100	**E300**	**E100**	**E300**
Density (Kg / m^3)	1076	1253	636	636
Viscosity (cP)	0.42	0.71	0.50	0.50

Looking at 3D and intersectional images of both the black-oil and compositional case of Figure 5.4, it can be observed that the CO_2 plume moves toward the upper part of the formation much faster in the compositional case; however, the migration process looks similar for both cases. Close to the well, a piston-like movement of CO_2 is observed, leading to a horizontal displacement of brine to some extent. A bit further from the well, the CO_2 cannot push away the in situ brine horizontally, thus it tends to migrate vertically and fill the top of the formation after some years that the injection operation stops. Simultaneous to the vertical migration of the CO_2 plume, some portion of the injected CO_2 will be left near the injection-well area since the brine that was displaced by the injected CO_2 in the drainage process starts to displace the CO_2 in the imbibition process and snaps off CO_2 in the pore bodies, leading to residual trapping as one of the essential trapping mechanisms for increasing the safety of the storage operation after that CO_2 plume migrates vertically and reaches the top of the formation, forming a thin plume layer on top and moving toward the northern part of the model. 3D map in the year 2200 shows that the CO_2 front in the compositional model has reached the northern part of the model, moving 11.5 km away from the well, while for the black-oil case, the CO_2 front is around 10 km away from the well and has not yet reached the boundary.

The intersectional view of both models in the same period confirms the CO_2 plume being faster in the compositional case, where the vertical migration close to the well has occurred faster. At the end of the simulation, 3D map of the reservoir shows that the CO_2 plumes on top of the formation are almost identical for both cases, with minor differences on some parts. Observing the intersectional views, it can be seen that more CO_2 has been left near the injection well region in the black-oil case compared to the compositional case, which also confirms the fact that the thickness of the CO_2 on top of the formation with the extended lateral move is lower for the black-oil case. Lastly, looking closely at the intersectional view close to the injection well, it can be seen that for the black-oil case, the injected CO_2 has managed to push away the brine horizontally around 500 m, while in the compositional model, the horizontal movement of the CO_2 is around 250 m, half of the one in the black-oil case.

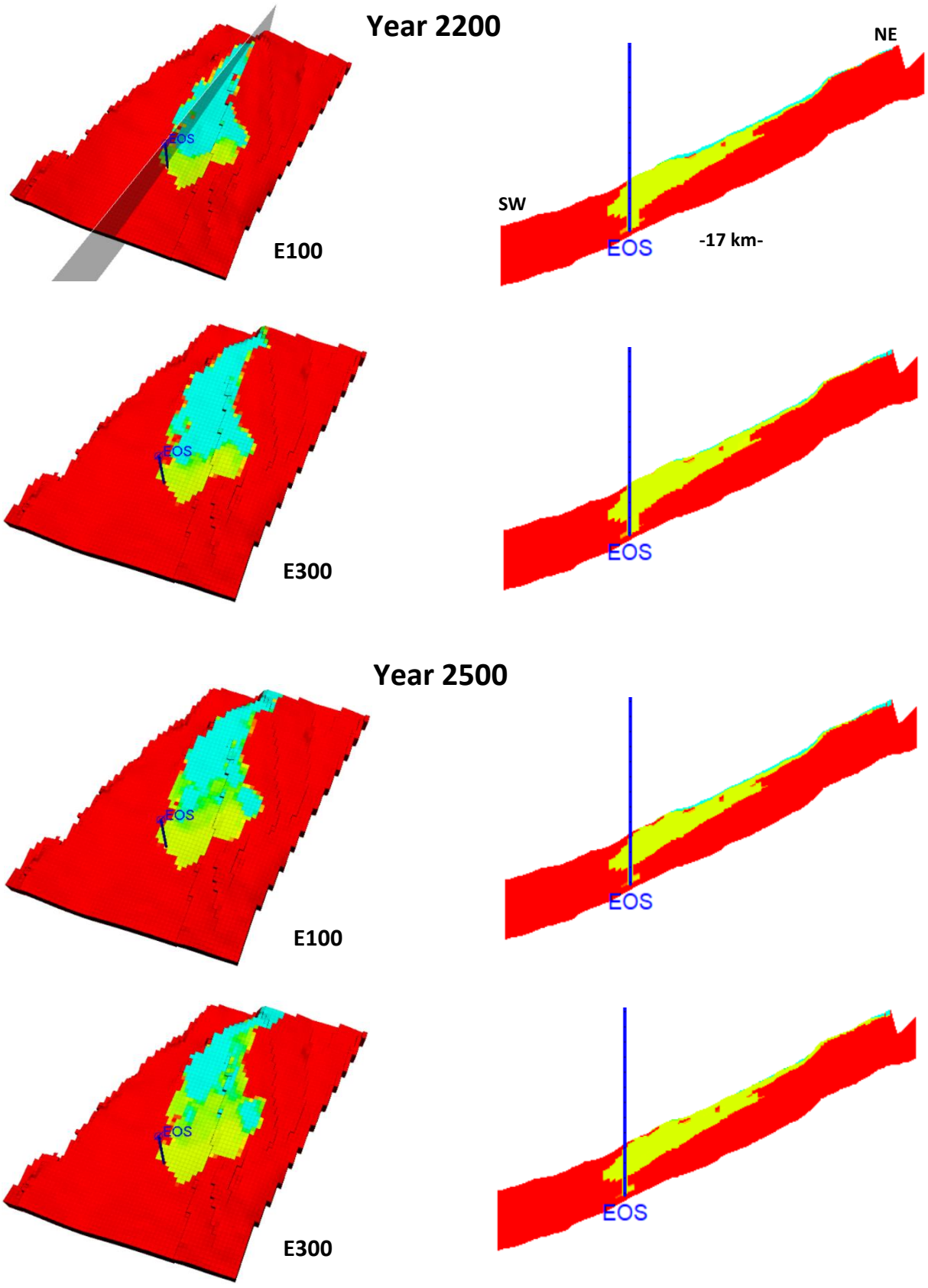

Figure 5.4 CO_2 footprint in the Aurora model in the years 2200 and 2500 for different simulation methods (Left) 3D map view (Right) Northern-Southern intersectional view.

Simulation runs for the black-oil, and compositional models showed close results with some differences. In terms of the non-linear convergence, there were some convergence problems (not errors) for the black-oil model where the time-step needed to be decreased to reach a sufficient residual value, meaning more iterations to be accepted by the simulator. At the same time, the compositional simulation did not face any convergence problems, meaning all of the residuals were calculated with low iterations, without any difficulties. As expected, the compositional model took much longer for each simulation run in terms of the computation time. The computation time for the compositional case, using two processors, was around 9 hours for each simulation case, while for the black-oil model, it took around 2.5 hours for each simulation case, meaning 3.5 times less than the compositional case, which is significant when the time is limited, and several simulation cases are needed for updating, refining, comparison, and sensitivity studies (see Table 5.4).

Table 5.4 Computation time comparison between using the black-oil and compositional simulation

Simulator	**Simulation time**	
	Second	***Hour***
Black Oil	9176	2.548
Compositional	31720	8.811

Black-oil and compositional simulators showed that after around 500 years, 8-11% of the injected CO_2 will be considered as dissolved. CO2STORE option can report the amount of mobile and immobile CO_2; however, the black-oil model has not been made for that purpose. Thus, it can only report the amount of free CO_2, which can be considered the equivalent of immobile and mobile gas summation in the compositional case using CO2STORE. The mobile and immobile CO_2 together make up 92% of the CO_2 injection in the compositional model, and the free CO_2 at the end of the black-oil's case is 88%. As a result, they both reflect the high end-point values used in the relative permeability curve, especially the residual gas saturation. In general, the results are almost compatible, but the differences should always be considered.

The most important reason for having slightly different results is the approach both models use to calculate the amount of free or dissolved CO_2. In the black-oil simulation, the amount of dissolved gas is calculated depending on the CO_2-brine phases contact in grid cells and the PVT property provided for the model, whereas the pressure elevation in the reservoir, the solution gas-oil ratio (R_s) will increase accordingly (oil represents water in black-oil CO_2 storage modeling). Thus, the amount of dissolved CO_2 in the brine phase increases in the injection

period due to more CO_2 entering the formation; however, it does not increase considerably in the post-injection period since the pressure starts to stabilize at an almost constant rate. It means the pressure will not affect dissolution, and only the contact between fluid phases can lead to the dissolution of CO_2 in the brine phase due to convection for long-term periods, and the rest will be considered as free gas. In the compositional case, the amount of dissolved CO_2 in the brine phase is based on the procedure given by Spycher and Pruess and was explained in more detail in previous sections. Even though both simulation methods use different approaches to calculate the amount of dissolved CO_2, the results are not entirely different and can be considered reliable calculations. To make the black-oil case more compatible with the compositional case using CO2STORE, which specifically was developed for CO_2 storage in saline aquifers, the PVT table used in the black-oil model can be modified by changing the amount of solution gas-oil ratios at different saturation pressures; however, much care needs to be taken while changing these values, since they are correlated by CO_2 storage research groups, specifically for CO_2 injection in brine systems.

Both simulation methods' amount of mobile and immobile gas rely heavily on the residual gas saturation assigned in the saturation-dependent tables. Each grid cell has a total fluid saturation of 100%, which is the total of CO_2 saturation and brine saturation. The residual gas saturation in the model is 29.8%, where the gas relative permeability is zero, and the fluid cannot move anymore in the simulation. The irreducible water saturation is 33.7%, meaning that when CO_2 enters a grid cell filled by brine, it cannot invade 100% of the pores, and the maximum gas saturation it can reach is subsequently 66.3%, where the brine relative permeability is zero and remains the pores. In the compositional model, if as an example, the gas saturation of grid ‘A’ is 40%, around 30% of it will be considered as trapped gas since the gas relative permeability is zero and the rest will be mobile, with non-zero relative permeability, which can move through the porous medium. In general, only the compositional case can differentiate between mobile and immobile gas and report the values in the simulation while the black-oil model, as mentioned before, can differentiate between the immobile and mobile CO_2 through the given relative permeability values but it is not able to report the values.

Despite the limitations of the black-oil case, the PVT property to adapt the CO_2-brine behavior has been proven to obtain reasonable results, which can be confirmed due to very slight differences with the values obtained from the case using the CO2STORE option in the compositional model. To have a more accurate result in terms of immobilization of the injected CO_2, some factors must be taken into consideration. The most important factor is obtaining

accurate saturation end-point values since any changes in the residual gas saturation can lead to various trapped CO_2 values. More residual gas saturation value in the relative permeability data means that after the imbibition process of brine that displaces the CO_2 in the pores, especially close to the injection well area, more CO_2 will stay in the pores, and despite being buoyant, it loses its mobility. One practical approach is to obtain core samples from different parts of the reservoir and obtain their relative permeability curves. Several saturation tables can be assigned to different regions in the model and have a more realistic simulation of saturation end-point values and residual trapping. Petrophysical properties are also vital factors in dictating the fluid distribution in the reservoir, where any lateral or vertical CO_2 movement is a strong function of porosity and permeability. Seismic inversion techniques have estimated the porosity of the model, and the permeabilities are based on the porosity measurements. Well logging, well testing, and taking core samples can be strong evidence for confirming the reservoir's porosity-permeability range. According to the stratigraphy of Aurora site, the primary sealing unit of the model is the Drake Formation with nearly 128 m thickness according to the confirmation well (Eos). Building several layers of grid cells on top of the reservoir to represent the sealing unit could make the reservoir more realistic regarding the amount of mobile or immobile CO_2 for long-term periods.

Obtaining more accurate values on how much of the CO_2 dissolves into the brine phase is done by proposing gravimetric monitoring over the years, where it is possible to calculate the amount of CO_2 that has been dissolved in the brine phase. In the Sleipner CO_2 storage project, gravimetric monitoring has been used to estimate the amount of dissolved CO_2 in the brine phase. In 2012 and after 17 years from the start of the injection operation, it was forecasted that 10-13% of the injected CO_2 was dissolved in the brine phase according to the mass changes observed from gravimetry surveys (Ringrose et al., 2021). The proportion of dissolved CO_2 in the brine phase in the simulations of this project is showing quite close values, which confirms almost accurate results, based on the previous research and studies in this field. The presence of siltstone and mudstone interlayers with low porosity-permeability have been found on the well logging data, mainly on the Johansen Formation, however, there is not much certain knowledge and predictability about their lateral extent. Suppose their lateral extent in the reservoir unit is confirmed (Sundal et al., 2015). In that case, they will play a huge role in preventing some portions of the CO_2 from migrating up, leading to more contact with brine formation in the pores, leading to more dissolution trapping.

Since the pore volume, geology, and injection rate are similar for both the black-oil and compositional models, the pressure change trends are expected to be the same for both cases. After 45 Mt injection of CO_2 for 30 years, the pressure elevation value is around 11 bar for both. However, a pressure difference was observed due to different brine density values, where the pressure trend for the compositional case is around 4 bar more than that of the black-oil case due to having higher brine density values at the same grid block. The pressure noise at the initial time is due to the boundary conditions that the simulator deals with and will not cause any problems for long-term calculations. Even though the pressure reports for grid blocks further from the injection well showed fewer noises in the initial time of the pressure plot, the pressure block in the injection area is favorable to observe since it would be possible to measure the maximized pressure inside the porous media due to injection, to estimate if any possible fracturing happens due to injection or in general what is the pressure difference between the maximized pressure and the fracture pressure. This could be due to both simulation methods' approaches to calculating the boundary condition pressure. In the post-injection period, the stabilized pressure for the black-oil simulation is slightly less (< 1bar) than that of the compositional model since more CO_2 was dissolved in the black-oil case. As a result, less CO_2 in the super-critical phase attempts to push the brine in the areas it faces the brine. According to the pressure depth function measurements in the Norwegian North Sea basin, at a depth of 2700 m, where Eos well is drilled for injection, the fracture pressure is approximately 500 bar, much higher than 296 and 292 bar maximum pressure values obtained by the compositional and black-oil cases (Bolås & Hermanrud, 2003). Thus, in terms of reservoir failure due to high pressure, it can be stated that the Johansen Formation has a high capability for 45 Mt of CO_2 injection and even more, as the maximum pressure that could be reached is far less than the approximate fracture pressure in the depth of 2700 m.

The CO_2 injection process for both cases is the same, with some differences that will be explained. Three important driving mechanisms, i.e., viscous, capillary, and gravity forces, contribute to the injection process. Depending on the location, time, and factors such as heterogeneity, pressure and density difference, and mobility ratio values, the domination of each one is more severe. Capillary pressure in the project was assumed to be negligible since the capillary pressure values were only available for the Tubåen formation, with relatively low values. Thus, it was preferred to ignore the capillary pressure effects until more recent values are calculated and can be used for further studies on the model. Close to the injection well area, the viscous force dominates the flow. The domination of viscous force, leading to a piston-like

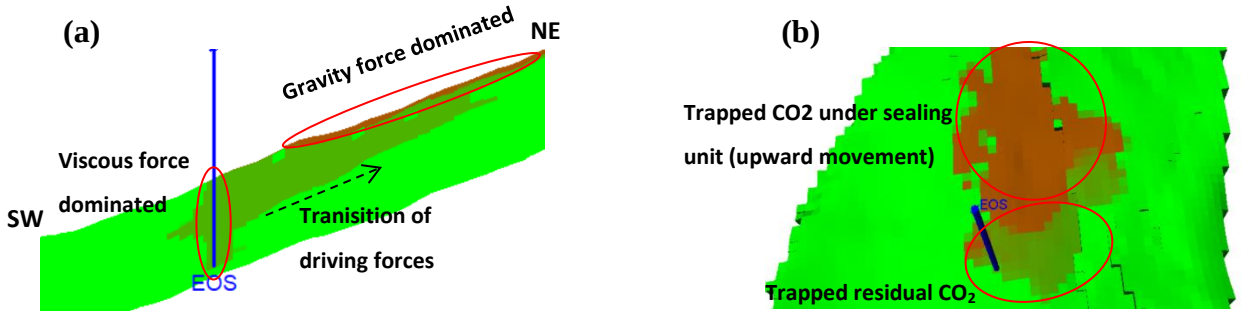

Figure 5.5 CO_2 plume distribution after around 500 years **(a)** intersectional view indicates the domination of viscous force close to the well followed by the domination of gravity force away from the well. Some portion of CO_2 will be left in the pores **(b)** Top view indicates the amount of trapped residual CO_2 near the injection well and the upward migration of the CO_2 plume when reaching the top of the formaion

movement of the CO_2 and pushing the brine away from the well, can be confirmed by Figure 5.5. The primary reason for such driving force is the high pressure difference between the bottomhole and the formation, leading to a horizontal movement of CO_2. The extension of the piston-like movement of CO_2 depends on how high or low the sweep efficiency is. Different parameters can impact the magnitude of sweep efficiency, including the well placement, reservoir thickness, permeability, heterogeneity effects, density difference, flow rate, and mobility ratio. The high density difference between the CO_2 and brine and high mobility ratio due to the super-critical gas-like viscosity will lead to low sweep efficiency, resulting in more vertical movements of the injected CO_2. The transition of driving forces from viscous to gravity happens away from the well, where the CO_2 plume migration changes its direction from being completely horizontal close to the well to become more vertical as the distance from the injection well increases. The main reason for such flow is that the pressure gradient is relatively low inside the reservoir, leading to vertical migration of CO_2 due to having a lower density than the *in situ* brine. As the super-critical CO_2 moves vertically, a trail of residual CO_2 remains in the pores and become immobile due to the high residual gas saturation that was assigned in this project ($S_{gr}=0.298$). Thus, residual trapping as one of the essential trapping mechanisms that help retain some portion of the injection CO_2 can be confirmed in the model, increasing storage safety. Two main reasons cause the CO_2 to migrate to the northern part of the model; the slight N-S slope of the reservoir and a relatively low density of the injected CO_2. Even though the low permeable sealing unit is not included in the model, the structural trapping mechanism is also happening in the model, where the top of the model (assumed as the sealing unit) is retaining plume in the formation, and no more vertical migration occurs; instead, a thin layer of CO_2 distributes laterally toward the northern part of the reservoir. Due to the long lateral movement of CO_2, especially on top of the formation, dissolution trapping tends to occur where there's a relatively long CO_2-brine contact which leads to mutual solubilities between two phases, mainly

the solubility of the CO_2 into the brine phase and increased dissolution rates. The CO_2 plume in the simulations will not reach the northern boundary near the Troll Field, at least for 150 years after the injection (the year 2200). The fact is that Troll Field is producing from the Sognefjord formation, which is on top of the Johansen and Cook formation. Thus, even if the Troll Field continues the hydrocarbon production for the next 70-80 years (probably impossible), there's no risk associated with the CO_2 plume leaking to that area. Undoubtedly, the flow simulations will be more accurate after refining the model based on repeating seismic surveys as the best tool to observe the domination of driving mechanisms, heterogeneities, sealing unit integrity, and the effect of faults that the CO_2 front faces.

The main reason for having a faster CO_2 distribution of the compositional case compared to the black-oil case is fluid properties and the CO_2-brine interactions in the reservoir. In the black-oil case, the density of fluid phases depends on the given density at surface conditions and the value of the formation volume factor in the PVT table, which changes as a function of pressure. Moreover, the viscosity also is provided in the PVT table and changes slightly as pressure changes in the reservoir. In contrast, the compositional model using the CO2STORE module is not provided with PVT table values since it uses a cubic EoS to calculate the fluid properties in the simulation. It was observed that the brine density and viscosity calculated in the compositional case were higher than those of the black-oil case (see Table 5.3). As mentioned, the gas viscosity and density for both simulation cases are identical. Since the density difference between fluid phases is higher in the compositional case than the black-oil case, a faster vertical migration is expected from the injected CO_2, which leads to filling the top of the formation and upward movement towards the northern part of the model. In addition, the mobility ratio is larger for the compositional case since the viscosity difference in the compositional case is more substantial than the black-oil case. In total, it can be stated that both density and viscosity were the primary reasons for having CO_2 distributions with different paces and mobility. Forecasting CO_2 footprint and CO_2-brine behavior are associated with high ambiguity, especially at the early stages of the project before the injection starts to operate. Nevertheless, reservoir simulation is the best tool to approximate the possible behavior of fluids and the extension of the super-critical fluid, especially to convince the public and the authorities of the capability of some suitable reservoirs with low risk and cost-effective approaches.

Due to the presence of components rather than phases and the need to solve more equations, such as cubic equations of state to describe the state of components and calculate some crucial properties such as density in the reservoir based on pressure and temperature, compositional

simulations are computationally more expensive than black-oil models (constant in our project). According to this project, the computing time for the compositional simulation is around 3.5 times that of the black-oil simulation. The compositional model is the best option for projects with sufficient time to study or access computer clusters, especially because the calculations can be more closely tied to what is predicted to happen in the reservoir. Furthermore, ECLIPSE Schlumberger has developed the CO2STORE module for CO_2 storage in saline aquifers, which is worth testing or using as a benchmark. On the other hand, black-oil simulations can generate findings much faster than the compositional model, with minor differences in some parameters. As a result, the black-oil simulator is a better choice when working on a project with a limited amount of time or sensitivity studies with many simulated scenarios to compare.

5.2 Sensitivity analysis

Reservoir models used for numerical simulation are based on field observation, geological studies, and interpretations; thus, they can be highly uncertain in different aspects, especially at the early stages of a field development. CO_2 storage in saline aquifers is an emerging field, where the industry started to gain experience after the Sleipner CO_2 storage project in 1996, followed by In Salah and Snøhvit projects. This means that the data available and the industry's experience are much less than other subsurface projects such as hydrocarbon production or even CO_2 EOR. Thus, it is necessary to quantify and analyze the risks associated with CO_2 storage in saline aquifers before significant investments can lead to failure.

Several numerical reservoir simulation runs are required to observe the impact of uncertain parameters such as faults, the true connected pore volume to the reservoir, porosity, and permeability values, and other factors affecting pressure and CO_2 plume distribution in the reservoir to comprehensively study and quantify the risks associated with CO_2 storage projects in saline aquifers. The uncertainty and risk associated with CO_2 storage will decrease significantly after several years of injection, collecting sufficient data about pressure, temperature values and observing the CO_2 footprint using repetitive seismic surveys and/or other helpful monitoring tools. Reservoir models could be modified accordingly to predict the CO_2 storage process in the reservoir more accurately. This project's sensitivity analysis covers six uncertain parameters. It highlights the influence on pressure, free and dissolved CO_2 levels, and CO_2 plume distribution over 500 years. It should be emphasized that the impact of each sensitivity parameter can vary in magnitude over time, with some examples having a long-term (>500 years) influence and others having a short-term (50-200 years) impact. As a result, the time chosen for displaying 3D map views of CO_2 footprint may vary from case to case. However, in Appendix D, recorded videos covering the whole simulation period have been provided to help better comprehend each sensitivity. The following are the uncertain parameters:

- Permeability ratio
- F6 Fault transmissibility
- Relative permeability curve
- Residual gas saturation
- Pore volume
- Rock Compressibility

Permeability ratio

Vertical permeability is usually obtained as a ratio with horizontal permeability, which can be obtained either by correlations or lab measurements. For the base case model, the vertical to horizontal permeability is considered to be $K_V/K_H = 0.1$. To do the sensitivity studies, three other values of 0.3, 0.5, and 0.7 were assigned to K_V/K_H.

Figure 5.6 indicates that the initial pressure in the injection area is around 278 bar for all cases, followed by a 16 bar increase in pressure after 45 Mt of CO_2 injected in the and reaching the maximum pressure value of 293 bar. After the injection stops, the pressure decreases dramatically and stabilizes from 2070 till 2500 at the pressures between 285.6 and 285.8 bar. With higher K_V/K_H, the stabilized pressure increases, but very slightly, and the most considerable pressure difference is between the base case (K_V/K_H=0.1) and Case 3 (K_V/K_H=0.7), which is less around 0.2 bar. Thus, it can be stated that the pressure is a weak function of the permeability ratio since the differences are not extreme for all simulation cases.

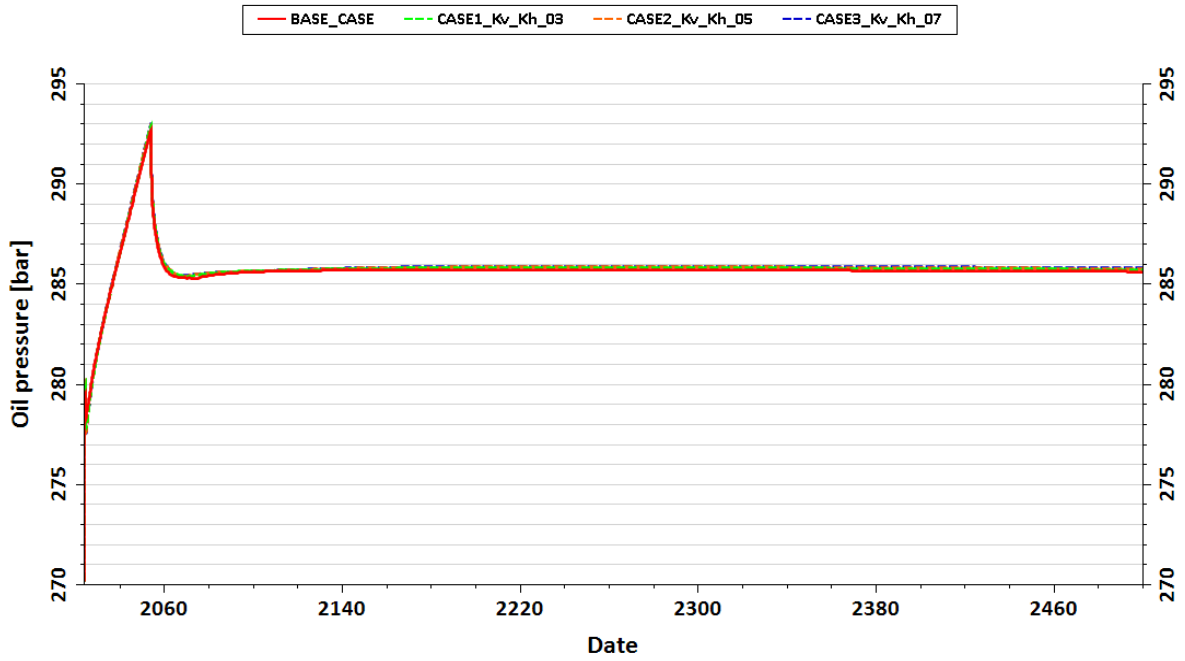

Figure 5.6 Reservoir pressure in the injection area (Grid 43,49,44) for different permeability ratios. The base case is assigned with permeability ratio of 0.1, while Case 1, Case 2 and Case 3 are assigned with permeability ratios 0.3, 0.5 and 0.7, respectively.

According to Table 5.5, the amount of free CO_2 is more for cases with a higher permeability ratio for three different time intervals. Subsequently, for the base case with the horizontal to permeability ratio K_V/K_H =1, there is more dissolved gas in 2100, 2300, and 2500. It is shown that no free gas reaches the boundary at least until the year 2100. Cases 1, 2, and 3 will have some amount of free CO_2 in the next time interval, the year 2300, while for the base case, there's

no free CO_2 that has reached the boundary yet. By the year 2500, Case 3 has the highest amount of free and dissolved CO_2 in the boundary region, while the base case has the least amount of free and dissolved CO_2 in the same region. The fact that more dissolved CO_2 has been reported for the base case can be confirmed by its stabilized pressure value in the pressure plot, which is the least among all four cases.

Table 5.5 The amount of free/dissolved CO_2 in the boundary and the model over three time intervals 2100, 2300, and 2500 for different permeability ratios.

45 Mt injection		**Permeability ratio**							
		Base Case		**$K_V/K_H = 0.3$**		**$K_V/K_H = 0.5$**		**$K_V/K_H = 0.7$**	
	Year	**Model**	**Boundary**	**Model**	**Boundary**	**Model**	**Boundary**	**Model**	**Boundary**
Free CO_2 (Mt)	2100	40.60	0.00	41.03	0.00	41.20	0.00	41.30	0.00
	2300	39.94	0.06	40.13	0.18	40.15	0.26	40.16	0.33
	2500	39.26	0.43	38.75	1.14	38.51	1.45	38.38	1.65
Dissolved CO_2 (Mt)	2100	4.40	0.00	3.96	0.00	3.80	0.00	3.69	0.00
	2300	5.06	0.00	4.67	0.02	4.57	0.02	4.49	0.02
	2500	5.30	0.01	5.07	0.04	4.99	0.05	4.92	0.05

The 3D images and the intersectional view of Figure 5.7 indicate that in the year 2120, more CO_2 has been moved vertically to accumulate on top of the formation. The CO_2 accumulated in deeper parts of the formation increases with increasing the permeability ratio. In the base case, CO_2 faces low permeable layers in some regions that help prevent some amount of injected fluid from further vertical migration. In addition, more viscous dominating flow is observed in the base case compared to three other cases with a higher permeability ratio. Cases 1, 2, and 3 show similar CO_2 distributions with minor vertical migration differences. Results show that increasing the permeability ratio affects the vertical migration considerably where the injected fluid does not face difficulties reaching the top of the formation, meaning that the domination of gravity force is more significant when the vertical permeability ranges in the formation are closer to the horizontal permeability ranges. Subsequently, viscous forces will lose their impact, and sweep efficiency will be insignificant.

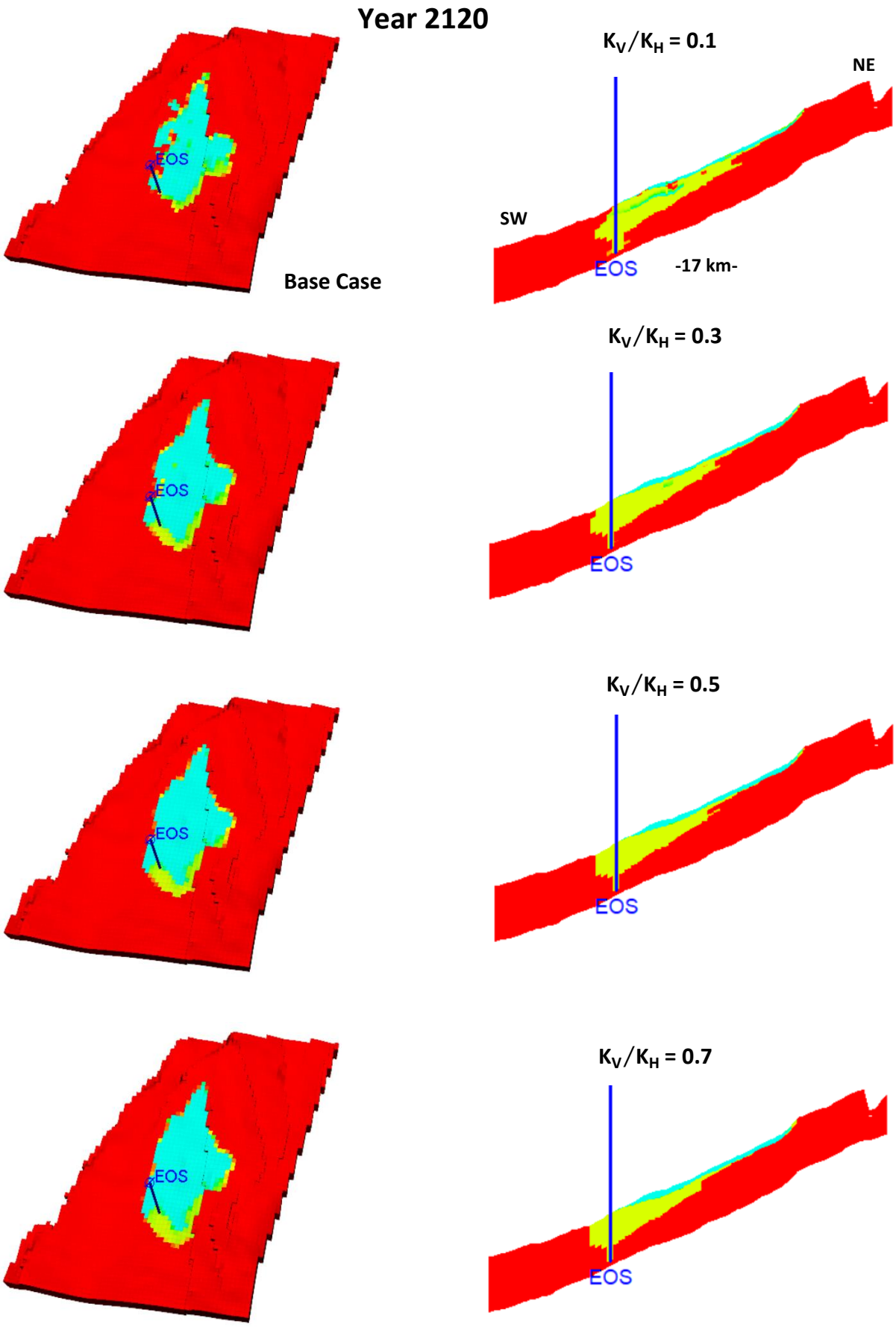

Figure 5.7 CO_2 footprint in the Aurora model in the year 2120 for different permeability ratios **(Left)** 3D map view **(Right)** Northern-Southern intersectional view.

Fault transmissibilities

The model's closest and most important fault is the F6 Fault, with an uncertain fault transmissibility value. In addition to the base case model with 0.1 as the fault transmissibility multiplier for F6, three more cases were used with the transmissibility multipliers 0.001, 1, 10 classified as sealing, conduit, and fully conduit, respectively.

The initial pressure in the injection area is around 278 bar for all cases except for Case 1 (sealing) with 279 bar of pressure, followed by a 16 bar increase in pressure after 45 Mt of CO_2 injected in and reaching the maximum pressure value of 293 bar, except the maximum pressure for Case 1 which is around 297 bar (Figure 5.8). After the injection stops, the pressure decreases dramatically and stabilizes from 2070 till 2500 at the pressures between 285.6 and 285.8 bar. As the fault transmissibility multiplier (MULTPV) increases for the F6 Fault, the pressure stabilizes at lower values; however, the highest pressure difference between Case 1 as the sealing case and Case 3 as the fully conduit case is around 0.2 bar. According to the results, the pressure effect is only significant during the injection period and when F6 acts as a sealing unit. The reason for obtaining such pressure is that the F6 Fault is relatively close to Eos well (2 km away). Subsequently, some part of the distributed CO_2 moves on the eastern part towards the fault. However, since CO_2 cannot migrate across the fault, the pressure cannot dissipate easily. Thus, the pressure experiences a higher pressure during the injection period.

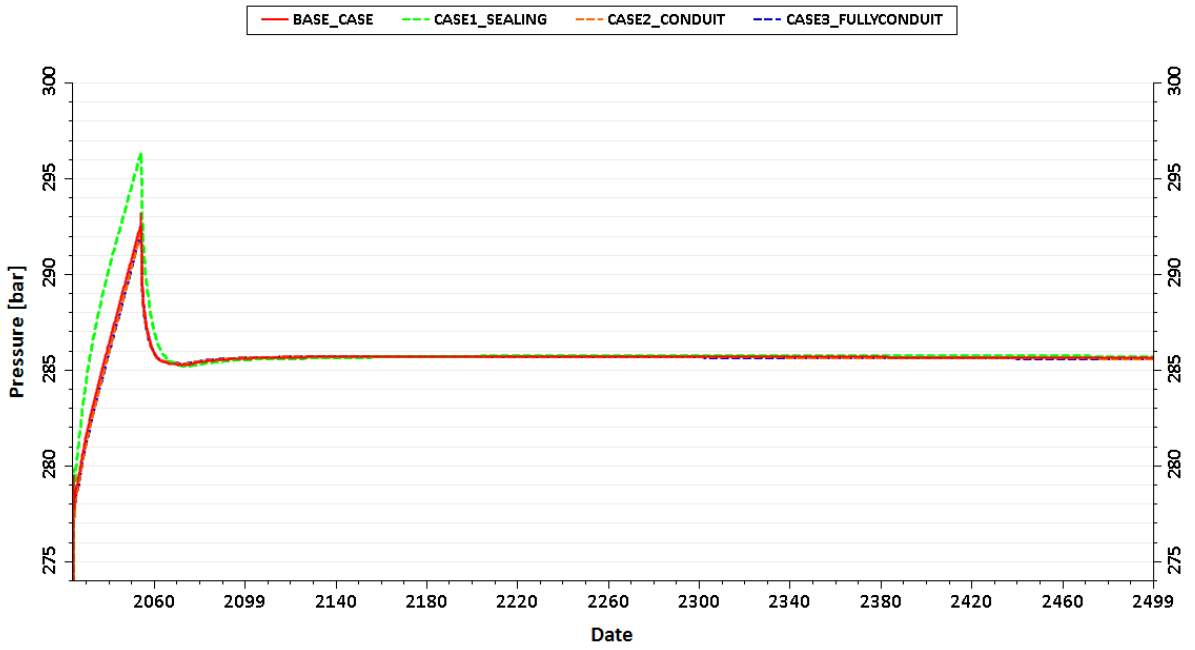

Figure 5.8 Reservoir pressure in the injection area (Grid 43,49,44) for different F6 Fault transmissibilites. The base case is assigned fault transmissibility multiplier of 0.1, while Case 1, Case 2 and Case 3 are assigned fault transmissibility multipliers of 0.001, 1 and 10, respectively.

Table 5.6 shows that the amount of free CO_2 is more as the fault transmissibility value decreases for three different time intervals shown in the table. As a result, for the sealing case where F6 fault act as a sealing unit, less dissolved gas is seen in the dissolved gas reported in 2100, 2300, and 2500. It is shown that no free gas reaches the boundary at least until the year 2100. In 2300, a small portion of free gas has reached the northern region for the base case and the sealing case, while no CO_2 was seen in the same region for the conduit and fully conduit case. In the year 2500 has the highest amount of free and dissolved CO_2 in the boundary region, while conduit and fully conduit cases have the least amount of free and dissolved CO_2 in the same region. The main reason that more CO_2 is dissolved for cases with higher fault transmissibility is due to the fact that CO_2 has been distributed more widely in the reservoir, and hence there's more contact between the two phases, leading to more dissolved CO_2 in the brine phase.

Table 5.6 The amount of free/dissolved CO_2 in the boundary and the model over three time intervals 2100, 2300, and 2500 for different F6 Fault transmissibilities.

45 Mt injection		**F6 Fault transmissibility**							
		Base Case		**Sealing**		**Conduit**		**Fully conduit**	
	Year	**Model**	**Boundary**	**Model**	**Boundary**	**Model**	**Boundary**	**Model**	**Boundary**
Free CO_2 (Mt)	2100	40.60	0.00	40.67	0.00	40.61	0.00	40.58	0.00
	2300	39.94	0.06	39.81	0.34	39.99	0.00	39.98	0.00
	2500	39.26	0.43	38.62	1.25	39.54	0.13	39.50	0.14
Dissolved CO_2 (Mt)	2100	4.40	0.00	4.33	0.00	4.39	0.00	4.42	0.00
	2300	5.06	0.00	4.83	0.02	5.01	0.00	5.02	0.00
	2500	5.30	0.01	5.09	0.04	5.32	0.01	5.35	0.01

The 3D images and the intersectional view of Figure 5.9 in the year 2200 indicate that no portion of the CO_2 managed to cross the F6 fault in the sealing case. Consequently, it has moved to the northern part of the model and reaches the boundary faster than other cases. In the Base case, some portion of the injected CO_2 enters the eastern part of the F6 fault. In contrast, more CO_2 is seen on the eastern part of the F6 Fault for the conduit and fully conduit cases. It can be concluded CO_2 footprint is similar for the conduit case and the fully conduit case, with a slight difference to the base case. The most significant effect on the CO_2 plume is shown when the fault transmissibility value is close to zero, leading to substantially changing the direction of the CO_2 plume.

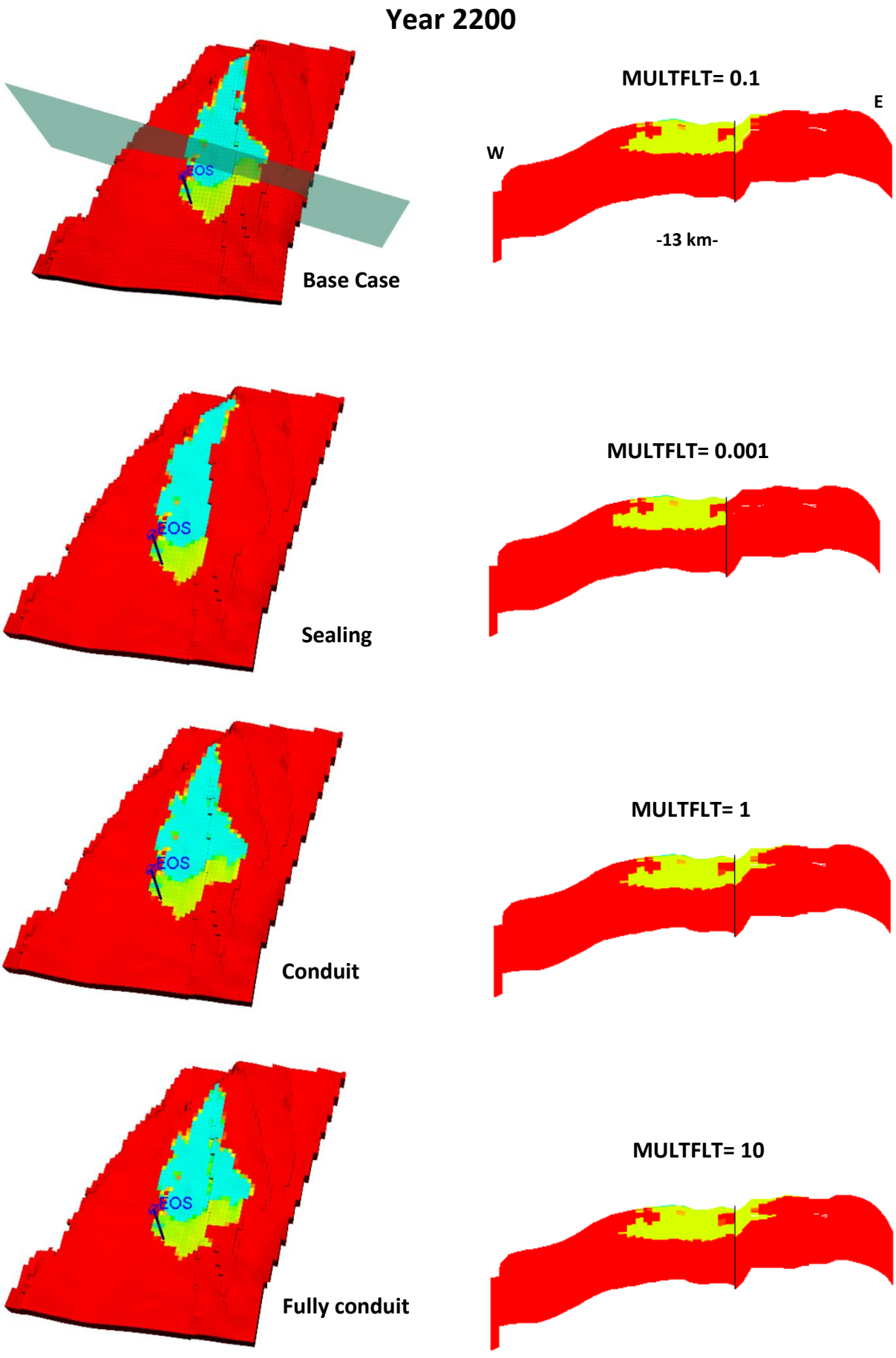

Figure 5.9 CO_2 footprint in the Aurora model in the year 2200 for different F6 fault transmissibility values **(Left)** 3D map view **(Right)** Eastern-Western intersectional view.

Relative permeability curve

A sensitivity study was done using the relative permeability curves of the Utsira, Tubåen, and Johansen Formation. The base case model is based on the saturation end-point values of the Johansen Formation, reported by Gassnova (2012). Two more cases were also studied, with one using Utsira's relative permeability curve that was used in the default model and Tubåen's relative permeability curve that was included in the data file of the model but was not used.

The highest pressure elevation occurs during the injection phase in Case 1, where the saturation end-points of Tubåen's formation have been input, while the highest stabilized pressure occurs in Case 2, where the Utsira saturation end-point values have been entered (Figure 5.10). The base case has the maximum stabilized pressure before the year 2150, after which the Utisra case has the maximum stabilized pressure. The highest pressure difference is almost 1 bar between Case 1 and Case 2. After 500 years, the pressure near the well injection remains stable between 285.5 and 286 bar, corresponding to Utsira and Tubåen's end-point values, respectively.

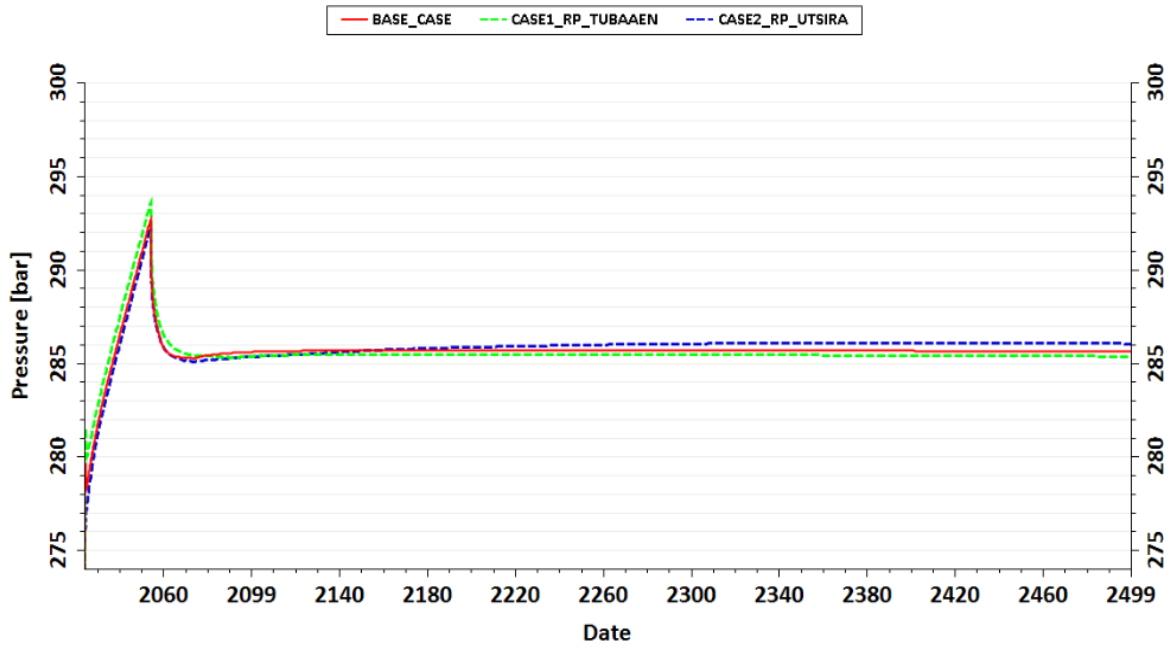

Figure 5.10 Reservoir pressure in the injection area (Grid 43,49,44) for different relative permeability curves. The base case is assigned with saturation end-point values of the Johansen Formation, while Case 1 and Case 2 are assigned with saturation end-points of the Tubåen and Utsira formations, respectively.

According to Table 5.7, the amount of free or dissolved CO_2 obtained by three cases using different saturation end-point values is not generally highly different. In the year 2100, the CO_2 plume stays in the model region for all three cases, with more dissolution of CO_2 for the base case than other cases. In 2300, the only case with CO_2 plume extension in the northern boundary is the Utsira case, with a dissolution amount of CO_2 extremely close to the base case. In the year 2500, the amount of free CO_2 and dissolved CO_2 in the Utsira and base cases are quite

close, with slight differences. In the same period, all of the injected fluid for the Tubåen case stays in the model region and has the least dissolved CO_2.

Table 5.7 The amount of free/dissolved CO_2 in the boundary and the model over three time intervals 2100, 2300, and 2500 for different relative permeability curves.

45 Mt injection		**Relative permeability curve**					
		Base Case		**Tubåen**		**Utsira**	
	Year	**Model**	**Boundary**	**Model**	**Boundary**	**Model**	**Boundary**
Free CO_2 (Mt)	2100	40.60	0.00	41.16	0.00	41.31	0.00
	2300	39.94	0.06	40.41	0.00	35.94	4.32
	2500	39.26	0.43	40.10	0.00	33.05	6.70
Dissolved CO_2 (Mt)	2100	4.40	0.00	3.84	0.00	3.69	0.00
	2300	5.06	0.00	4.59	0.00	5.00	0.05
	2500	5.30	0.01	4.89	0.00	5.14	0.11

The reservoir's 3D images and intersectional views show considerably varying results in both the amount of CO_2 trapped near and away from the well and the mobility of the CO_2 (Figure 5.11). In the year 2500, Case 1 (Tubåen) shows that the CO_2 plume has much less mobility than other cases. Since the Tubåen case has the highest residual gas saturation value, more CO_2 remains trapped in the pores due to the imbibition of brine; thus, less CO_2 accumulates on top of the formation for upward movement towards the northern part of the model. However, since the irreducible water saturation is low ($S_{wirr} = 0.1$), it can invade the majority of the pores and displace brine on top of the formation. Case 2 (Utsira) has the lowest residual gas saturation and irreducible water saturation between the three cases. Accordingly, more CO_2 can escape from the pores and migrate vertically, draining 93% of the brine in the pores and moving significantly faster than in the other cases. More CO_2 is trapped in the pores in the base case (Johansen) than in the Utsira case, but less CO_2 is trapped in the Tubåen scenario. In addition, the Johansen case has a smaller CO_2 plume extent than the Utsira case and a larger CO_2 plume extension than the Tubåen case. In total, Residual gas saturation and irreducible water saturation can considerably impact the CO_2 plume extension in the reservoir and the amount of CO_2 trapped in the pores and immobilized. The shape of the saturation function also affects the amount of mobile CO_2, where more curvature relative permeability curves will make CO_2 less mobile for lower gas saturations

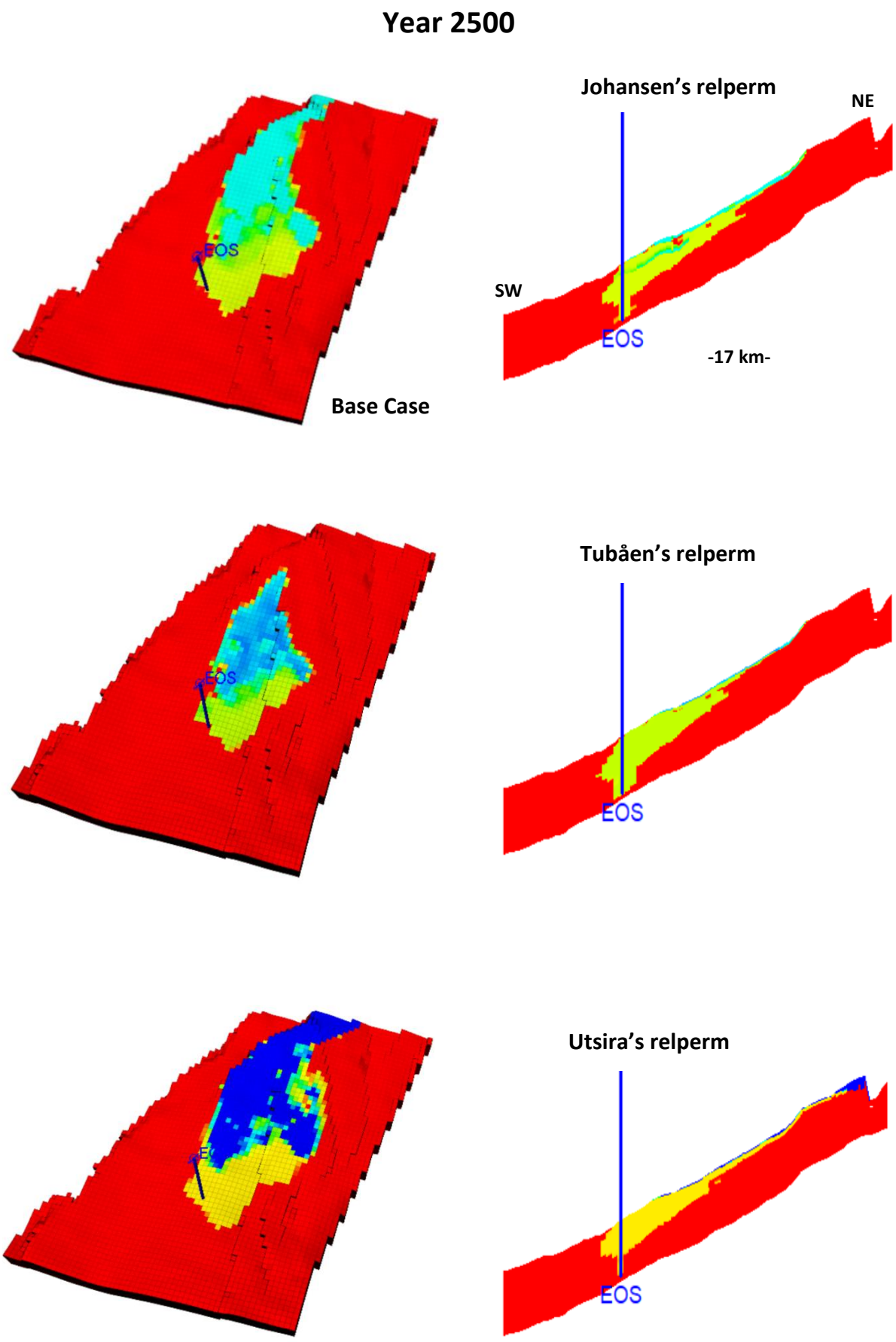

Figure 5.11 CO_2 footprint in the Aurora model in the year 2500 for different relative permeability curves **(Left)** 3D map view **(Right)** Northern-Southern intersectional view.

Residual gas saturation

Usually, drainage relative permeability curves are provided and utilized for the reservoir simulation, where the residual gas saturation values can strongly impact the amount of CO_2 that can be trapped in the pores. Since the uncertainty on the most representative residual gas saturation in the Johansen Formation is still high, a sensitivity study on different residual gas saturation values was conducted in this project. The base case model has a residual gas saturation of around 30%, while two other cases were assigned the residual gas saturation values of 25% and 20%.

Figure 5.12 indicates that the initial pressure in the injection area is around 278 bar for all cases, followed by a 16 bar increase in pressure after 45 Mt of CO_2 injected in the and reaching the maximum pressure value of 293 bar. After the injection stops, the pressure falls substantially. It stabilizes from 2070 till 2500 at the pressures between 285.6 in the Base case and 285.7 in Case 2, meaning the maximum stabilized pressure difference is about 0.1 bar. It can be concluded that changing the residual gas saturation does not considerably affect the reservoir pressure.

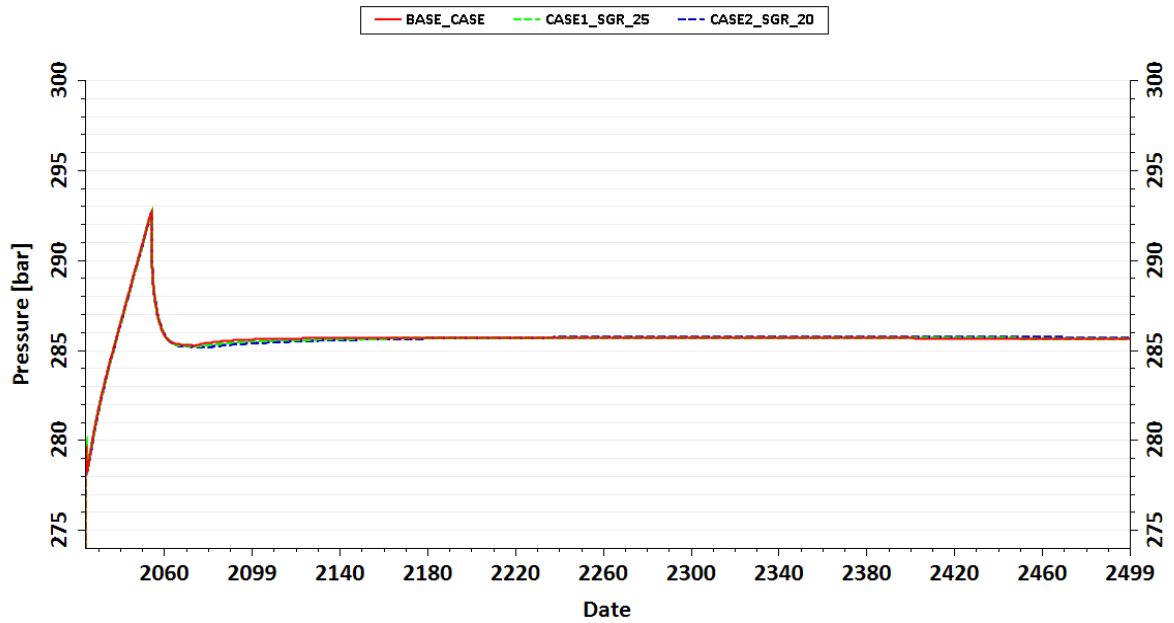

Figure 5.12 Reservoir pressure in the injection area (Grid 43,49,44) for different residual gas saturations. The base case is assigned with residual gas saturation of 0.298, while Case 1 and Case 2 are assigned with residual gas saturations 0.25 and 0.20, respectively.

Looking at Table 5.8, it can be stated that the amount of free CO2 is less as the residual gas saturation decreases for three different time intervals shown in the table. By 2100, the CO2 plume front does not reach the boundary, meaning any free or dissolved CO2 in the first time

interval. However, more gas is dissolved for Case 2, where the residual gas saturation is at its lowest value. In the year 2300, it can be observed that free CO2 has reached the northern boundary, where for Case 2, more free CO2 exist in that region, and some portion of it has been dissolved, while the amount of dissolved CO2 for Case 1 is less and for the base case is almost zero. Lower residual gas saturation means more free CO2 exists in the formation, leading to more contact with the brine phase in the formation. As more CO2 is in contact with the brine phase, the dissolution of CO2 in the brine phase increases, and as a result, CO2 occupies less volume, and the pressure dissipates easier, leading to a lower pressure stabilization.

Table 5.8 The amount of free/dissolved CO_2 in the boundary and the model over three time intervals 2100, 2300, and 2500 for different residual gas saturations.

45 Mt injection		**Residual gas saturation**					
		Base Case		**S_{gr}=0.25**		**S_{gr}=0.20**	
	Year	**Model**	**Boundary**	**Model**	**Boundary**	**Model**	**Boundary**
Free CO_2 (Mt)	2100	40.60	0.00	40.32	0.00	40.05	0.00
	2300	39.94	0.06	39.01	0.45	37.01	1.94
	2500	39.26	0.43	37.33	1.74	34.88	3.60
Dissolved CO_2 (Mt)	2100	4.40	0.00	4.68	0.00	4.95	0.00
	2300	5.06	0.00	5.51	0.03	5.98	0.07
	2500	5.30	0.01	5.87	0.06	6.42	0.10

The CO_2 footprint shown by the 3D and intersectional view of three cases indicates that as the residual gas saturation decreases, more amount of CO_2 has the ability to escape vertically and fill the top of the formation (Figure 5.13). Thus, the CO_2 on top of the formation tends to move upward and touch more grid cells in the northern part of the model with less residual gas saturation values. As mentioned previously, during CO_2 distribution in the reservoir, brine imbibition causes a portion of the CO_2 phase to be trapped in the pores and left behind the CO_2 plume in residual trapping. Therefore, it can be stated that when the residual gas saturation increases, more amount of CO_2 is trapped in the pore bodies, leading to less mobile CO_2 and consequently a minor CO_2 plume extension.

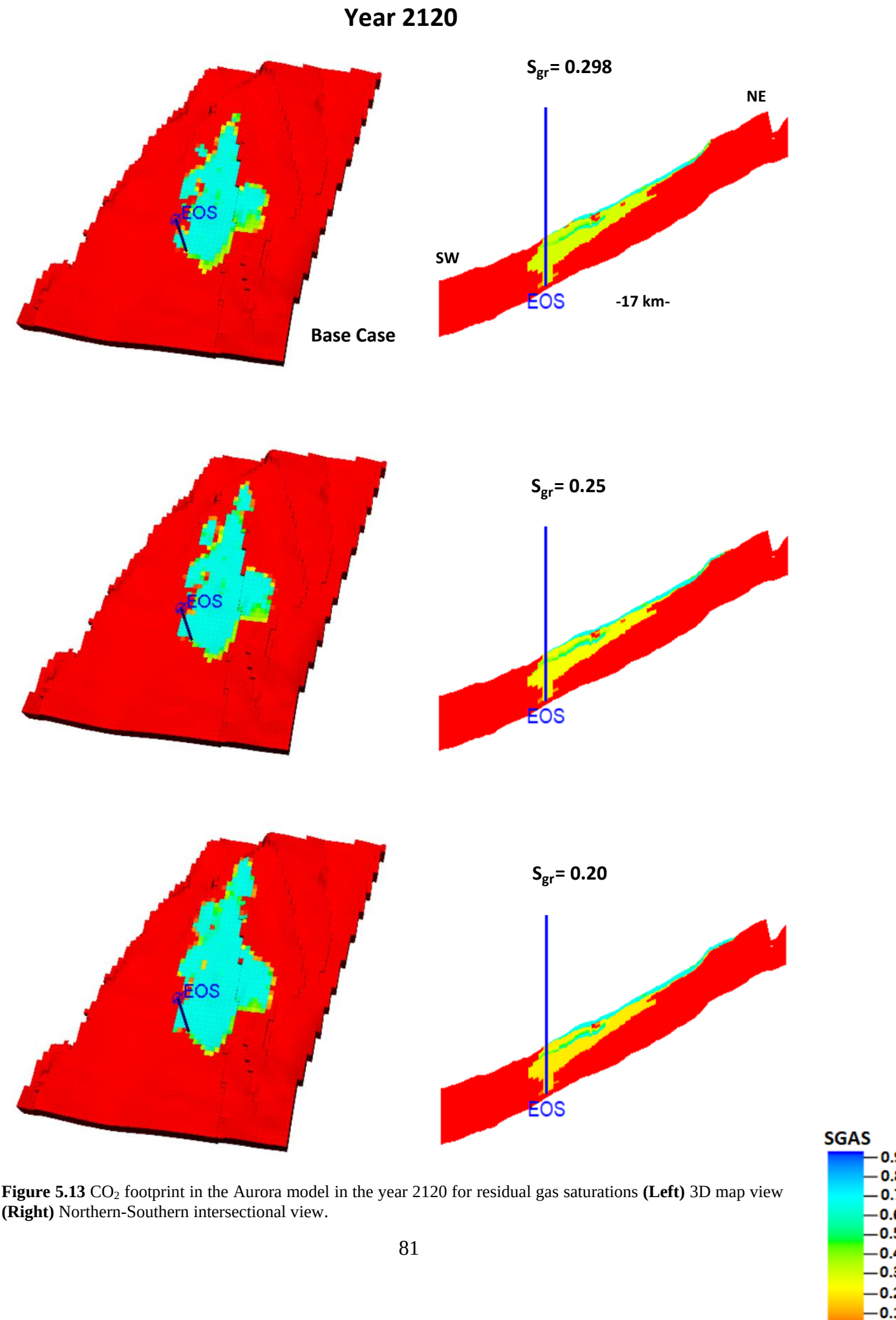

Figure 5.13 CO_2 footprint in the Aurora model in the year 2120 for residual gas saturations **(Left)** 3D map view **(Right)** Northern-Southern intersectional view.

Pore volume

A sensitivity study has been done on the pore volume of the model as one of the major uncertainties of the Aurora model. The base case has a total pore volume of 50 Sm^3 to account for the western part of the Vette fault. Two other cases with 90 Sm^3 and 150 Sm^3 has been included to observe the major differences and similarities.

Figure 5.14 reveals that the initial pressure is around 278 bar for all three cases, followed by various pressure build-up values. The maximum pressure in the base case, which has the smallest pore volume in the model, is 293 bar, whereas it is 287 and 284 bar in Cases 1 and 2, with pore volumes of 90 and 150 Gm^3, respectively. Additionally, all three cases stabilize the pressure to varying degrees. The base case saw the greatest pressure stabilization at the pressure of 286 bar, while Case 1 and Case 2 had stabilization pressures of 278 and 275 bar, respectively. The primary reason for obtaining different pressure values is different connected pore volumes in each case. The injected CO_2 starts to displace the brine near, and hence the brine is compressed, leading to pressure increase, especially near the well area. With the available pore volume being smaller, injecting the same amount of CO_2 will compress a smaller volume of brine, leading to a higher pressure build-up during the injection period and higher stabilization pressure during the post-injection period. As a result, it can be stated that pore volume strongly affects the maximum pressure during the injection period and the stabilization of pressure during the post-injection period.

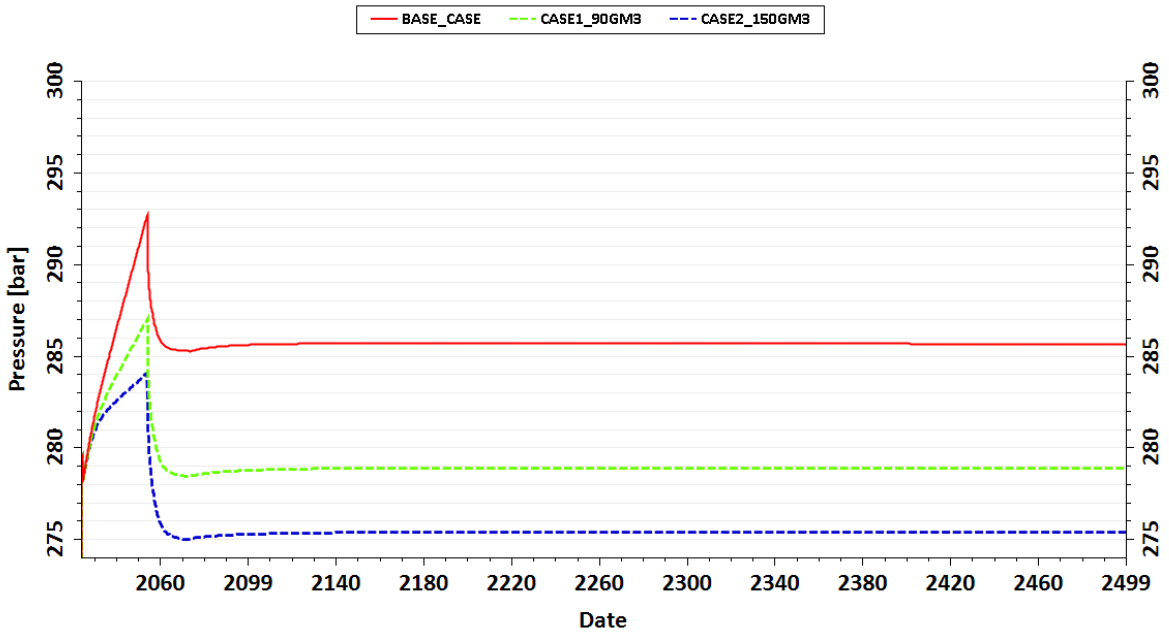

Figure 5.14 Reservoir pressure in the injection area (Grid 43,49,44) for different connected pore volumes. The base case is assigned the total pore volume of 50 Gm^3, while Case 1 and Case 2 are assigned with the total pore volumes of 90 and 150 Gm^3, respectively.

Table 5.9 demonstrates that the amount of free CO_2 is larger with smaller pore volumes. The CO_2 plume front does not reach the boundary in any of the three examples in the year 2100, implying no free or dissolved CO_2 at the northern boundary in the first time interval. The CO_2 plume reaches the northern boundary for all models by the end of simulation time. More free CO_2 remains in the boundary region for Case 2, and a tiny portion of CO_2 is dissolved in the brine system in the same region. Likewise, more CO_2 appears in the boundary for Case 2 in the last time interval; yet the amount of dissolved gas in the same region for Cases 1 and 2 is equivalent to the amount of dissolved gas in the base case with a subtle difference. In general, the variations in free and dissolved CO_2 for all three cases are minor. It can be claimed that changing the pore volume slightly affects the amount of free or dissolved CO_2 and minor differences are due to obtaining different pressure values when changing the pore volume, leading to different density and viscosity values for the CO_2 and brine phases.

Table 5.9 The amount of free/dissolved CO_2 in the boundary and the model over three time intervals 2100, 2300, and 2500 for different connected pore volumes.

45 Mt injection		**Pore volume**					
		50 Gm^3		**90 Gm^3**		**150 Gm^3**	
	Year	**Model**	**Boundary**	**Model**	**Boundary**	**Model**	**Boundary**
Free CO_2 (Mt)	2100	40.60	0.00	40.55	0.00	40.52	0.00
	2300	39.94	0.06	39.86	0.09	39.81	0.13
	2500	39.26	0.43	39.07	0.57	38.97	0.65
Dissolved CO_2 (Mt)	2100	4.40	0.00	4.44	0.00	4.49	0.00
	2300	5.06	0.00	5.05	0.00	5.06	0.00
	2500	5.30	0.01	5.33	0.03	5.35	0.03

Figure 5.15 indicates that in the year 2300, the injected CO_2 has invaded the same parts of the model for all three cases, which signifies that all of the CO_2 footprints, whether close to the well in terms of horizontal or vertical movement and distant from the well towards to the northern boundary, are nearly identical. However, the CO_2 movement with the largest pore volume is slightly faster. In fact, the pore volumes in the boundaries should not influence the mobility of CO_2 distribution since the injected fluid cannot determine how small or large the reservoir is before it hits the reservoir's boundary. Small differences in CO_2 distribution is due to the pressure variations as a result of changing the total pore volume that leads to different density and viscosity values for the CO_2 and brine phases.

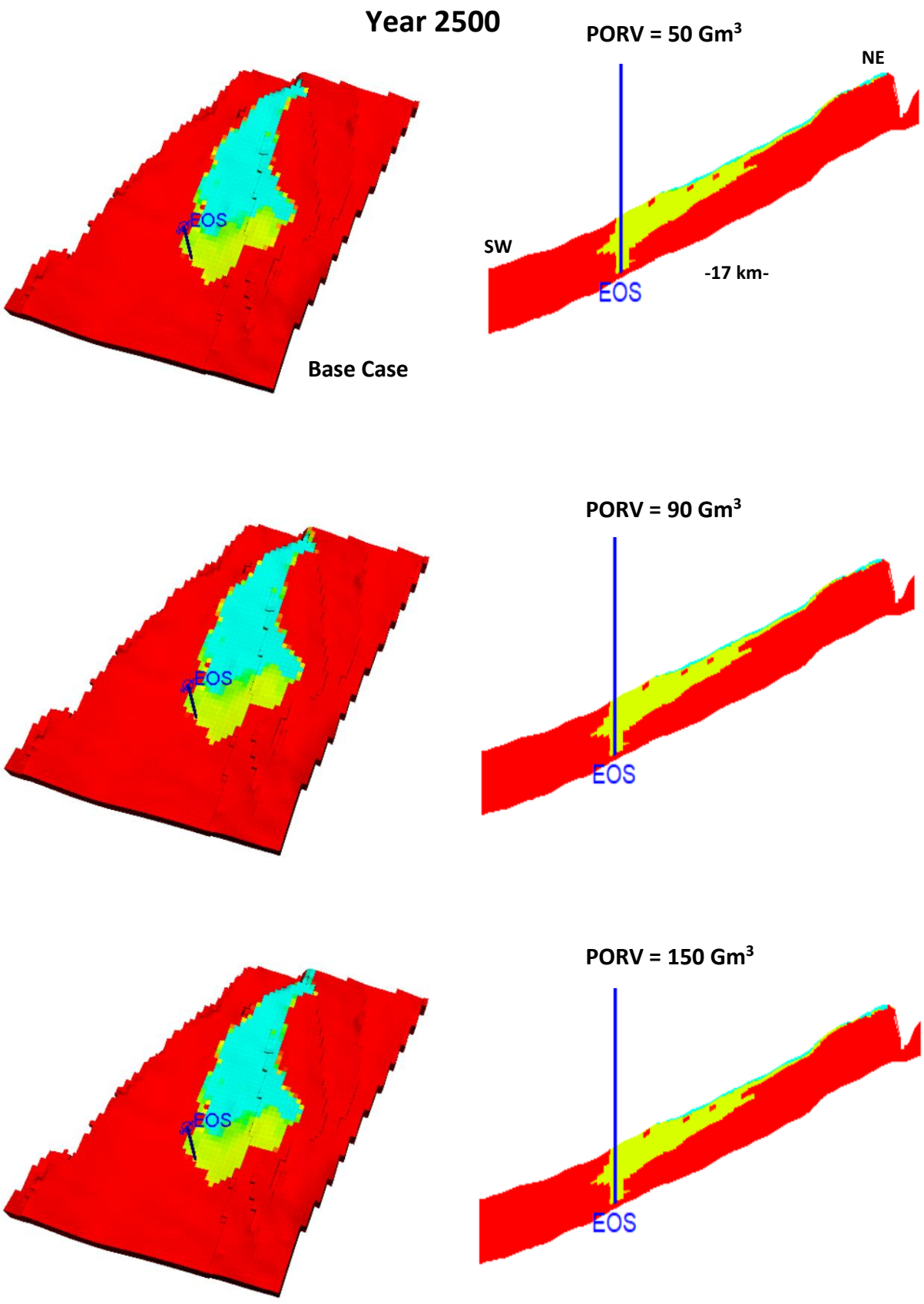

Figure 5.15 CO_2 footprint in the Aurora model in the year 2500 for different pore volumes **(Left)** 3D map view **(Right)** Northern-Southern intersectional view.

Rock compressibility

A sensitivity study has been done on the rock compressibility of the model, which has been found to lie in the range of C_r= 3.5E-5 - 5.2E-5 bar^{-1} in the Johansen Formation (Gassnova, 2012). The base case has rock compressibility of C_r= 5E-5 bar^{-1}, followed by two other cases with rock compressibility of C_r= 4E-5 bar^{-1} and C_r= 3E-5 bar^{-1}.

The initial pressure for all three cases is roughly 278 bar, although the pressure build-up is larger for cases with lower rock compressibility (Figure 5.16). Case 1, with the lowest rock compressibility, has a maximum pressure of 297 bar. In contrast, Case 2, with lower rock compressibility than the base case, has a maximum pressure of 295 bar. The base case does have a maximum pressure of 293 bar. Depending on their rock compressibility value, the cases are subjected to varying stabilization pressures during the injection and post-injection phases. Case 1, with the lowest rock compressibility, stabilizes at the highest pressure of 290 bar, followed by Case 2 and the base case at 288 and 286 bar, respectively. The difference in pressure levels during the injection and post-injection periods is that pore pressure increases once the injected fluid enters the formation, attempting to stress the porous medium to generate more void space (porosity) to release the pressure. For cases with higher rock compressibility, pressure elevation will more significantly affect the formation's porosity, making more void space for the pressure to dissipate in the reservoir.

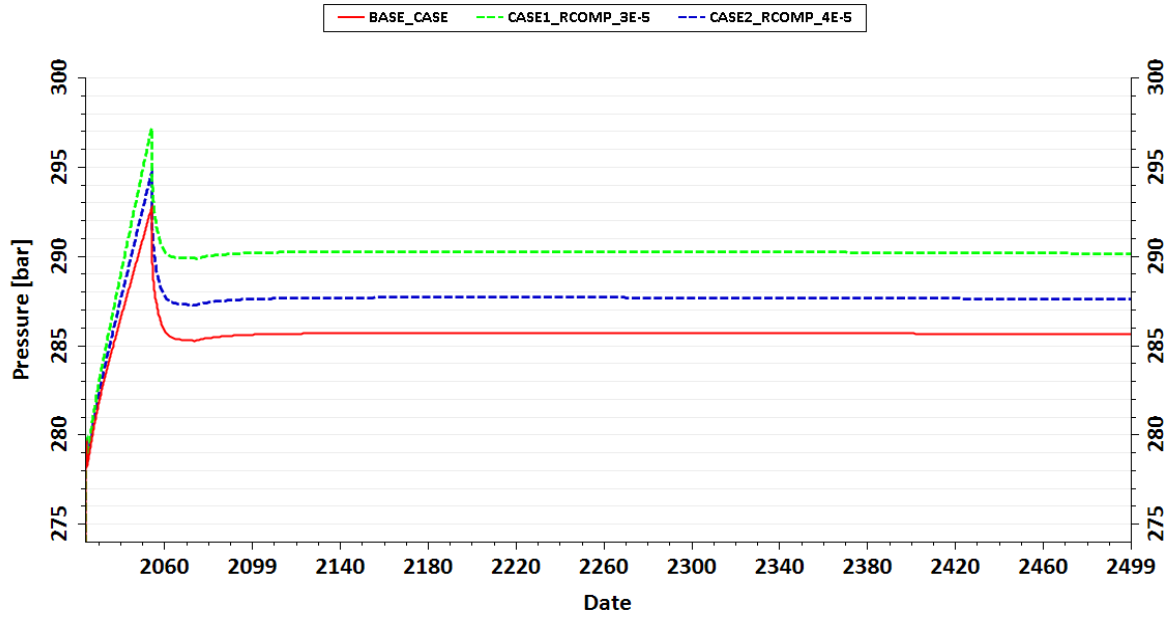

Figure 5.16 Reservoir pressure in the injection area (Grid 43,49,44) for different rock compressibilities. The base case is assigned with rock compressibility of 5E-5 bar^{-1}, while Case 1 and Case 2 are assigned with rock compressibilities of 3E-5 and 4E-5 bar^{-1}, respectively.

Free or dissolved CO_2 amount is almost consistent in all three instances with slight differences, as shown in Table 5.10. The CO_2 plume does not touch the northern boundary within the first period. The levels of dissolved CO_2 in the model region are only slightly greater for the base case with the highest compressibility. The CO_2 front reaches the grid cells in the north over the next time, the year 2300, with the state of being free. In the year 2500, more free CO_2 accumulates in the northern region, and a tiny fraction of CO_2 for all three cases is dissolved in the brine phase. In all three time intervals, the amount of CO_2 dissolved in the brine system is higher for the base case, resulting in less free CO_2. Nevertheless, more free CO_2 is collected in the base case's northern region at the end of the simulation. Altogether, there is a slight difference in the amount of free or dissolved CO_2, mainly due to the difference in pressure developments. In total, the rock compressibility has weak effects on the state of CO_2 in the free or dissolved in the brine phase.

Table 5.10 The amount of free/dissolved CO_2 in the boundary and the model over three time intervals 2100, 2300, and 2500 for different rock compressibilities.

45 Mt injection		**Rock compressibility**					
		Base Case		**4E-5 bar^{-1}**		**3E-5 bar^{-1}**	
	Year	**Model**	**Boundary**	**Model**	**Boundary**	**Model**	**Boundary**
Free CO_2 (Mt)	2100	40.60	0.00	40.63	0.00	40.65	0.00
	2300	39.94	0.06	39.97	0.04	40.00	0.03
	2500	39.26	0.43	39.30	0.39	39.36	0.35
Dissolved CO_2 (Mt)	2100	4.40	0.00	4.37	0.00	4.34	0.00
	2300	5.06	0.00	4.98	0.01	4.96	0.01
	2500	5.30	0.01	5.28	0.03	5.26	0.03

According to the 3D and intersectional images in Figure 5.17, in the year 2120, The CO_2 front has contacted more grid cells toward the northern part of the model for the base case compared to other cases, although the difference is not extreme. In intersectional images, the vertical movement and the amount of trapped CO_2 show similar results. As a result, altering the rock compressibility does not influence CO_2 distribution, which is true in practice. In conclusion, rock compressibility is a geology feature that has a massive effect on the severity of pressure fluctuations but has no major impact on CO_2 plume extension in the reservoir.

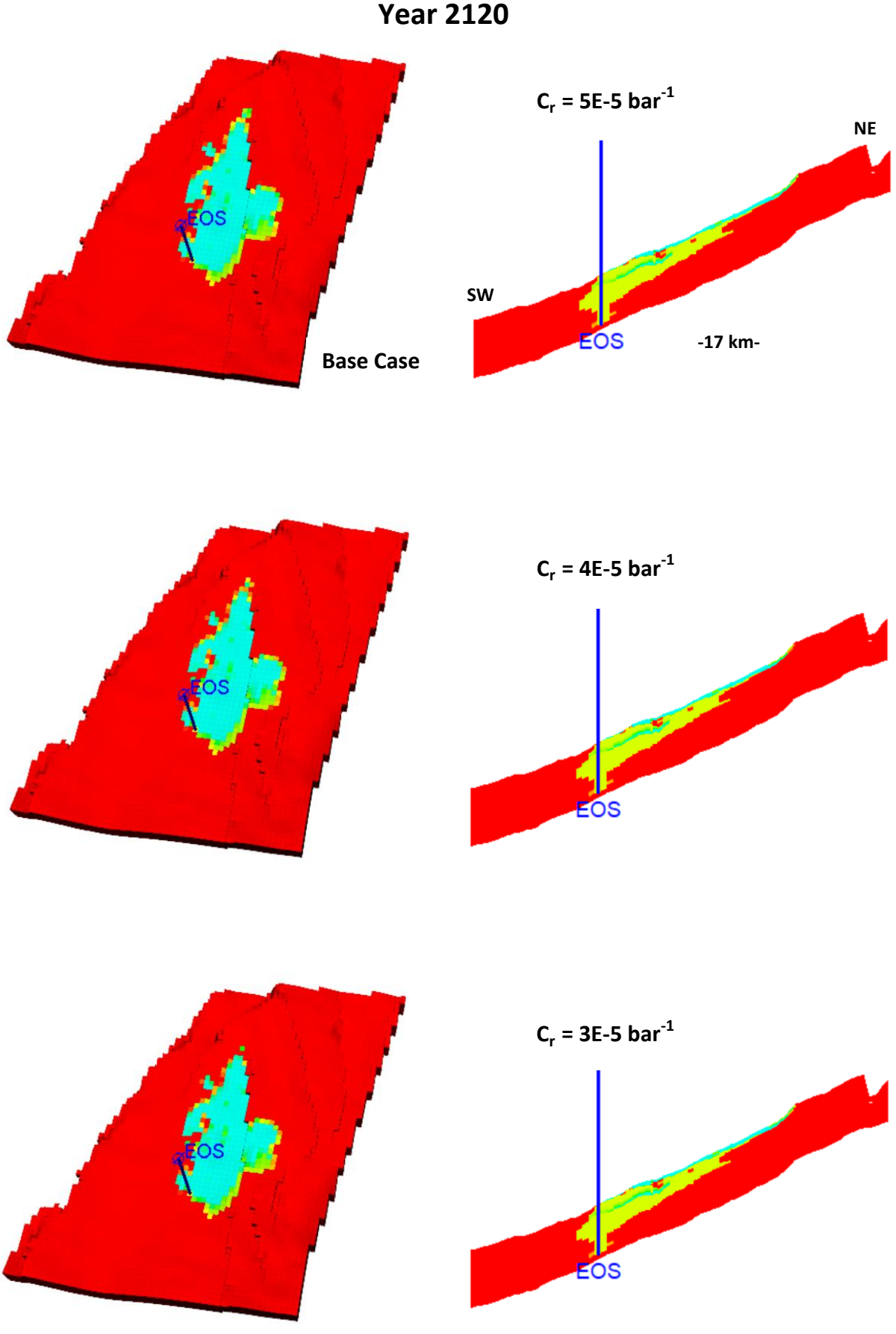

Figure 5.17 CO_2 footprint in the Aurora model in the year 2120 for different rock compressibilites **(Left)** 3D map view **(Right)** Northern-Southern intersectional view.

Overall, the impact of changing different uncertain parameters at different times within the uncertainty range on pressure build-up and stabilization, the amount of CO_2 that will be dissolved versus the rest that will be free, and the CO_2 plume extent over the reservoir for a period of around 500 years were investigated. Permeability ratio is a key element in preventing some portion of the injected CO_2 from migrating up, resulting in successful residual trapping and subsequent dissolution trapping. Furthermore, viscous force dominance will be extended to cases with a low permeability ratio, which will improve storage efficiency. Whether the fault property functions as a sealing unit with permeability close to zero or as a conduit that allows fluid to pass through it and diffuse more easily have a significant impact on CO_2 distribution. Compared to other cases, the F6 Fault, when functioning as sealing, has the greatest impact on CO_2 plume extent and pressure. The relative permeability curve was examined as one of the primary unknown parameters. It was discovered that modifying the saturation end-points significantly impacts the residual trapping and CO_2 distribution. The most significant feature of an efficient trapping mechanism, residual gas saturation, was examined. It moderately affected CO_2 plume extension, particularly vertical CO_2 migration, where more CO_2 was trapped with greater residual gas saturation conditions. Pore volume sensitivity revealed that the pore volume of the reservoir has a significant impact on pressure variations, as pressure must be dissipated, and higher volume allows for easier dissipation, resulting in lower pressure build-up and stabilization. Finally, the rock compressibility sensitivity demonstrated that changing the compressibility of the rock has a significant impact on the pressure. This is because rocks with poorer compressibility are unaffected by pressure, and the size of the pores remains nearly constant, implying that the higher pore pressure in the pores caused by the injected fluid cannot rapidly dissipate, resulting in higher reservoir pressure levels. The effect magnitude of all six parameters on pressure, free and dissolved CO_2, and the CO_2 plume growth has been provided in Table 5.11.

Table 5.11 The magnitude of each parameter's effect on pressure, free/dissolved CO_2, and CO_2 plume extension have been classified into strong (2), moderate (1), and weak or no effect (0).

	Effect Magnitude		
Sensitivity	**Pressure**	**Free/Dissolved CO_2**	**CO_2 plume extension**
Permeability Ratio	0	1	2
F6 Fault transmissibility	1	1	2
Relative permeability curve	1	1	2
Residual gas saturation	0	1	1
Pore volume	2	0	0
Rock compressibility	2	0	0

6 Conclusion

After refining the Aurora model created in 2015 (Sundal et al., 2015) and updating the model according to the last decisions made by the Norwegian government and operators involved in the Northern Lights project (https://northernlightsccs.com), two different studies were conducted in this project. The first study compared the performance of the CO_2 storage model in saline aquifer reservoirs using ECLIPSE 100, a black-oil simulator, and ECLIPSE 300, a compositional simulator with the CO2STORE option to activate the CO_2 storage module in saline aquifers. The second study did sensitivity analysis of six parameters that can affect the reservoir or fluid characterization of a model. The reservoir parameters analyzed in this project were permeability ratio, F6 Fault transmissibility, relative permeability curve, residual gas saturation, pore volume, and rock compressibility.

The first study revealed that despite slight variations in some calculations between the black-oil and compositional simulators, primarily due to different density-viscosity computation approaches, both simulation methods can be used to gain a clear understanding of pressure elevation and stabilization during the injection and post-injection periods, the amount of free and dissolved CO_2 that can be achieved and forecasting the CO_2 footprint in the reservoir over a long period. Since the simulation time for black-oil cases is roughly four times less than for compositional cases, the black-oil simulator could be used when there is a time limitation to investigate a reservoir and/or when several simulations are required to refine the model or conduct sensitivity analysis of uncertain parameters. In contrast, the compositional case with CO2STORE option might indeed produce more accurate results. Since the compositional model takes much longer to compute the final results, especially for long-term simulations, it is recommended to employ them if computer clusters are available to accelerate the time efficiency of the study.

The second study showed that parameters chosen for sensitivity studies affect the pressure, CO_2 dissolution, and CO_2 plume distribution differently. It was concluded that changing pore volume and the rock compressibility have the strongest impact on pressure changes; however, they have almost no effect on the dissolution of CO_2 and CO_2 plume distribution. Changing permeability ratio, F6 fault transmissibility, and relative permeability affect the CO_2 plume migration significantly and moderately impact the amount of CO_2 dissolved in the brine phase. Lastly, the change of permeability ratio and residual gas saturation did not affect pressure changes.

Room for improvements

One of the study's limitations was the model's small size, which was designed to place CO_2 injection wells in the southern part of the Johansen Formation. However, because one of the project's goals was to place the confirmation well (Eos) in the actual geographical location, the CO_2 injected reaches the northern part of the model faster after around 500 years of simulation. As a result, most simulation cases show the same extension of the CO_2 plume, especially in the J-direction. Collaboration with geology groups could address this issue to extend the Johansen Formation to the northern part of the model and then run the simulations with the same cases. The CO_2 plume distribution in the northern part will be different, most probably with different cases.

Obtaining more accurate results on the porosity-permeability distribution should be considered, as they can affect the reservoir's injectivity, pressure, capacity, and CO_2 distribution. In addition, adding heterogeneity to the model, especially the possible presence of lateral siltstones inside the Johansen Formation, will affect the migration or retention of the injected CO_2, where the more inverted cone shape plume can change to different lateral CO_2 plumes accumulated beneath the siltstones present in the formation, leading to higher trapped and dissolved CO_2 over time.

ECLIPSE has been proven as one of the most advanced tools for reservoir simulation, especially for CO_2 sequestration in saline aquifers. However, there are other reservoir simulators developed by engineers and researchers that are being used in the industry and academia. CMG (Computer Modelling Group) reservoir simulation software has provided a specific module called GEM for CO_2 storage in saline aquifers, and MRST-co2lab (Matlab Reservoir Simulation Toolbox) developed specifically for the study of CO_2 storage in large-scale saline aquifer systems. It would be beneficial to run the simulations using different tools, compare their performance and compatibility, and find some valuable insights from these studies.

The smart proxy model (SPM) is a new tool that the oil and gas industry has started to use for sensitivity analysis and uncertainty assessments in reservoir simulations leveraging artificial intelligence (AI) and machine learning techniques (ML). Since it has shown accurate results in a much shorter time than conventional reservoir simulation, it can be utilized to propose more sensitivity analysis with high accuracy and much faster computation than reservoir simulations.

Appendix A

Conversion factors

Volume to mass (ECLIPSE 100):

1 year = 365 days

534 Sm^3 = 1 tonne

10^6 tonnes= 1 million tonnes

Cumulative Injection volume of 30 years:

$$2{,}194{,}520.548 \ \frac{Sm^3}{day} \times \frac{365 \text{ days}}{1 \text{ year}} \times 30 \text{ years} = 2.403 \times 10^{10} \ Sm^3$$

$$2.403 \times 10^{10} \ Sm^3 \times \frac{1 \text{ tonne}}{534 \ Sm^3} \times \frac{1 \text{ Mt}}{10^6 \text{ tonnes}} = 45 \text{ Mt}$$

Mass-mole to mass (ECLIPSE 300 – CO2STORE):

mol = mole = g-mole

1 mole = 1 g-mole CO_2 = 44.01 g CO_2

1 kg-mole CO_2= 1000 g-mole CO_2= 1000 mole CO_2

$$1 \text{ kg-mole } CO_2 \times \frac{1000 \text{ mole } CO_2}{1 \text{ kg-mole } CO_2} \times \frac{44.01 \text{ g } CO_2}{1 \text{ mole } CO_2} \times \frac{1 \text{ kg}}{1000 \text{ g}} \times \frac{1 \text{ tonne}}{1000 \text{ kg}} \times \frac{1 \text{ Mt}}{10^6 \text{ tonnes}} = \text{Mt}$$

CO_2 trapped in the gas phase at the end of simulation:

$$8.9\text{E}{+}8 \text{ kg-mole } CO_2 \times \frac{10^3 \text{ mole } CO_2}{1 \text{ kg-mole } CO_2} \times \frac{44.01 \text{ g } CO_2}{1 \text{ mole } CO_2} \times \frac{1 \text{ kg}}{10^3 \text{ g}} \times \frac{1 \text{ t}}{10^3 \text{ kg}} \times \frac{1 \text{ Mt}}{10^6 \text{ t}} = 39.2 \text{ Mt}$$

CO_2 mobile in the gas phase at the end of simulation:

$$8.3\text{E}{+}7 \text{ kg-mole } CO_2 \times \frac{1000 \text{ mole } CO_2}{1 \text{ kg-mole } CO_2} \times \frac{44.01 \text{ g } CO_2}{1 \text{ mole } CO_2} \times \frac{1 \text{ kg}}{10^3 \text{ g}} \times \frac{1 \text{ t}}{10^3 \text{ kg}} \times \frac{1 \text{ Mt}}{10^6 \text{ t}} = 3.66 \text{ Mt}$$

CO_2 dissolved in the water phase at the end of simulation:

$$8.3\text{E}{+}7 \text{ kg-mole } CO_2 \times \frac{1000 \text{ mole } CO_2}{1 \text{ kg-mole } CO_2} \times \frac{44.01 \text{ g } CO_2}{1 \text{ mole } CO_2} \times \frac{1 \text{ kg}}{10^3 \text{ g}} \times \frac{1 \text{ t}}{10^3 \text{ kg}} \times \frac{1 \text{ Mt}}{10^6 \text{ t}} = 1.77 \text{ Mt}$$

Appendix B

Aurora model base case (E100)

```
RUNSPEC
TITLE
3DCO2 Injection Johansen Formation, Grid from Anja Sundal
Modified by Vahid Marashi
-- Grid 400x400m faults sealing
DIMENS
-- Grid Dimensions
-- NX       NY       NZ
-- ------  --------  ------
    78      130       120  /
-- Active Phases Present
OIL
GAS
DISGAS
METRIC
-- Unit Convention
-- BIGMODEL
-- DIFFUSE
-- Enables Molecular Diffusion
PARALLEL
2 DISTRIBUTED /
--MEMORY
--30000 /
TABDIMS
-- Table Of Dimensions
-- NTSFUN  NTPVT  NSSFUN
-- ------  -----  ------
     1       1      40   1* 2 /
-- NTSFUN: No. of saturation tables entered.
-- NTPVT : No. of PVT tables entered (in the PROPS section).
-- NSSFUN: Max. no. of saturation node in each saturation table, ie.,
--         Max. no. of data points in each table.
WELLDIMS
-- Well Dimension Data
-- NWMAXZ NCWMAX NGMAXZ NWGMAX
-- ------ ------ ------ ------
     20      120    5    10    /
-- NWMAXZ: Max. no. of wells in the models.
-- NCWMAX: Max. no. of connections per well (i.e., no. of
perforations).
-- NGMAXZ: Max. no. of groups in the model.
-- NWGMAX: Max. no. of wells in any group.
REGDIMS
-- NTFIP   NMFIPR----
 9 3 /
-- NTFIP: Max. no. of fluid-in-place regions
-- NMFIPR: No. of sets of fluid-in-place regions
--EQLDIMS
-- 6 /
FAULTDIM
 2000 /
START
```

```
-- Specifies a Start Date
-- DAY    MONTH   YEAR
-- ----   -----   ----
    1     JAN     2024 /
NSTACK
-- Stack Size For Linear Solver
250/
UNIFOUT
-- Restart And Summary Files Are To Be Unified
UNIFIN
-- Restart From A Unified Restart File
--NOSIM
--
================================================================================
========
GRID
--
================================================================================
========
INIT
INCLUDE
'../INCLUDE/Regional_NEW_JOINED.GRDECL' /
--       ARRAY   VALUE     ------- BOX ------
EQUALS
      'ACTNUM'      0            2   67  70  130  1   120 /
      'MULTPV'     18.5          10  67  67  69   1   120 /
      'MULTPV'     1             38  78  1   5    1   59 /
       'MULTPV'     215           38  78  1   5    60  120 /
/
INCLUDE
'../INCLUDE/Regional_NEW_FAULTS_AAG.grdecl' /
COPY
'PERMX' 'PERMY' /
/
MINPV
-- Minimum pore volume a cell must have to be active
 3000 /

--
================================================================================
========
EDIT
MULTFLT
 'F*' 1.0 /
 /
--
================================================================================
====
PROPS
--
================================================================================
========
INCLUDE
 '../INCLUDE/PVT_SH_TUBAAEN98C_1.TXT' /
-- PVT Data used Tubåen's
-- Using Johansen saturation End-points
-- Swirr=0.337
-- Sgr= 0.298
```

```
-- =========================
-- Saturation Dependent Data
-- =========================
SOF2
-- Oil Saturation Functions (2-phases)
--  So      Krog
-- ----    -------
--drainage
0.00    0.00000
0.05    0.00000
0.10    0.00000
0.15    0.00000
0.20    0.00000
0.25    0.00000
0.337   0.00000
0.35    0.00595
0.40    0.01235
0.45    0.02287
0.50    0.03902
0.55    0.06250
0.60    0.09526
0.65    0.13947
0.70    0.19753
0.75    0.27207
0.80    0.36595
0.85    0.48225
0.90    0.62430
0.95    0.79562 /
/
SGFN
--Gas Saturation Functions UPSCALED
--  Sg       krg    Pc_og
-- ----    -------  ----
--Drainage
0.00  0.00000  0.0
0.03  0.00000  0.0
0.05  0.00000  0.0
0.10  0.00000  0.0
0.15  0.00000  0.0
0.20  0.00000  0.0
0.25  0.00000  0.0
0.28  0.00000  0.0
0.298 0.00000  0.0
0.35  0.01000  0.0
0.40  0.05000  0.0
0.45  0.15000  0.0
0.50  0.25000  0.0
0.55  0.35000  0.0
0.60  0.45000  0.0
0.65  0.55000  0.0
0.70  0.65000  0.0
0.75  0.75000  0.0
0.80  0.85000  0.0
0.85  0.95000  0.0
0.95  0.95000  0.0 /
/
-- Saturation Dependent data used UTSIRA's relative permeability curve
```

```
--============================ls
================================================
REGIONS
--
================================================================================
========
--       ARRAY   VALUE     ------- BOX ------
EQUALS
           'FIPNUM'      1       1  78  6  66 1 120 /
           'FIPNUM'      2       1  78  1  5  1 120 /
/
--
================================================================================
========
SOLUTION
--
================================================================================
========
EQUIL
-- Equilibration Data Specification
-- Datum  Pi@Datum  WOC   Pc@WOC   GOC   Pc@GOC  Rs  Rv  Accuracy
-- -----  --------  ---   ------  -----  ------  --  --  --------
    2600    260.0   5050.0  0.0   100.0   0.0    1    0          /

/
RPTRST
BASIC=2 DENO PORV/
RPTSOL
DENO /
RSVD
-- Variation Of Solution GOR With Depth
-- Depth     Rs
-- -----  --------
   800   0.00000
   4150   0.00000 /
/
--
================================================================================
========
SUMMARY
--
================================================================================
========
--FIELD AVERAGES
FPR
FRS
FGIR
FGSAT
FGIT
FOPR
FOPT
FGIPL
FGIPG
FGIP
FGVIS
FGDEN
FOIP
FOIPR
```

```
FRPV
FOPV
FGPV
RGIP
/
RGIPL
/
RGIPG
/
--WELL
WBHP
/
WGIR
/
WGIT
/
WGOR
/
WOPR
/
WOPT
/
--Pressure in blocks around the well
BPR
43 49 44 /
/

BVOIL
44 40 44 /
/

BDENO
44 40 44 /
/

BVGAS
44 40 44 /
/

BDENG
44 40 44 /
/

EXCEL
--
================================================================================
========
SCHEDULE
--
================================================================================
========
MESSAGES
-- Resets Message Print and Stop Limits
-- Messages   Comments  Warnings  Problems  Error    Bug
-- --------   --------  --------  --------  -----    ---
    10000  10000 10000 10000  100 100 100000 100000 100000 10000 /
--RPTSCHED
--'RESTART' 'FIP=2' 'CPU=2' /
```

```
--/
RPTSCHED
 PRESSURE SGAS SWAT DENG DENW VGAS VWAT XMF AQPH SSOLID /
WELSPECS
-- Wellname Wellgroup   I-loc  J-loc   Ref. Depth    Pref. Phase  -----
-----------  ------ ------- -----------  -----------   ---------------
    Eos         'G1'      43     49        1*         'GAS'

--Drainage Radius
---------------
0.2   /
/

COMPDAT
-- Wellname  I-loc  J-loc   Upper K-loc  Lower K-loc   Connection  -- -
-------      ------ -----   -----------  -----------   ------------ ---
------------------- -------------   ----------
    Eos       43       49         44           109       'OPEN'         0

--Sat. table  Trans. factor  Well diameter   Pen. dir.
-----------  --------------- -------------    ---------
      1*       0.2               3*         Z     /
/
-- 1.5 Mt/y for 30 years (1 jan 24)
WCONINJE
'Eos'  'GAS'     'OPEN'     'RATE'     2194520.548 1*   450   /

/
-- Time steps until 2054
TSTEP
30*365.0
/
WELOPEN
 Eos SHUT /
/
DATES
 1 JAN 2060 /
 1 JAN 2070 /
 1 JAN 2080 /
 1 JAN 2090 /
 1 JAN 2100 /
 1 JAN 2120 /
 1 JAN 2140 /
 1 JAN 2160 /
 1 JAN 2180 /
 1 JAN 2200 /
 1 JAN 2250 /
 1 JAN 2300 /
 1 JAN 2350 /
 1 JAN 2400 /
 1 JAN 2450 /
 1 JAN 2500 /
/
END
```

Aurora model base case (E300)

```
RUNSPEC
TITLE
3DCO2 Injection Johansen Formation, Grid from Anja Sundal
Modified by Vahid Marashi
--E300
-- Grid 400x400m faults sealing
DIMENS
-- Grid Dimensions
-- NX       NY       NZ
-- ------  --------  ------
    78      130       120  /
CO2STORE
-- Capillary pressure mode
-- PW = P - PC
-- PG = P
OPTIONS3
250* 1 /

COMPS
3 /
METRIC
-- Unit Convention
PARALLEL
2 DISTRIBUTED /
MEMORY
200 /
TABDIMS
-- Table Of Dimensions
-- NTSFUN  NTPVT  NSSFUN
-- ------  -----  ------
     1       1      40   1* 2 /
-- NTSFUN: No. of saturation tables entered.
-- NTPVT : No. of PVT tables entered (in the PROPS section).
-- NSSFUN: Max. no. of saturation node in each saturation table, ie.,
--         Max. no. of data points in each table.
WELLDIMS
-- Well Dimension Data
-- NWMAXZ NCWMAX NGMAXZ NWGMAX
-- ------ ------ ------ ------
     20      120    5    10    /
-- NWMAXZ: Max. no. of wells in the models.
-- NCWMAX: Max. no. of connections per well (i.e., no. of
perforations).
-- NGMAXZ: Max. no. of groups in the model.
-- NWGMAX: Max. no. of wells in any group.
REGDIMS
-- NTFIP   NMFIPR----
 9 3 /
-- NTFIP: Max. no. of fluid-in-place regions
-- NMFIPR: No. of sets of fluid-in-place regions
--EQLDIMS
-- 6 /
FAULTDIM
 2000 /
START
-- Specifies a Start Date
```

```
-- DAY    MONTH   YEAR
-- ----   -----   ----
    1     JAN     2024 /
-- Stack Size For Linear Solver
NSTACK
40 /
UNIFOUT
-- Restart And Summary Files Are To Be Unified
UNIFIN
-- Restart From A Unified Restart File
--NOSIM
--
================================================================================
========
GRID
--
================================================================================
========
INIT
INCLUDE
'../INCLUDE/Regional_NEW_JOINED.GRDECL' /
--       ARRAY   VALUE     ------- BOX ------
EQUALS
      'ACTNUM'       0     2   67  70  130  1   120 /
    'MULTPV'       18.5    10  67  67   69   1   120 /
    'MULTPV'       1       38  78  1    5    1   59 /
    'MULTPV'       215     38  78  1    5    60  120 /
/
INCLUDE
'../INCLUDE/Regional_NEW_FAULTS_AAG.grdecl' /
COPY
'PERMX' 'PERMY' /
/
MINPV
-- Minimum pore volume a cell must have to be active
 3000 /

--
================================================================================
========
EDIT
MULTFLT
 'F*' 1.0 /
 /
--
================================================================================
====
PROPS
--
================================================================================
========
CNAMES
 CO2 H2O NaCl /

ZMFVD
--Total composition with respect to depth tables
-- depth  co2    h2o    nacl     cacl2
 2600      0     0.85   0.15 /
```

```
ROCK
-- Rock Compressibility
-- Ref. pressure     Compressibility
-- -------------     ---------------
       300.0              5.0E-05   /


RTEMP
98 /

-- Reference densities for solid phase
--SDREF
--2* 2170.0 /

-- =========================
-- Saturation Dependent Data
-- =========================
-- Critical gas saturation 0.2
-- Residual oil (water) saturation 0.07
-- Tentatively upscaled from laboratory values of 0.3 and 0.05,
respectively.
WSF
0.00    0.00000
0.05    0.00000
0.10    0.00000
0.15    0.00000
0.20    0.00000
0.25    0.00000
0.337   0.00000
0.35    0.00595
0.40    0.01235
0.45    0.02287
0.50    0.03902
0.55    0.06250
0.60    0.09526
0.65    0.13947
0.70    0.19753
0.75    0.27207
0.80    0.36595
0.85    0.48225
0.90    0.62430
0.95    0.79562 /
/
GSF
0.00  0.00000  0.0
0.03  0.00000  0.0
0.05  0.00000  0.0
0.10  0.00000  0.0
0.15  0.00000  0.0
0.20  0.00000  0.0
0.25  0.00000  0.0
0.28  0.00000  0.0
0.298 0.00000  0.0
0.35  0.01000  0.0
0.40  0.05000  0.0
0.45  0.15000  0.0
```

```
0.50  0.25000  0.0
0.55  0.35000  0.0
0.60  0.45000  0.0
0.65  0.55000  0.0
0.70  0.65000  0.0
0.75  0.75000  0.0
0.80  0.85000  0.0
0.85  0.95000  0.0
0.95  0.95000  0.0 /
/
--============================ls
================================================
REGIONS
--
================================================================================
========
--       ARRAY   VALUE     ------- BOX ------
EQUALS
           'FIPNUM'      1      1  78  6  66 1 120 /
           'FIPNUM'      2      1  78  1  5  1 120 /
/
--
================================================================================
========
SOLUTION
--
================================================================================
========
EQUIL
-- Equilibration Data Specification
-- Datum  Pi@Datum  WOC   Pc@WOC   GOC   Pc@GOC  Rs  Rv  Accuracy
-- -----  --------  ---   ------  -----  ------  --  --  --------
    2600    260.0   0  0.0   0   0.0   1    0          /
/
--RPTRST
--RESTART PRESSURE SGAS SWAT DENG DENW VGAS VWAT XMF AQSP AQPH SSOLID /
RPTSOL
PRESSURE SGAS SWAT DENG DENW VGAS VWAT XMF AQSP AQPH SSOLID /
--RSVD
-- Variation Of Solution GOR With Depth
-- Depth     Rs
-- -----  --------
--   800    0.00000
--   4150   0.00000 /
--/
--FIELDSEP
-- 1 15.0 1.01 /
--/
--
================================================================================
========
SUMMARY
--
================================================================================
========
--FIELD AVERAGES
FPR
FGIR
```

```
FGSAT
FGIT
FOPR
FOPT
FGIPL
FGIPG
FGIP
FGDEN
FOIP
FOIPR
FRPV
FWCD
FGCDI
FGCDM
RWCD
/
RGCDI
/
RGCDM
/
--FCMIT
--FCMIP
RGIP
/
RGIPL
/
RGIPG
/
--WELL
WBHP
/
WGIR
/
WGIT
/
WGOR
/
WOPR
/
WOPT
/
--Pressure in blocks around the well
BPR
43 49 44 /
/

BVGAS
44 40 44 /
/

BDENG
44 40 44 /
/

BVWAT
44 40 44 /
/
```

```
BDENW
44 40 44 /
/

EXCEL
--
================================================================================
========
SCHEDULE
--
================================================================================
========
RPTRST
ALLPROPS BASIC=2 PRESSURE SGAS SWAT SWAT SOIL XMF YMF ZMF SSOLID RPORV
BOIL BGAS BWAT AMF /
MESSAGES
-- Resets Message Print and Stop Limits
-- Messages   Comments  Warnings  Problems  Error    Bug
-- --------   --------  --------  --------  -----    ---
    10000  10000 10000 10000  100 100 100000 100000 100000 10000 /
RPTSCHED
'RESTART' 'FIP=2' 'CPU=2' /
/
-- Wellname Wellgroup   I-loc  J-loc   Ref. Depth    Pref. Phase  -----
-----------  ------ ------- -----------  -----------   ---------------
    Eos         'G1'       43     49        1*          'GAS'

--Drainage Radius
---------------
0.2   /
/

COMPDAT
-- Wellname  I-loc  J-loc   Upper K-loc  Lower K-loc   Connection  -- -
-------      ------ -----   -----------  -----------   ------------ ---
------------------- -------------   ----------
    Eos       43       49         44           109       'OPEN'         0

--Sat. table  Trans. factor  Well diameter   Pen. dir.
-----------  ---------------  -------------    ---------
      1*       0.2               3*          Z     /
/




-- Set Composition of injection gas stream
WELLSTRE
-- WellStreamName 1stCompMoleFrac  2ndCompMoleFrac
CO2INJ 1.0/
/
WINJGAS
-- WellName  NatureOfInjFluid WellStreamName
 'Eos' STREAM CO2INJ /
/
-- 1.5 Mt/y for 30 years (1 jan 24)
WCONINJE
```

```
      'Eos'  'GAS'     'OPEN'     'RATE'     2194520.548 1*   450   /

/
-- Time steps until 2054
TSTEP
30*365.0
/
WELOPEN
 Eos SHUT /
/
DATES
 1 JAN 2060 /
 1 JAN 2070 /
 1 JAN 2080 /
 1 JAN 2090 /
 1 JAN 2100 /
 1 JAN 2120 /
 1 JAN 2140 /
 1 JAN 2160 /
 1 JAN 2180 /
 1 JAN 2200 /
 1 JAN 2250 /
 1 JAN 2300 /
 1 JAN 2350 /
 1 JAN 2400 /
 1 JAN 2450 /
 1 JAN 2500 /
/

END
```

Appendix C

INTEGRATED BIOSTRATIGRAPHY OF THE EQUINOR ENERGY AS EXPLORATION WELL NO 31/5-7 "EOS", OFFSHORE NORWAY

Prepared by

Martin Pearce (coordinator), David Bailey, Paul Dodsworth,

Peter Morris and Stephen Packer

On behalf of the client

Equinor Energy AS

PROJECT NUMBER: 2020–09

APRIL, 2020

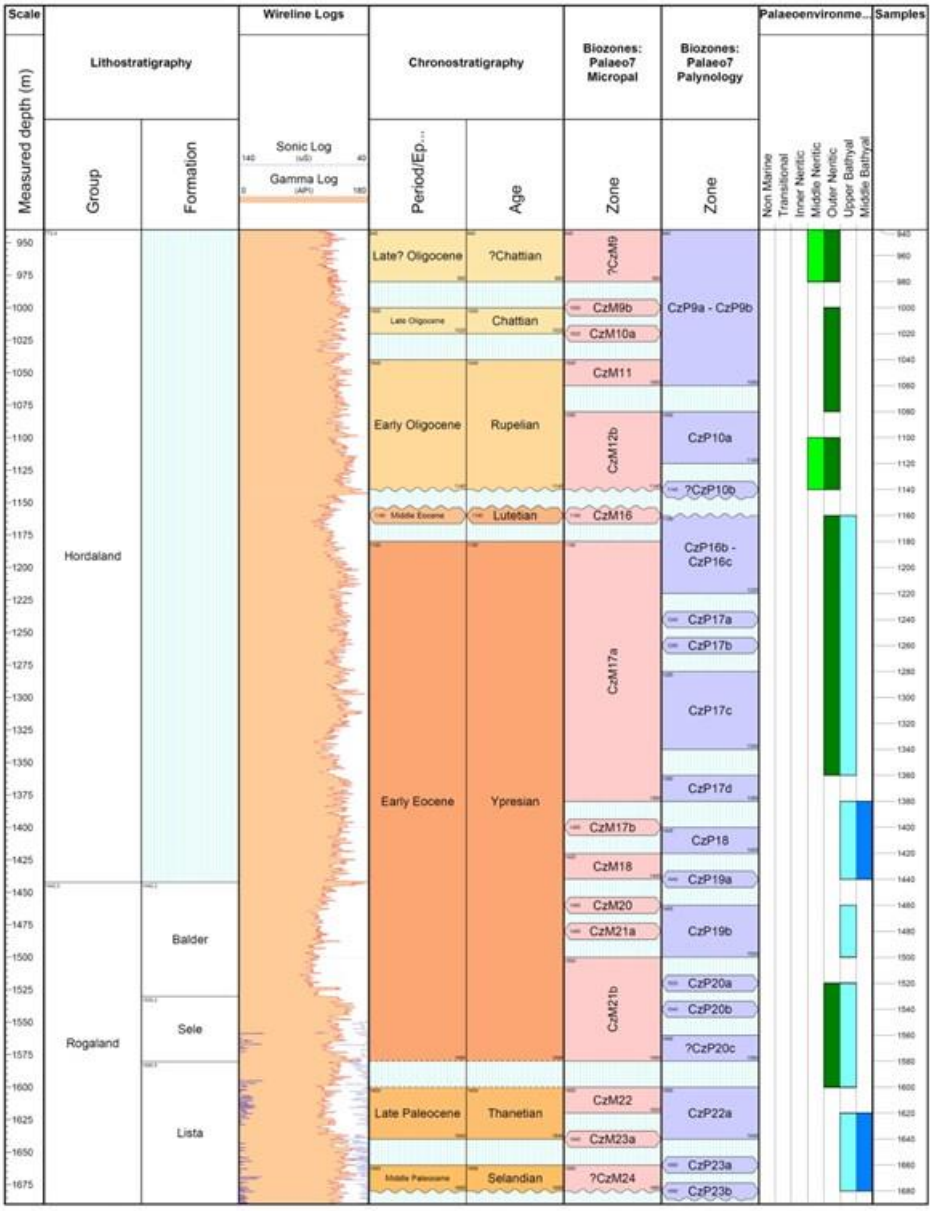

Figure 3. Biochronostratigraphic and palaeoenvironmental summary of the Hordaland to Rogaland groups of the NO 31/5-7 (Eos) well.

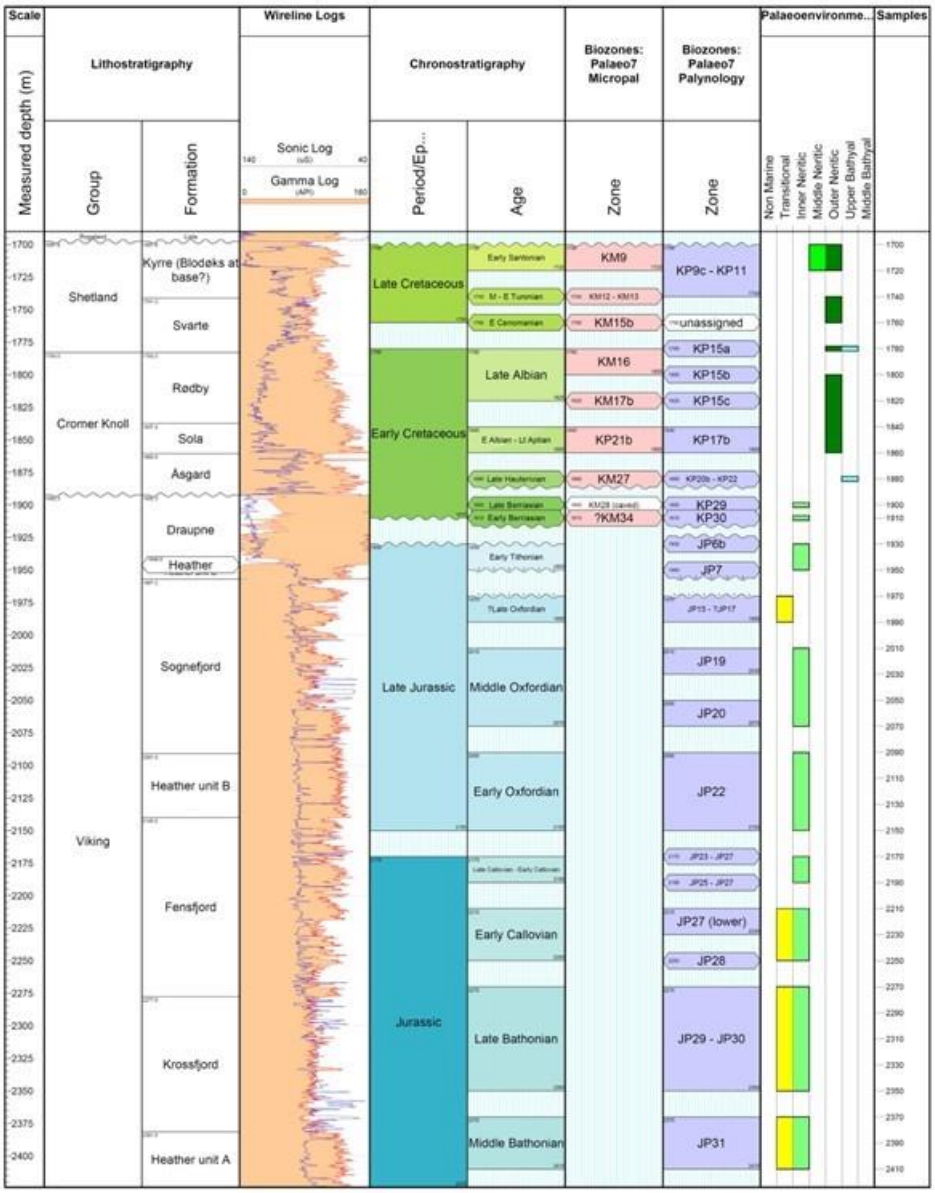

Figure 4. Biochronostratigraphic and palaeoenvironmental summary of the Shetland to Viking groups of the NO 31/5-7 (Eos) well.

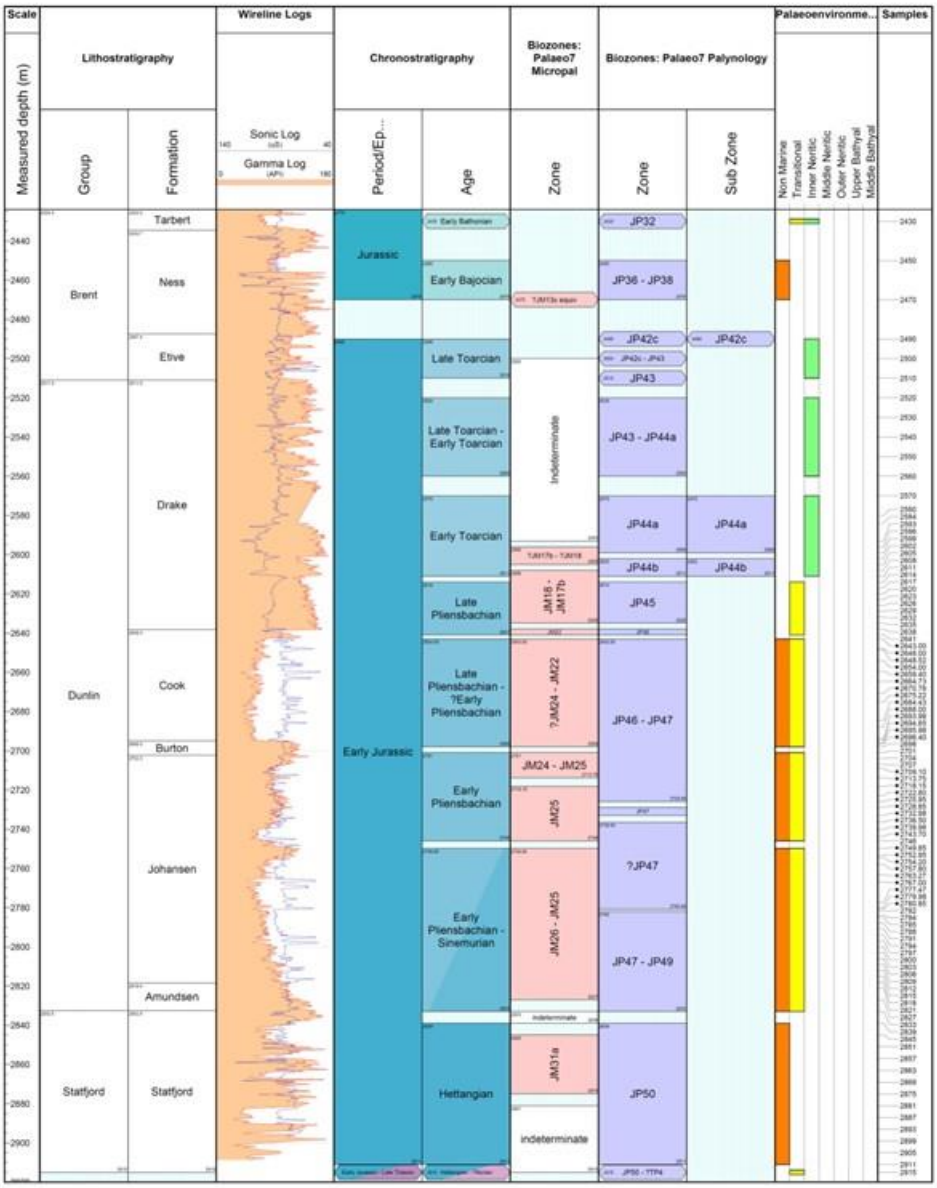

Figure 5. Biochronostratigraphic and palaeoenvironmental summary of the Brent to Statfjord groups of the NO 31/5-7 (Eos) well.

31/5-7 EOS					
			Actual		
System	Group	Formation tops	Depth (m TVD MSL)	Depth (m TVD RKB)	Depth (m MD RKB)
Quaternary/ Neogene/ Paleogene	Nordland	*Seabed*	307	338	338
		URU (Upper regional unconformity)	457	488	488
	Hordaland	*Skade*	741	772	772
		Hordaland "Green Clay"	1113	1144	1144
	Rogaland	*Balder*	1411	1442	1442
		Sele	1499	1530	1530
		Lista	1549	1580	1580
Cretaceous	Shetland	*Hardraade*	1667	1698	1698
		Svarte	1710	1741	1741
	Cromer Knoll	*Undefined*	1747	1778	1778
		Sola	1806	1837	1837
		Åsgard	1830	1861	1861
		BCU	1861	1892	1892
Jurassic	Viking	*Draupne*	1861	1892	1892
		Heather C	1915	1946	1946
		Sognefjord	1926	1957	1957
		Heather B	2073	2104	2104
		Fensfjord	2109	2140	2140
		Krossfjord	2247	2278	2278
		Heather	2350	2382	2382
	Brent	*Tarbert*	2393	2424	2424
		Ness	2404	2435	2435
		Etive	2456	2487	2487
	Dunlin	*Drake 2*	2479	2510	2510
		Drake 1	2532	2563	2563
		Drake Intra Marine Shale Acoustic marker	2553	2585	2585
		Cook 4	2607	2638	2638
		Cook 3	2607	2638	2638
		Cook 2	2611	2642	2642
		Cook 1	2654	2685	2685
		Burton	2664	2695	2695
		Johansen Fm. 4	2671	2702	2702
		Johansen Fm. 3	2710	2741	2741
		Johansen Fm. 2	2721	2752	2752
		Johansen Fm. 1	2735	2766	2766
		Amundsen	2787	2818	2818
Triassic	Statfjord	*Eriksson*	2801	2832	2832
		TD	2884	2915	2915

Appendix D

All of the simulations have been recorded as videos and can be found here:

https://mega.nz/folder/81hx3YZS#DqdGdUQXMmuvTzP7IBAeyQ

You can reach me by the following email:

marashivahid@gmail.com

References

Bachu, S. (2002). Sequestration of CO2 in geological media in response to climate change: road map for site selection using the transform of the geological space into the CO2 phase space. *Energy Conversion and Management*, *43*(1), 87-102.

Bakke, K. (2020). Northern Lights–" open source" access to transport and storage service. Presentation at the 10th Trondheim CCS Conference (TCCS-10),

Beck, S., & Mahony, M. (2018). The IPCC and the new map of science and politics. *Wiley Interdisciplinary Reviews: Climate Change*, *9*(6), e547.

Bennion, D. B., & Bachu, S. (2006). Dependence on temperature, pressure, and salinity of the IFT and relative permeability displacement characteristics of CO2 injected in deep saline aquifers. SPE Annual Technical Conference and Exhibition,

Berg , C. F., & Slotte, P. A. (2020). *Reservoir Simulation Through Open Source Software*.

Berg, R. R. (1975). Capillary pressures in stratigraphic traps. *AAPG bulletin*, *59*(6), 939-956.

Bolås, H. M. N., & Hermanrud, C. (2003). Hydrocarbon leakage processes and trap retention capacities offshore Norway. *Petroleum Geoscience*, *9*(4), 321-332.

CO2CRC. (2021). https://co2crc.com.au/about-ccus/storage/

Eigestad, G. T., Dahle, H. K., Hellevang, B., Riis, F., Johansen, W. T., & Øian, E. (2009). Geological modeling and simulation of CO 2 injection in the Johansen formation. *Computational Geosciences*, *13*(4), 435.

Flude, S., & Alcade, J. (2021). *Carbon capture and storage has stalled needlessly – three reasons why fears of CO_2 leakage are overblown*. https://theconversation.com/carbon-capture-and-storage-has-stalled-needlessly-three-reasons-why-fears-of-co-leakage-are-overblown-130747

Furre, A.-K., Meneguolo, R., Pinturier, L., & Bakke, K. (2020). Planning deep subsurface CO2 storage monitoring for the Norwegian full-scale CCS project. *First Break*, *38*(10), 55-60.

Gassnova. (2012). *Geological storage of CO2 from Mongstad. Interim report Johansen Formation*.

Gough, C., Shackley, S., Holloway, S., Bentham, M., Bulatov, I., Mclachlan, C., Klemfa, J. J., Purdy, R. W., & Cockerill, T. T. (2006). An integrated assessment of carbon dioxide capture and storage in the UK.

Holden, N. (2021). *Structural characterization and across-fault seal assessment of the Aurora CO2 storage site*

Holt, T., Jensen, J.-I., & Lindeberg, E. (1995). Underground storage of CO2 in aquifers and oil reservoirs. *Energy Conversion and Management*, *36*(6-9), 535-538.

Liu, Y., Wang, L., Liu, X., & Ding, T. (2014). Effects of capillary pressure–fluid saturation–relative permeability relationships on predicting carbon dioxide migration during injection into saline aquifers. *Energy Procedia*, *63*, 3616-3631.

Lothe, A. E., Bergmo, P. E., & Grimstad, A.-A. (2019). Storage Resources for Future European CCS Deployment; A Roadmap for a Horda CO2 Storage Hub, Offshore Norway.

Lothe, A. E., Bergmo, P. E. S., Emmel, B., & Eliasson, P. (2018). Effects of uncertainties in fault interpretations on pressure depletion and CO2 storage injection at Horda

Platform, offshore Norway. 14th Greenhouse Gas Control Technologies Conference Melbourne,
Marchetti, C. (1977). On geoengineering and the CO 2 problem. *Climatic change*, *1*(1), 59-68.
Marjanac, T. (1995). Architecture and sequence stratigraphic perspectives of the Dunlin Group formations and proposal for new type-and reference-wells. In *Norwegian Petroleum Society Special Publications* (Vol. 5, pp. 143-165). Elsevier.
Marjanac, T., & Steel, R. J. (1997). Dunlin Group sequence stratigraphy in the northern North Sea: a model for Cook Sandstone deposition. *AAPG bulletin*, *81*(2), 276-292.
Metz, B., Davidson, O., De Coninck, H., Loos, M., & Meyer, L. (2005). *IPCC special report on carbon dioxide capture and storage*. Cambridge: Cambridge University Press.
Miri, R., & Hellevang, H. (2016). Salt precipitation during CO2 storage—A review. *International Journal of Greenhouse Gas Control*, *51*, 136-147.
Niemi, A., Bear, J., & Bensabat, J. (2017). *Geological storage of CO2 in deep saline formations* (Vol. 29). Springer.
NPD. (2014). *CO2 Atlas for the Norwegian Continental Shelf*. https://www.npd.no/en/facts/publications/co2-atlases/co2-atlas-for-the-norwegian-continental-shelf/
Rasmussen, K., & Maver, K. (1996). Direct inversion for porosity of post stack seismic data. European 3-D Reservoir Modelling Conference,
Riaz, A., Hesse, M., Tchelepi, H., & Orr, F. (2006). Onset of convection in a gravitationally unstable diffusive boundary layer in porous media. *Journal of Fluid Mechanics*, *548*, 87-111.
Ringrose, P. (2020). *How to Store CO2 Underground: insights from early-mover CCS Projects*. Springer.
Ringrose, P. S., Furre, A.-K., Gilfillan, S. M., Krevor, S., Landrø, M., Leslie, R., Meckel, T., Nazarian, B., & Zahid, A. (2021). Storage of Carbon Dioxide in Saline Aquifers: Physicochemical Processes, Key Constraints, and Scale-Up Potential. *Annual Review of Chemical and Biomolecular Engineering*, *12*, 471-494.
Schlumberger. (2020). *Eclipse 100/300 Reference Manual and Technical Description*.
Spycher, N., & Pruess, K. (2005). CO2-H2O Mixtures in the Geological Sequestration of CO2. II. Partitioning in Chloride Brines at 12–100 C and up to 600 bar. *Geochimica et cosmochimica acta*, *69*(13), 3309-3320.
Spycher, N., & Pruess, K. (2010). A phase-partitioning model for CO 2–brine mixtures at elevated temperatures and pressures: application to CO 2-enhanced geothermal systems. *Transport in porous media*, *82*(1), 173-196.
Sundal, A., Miri, R., Ravn, T., & Aagaard, P. (2015). Modelling CO2 migration in aquifers; considering 3D seismic property data and the effect of site-typical depositional heterogeneities. *International Journal of Greenhouse Gas Control*, *39*, 349-365.
Sundal, A., Nystuen, J. P., Rørvik, K.-L., Dypvik, H., & Aagaard, P. (2016). The Lower Jurassic Johansen Formation, northern North Sea–Depositional model and reservoir characterization for CO2 storage. *Marine and Petroleum Geology*, *77*, 1376-1401.
Thompson, N., Andrews, J. S., & Bjørnarå, T. I. (2021). Assessing Potential Thermo-Mechanical Impacts on Caprock Due to CO2 Injection—A Case Study from Northern Lights CCS. *Energies*, *14*(16), 5054.
Vollset, J., & Doré, A. G. (1984). *A revised Triassic and Jurassic lithostratigraphic nomenclature for the Norwegian North Sea*. Oljedirektoratet.
Williams, G., & Chadwick, R. (2021). Influence of reservoir-scale heterogeneities on the growth, evolution and migration of a CO2 plume at the Sleipner Field, Norwegian North Sea. *International Journal of Greenhouse Gas Control*, *106*, 103260.

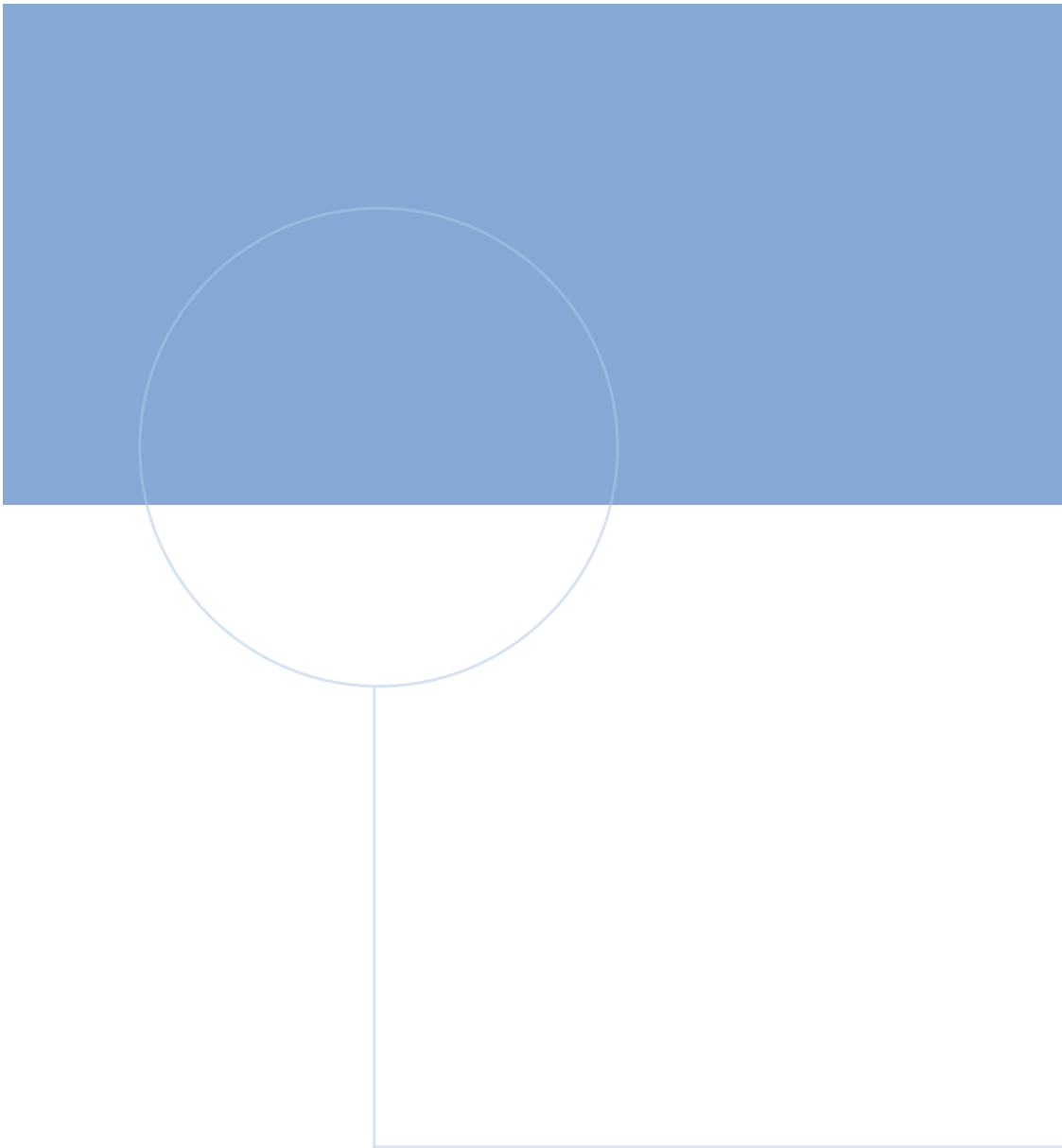

NTNU

Kunnskap for en bedre verden